MICROWAVE TORREFACTION OF NATURAL FIBERS FOR INCORPORATION INTO ENGINEERING THERMOPLASTIC BIOCOMPOSITES

A Dissertation
Submitted to the Graduate Faculty
of the
North Dakota State University
of Agriculture and Applied Science

By

Jessica Lynne Lattimer Vold

In Partial Fulfillment of the Requirements
for the Degree of
DOCTOR OF PHILOSOPHY

Major Department:
Mechanical Engineering

March 2015

Fargo, North Dakota

North Dakota State University
Graduate School

Title

Microwave Torrefaction of Natural Fibers for Incorporation into Engineering Thermoplastic Biocomposites

By

Jessica Lynne Lattimer Vold

The Supervisory Committee certifies that this ***disquisition*** complies with North Dakota State University's regulations and meets the accepted standards for the degree of

DOCTOR OF PHILOSOPHY

SUPERVISORY COMMITTEE:

Dr. Chad Ulven
Chair

Dr. Bret Chisholm

Dr. Bora Suzen

Dr. Xinnan Wang

Dr. Dean Webster

Approved:

4/13/2015
Date

Dr. Alan R. Kallmeyer
Department Chair

ABSTRACT

Little work has been done in the area of engineering thermoplastic biocomposites due to the increased processing temperatures which induce degradation of biomass. Torrefaction has been identified as an effective means of preparing biomass for introduction into engineering thermoplastics such as polyamide 6, however it is an energy and time intensive process. This work looks to microwave induced heating to reduce the required energy costs by 70% over a conventional heating method while producing a more homogeneous higher degree of torrefaction torrefied biomass. The torrefied biomasses were analyzed to understand how time, temperature, and power level affect the yield and thermal stability temperature of the fibers. The effects of the addition of torrefied flax shive, hemp hurd, and sunflower hulls to polyamide 6,6 on mechanical and thermal properties were also studied.

ACKNOWLEDGMENTS

I would like to first thank my advisor, Dr. Chad Ulven, for all the support and guidance he has shown me over the last five years. Had he not taken a chance on the aerospace engineer who had no knowledge of composite materials, aside from they exist, I can honestly say I would not be completing my doctorate today. I would also like to thank Dr. Bret Chisholm, Dr. Bora Suzen, Dr. Xinnan Wang, and Dr. Dean Webster for their time and input throughout the dissertation research.

I would also like to thank my parents, Bob and Debbie Lattimer, for all their love, encouragement, and support throughout the years. You never ceased to show me that hard work and determination could accomplish anything I could dream of.

Last but certainly not least I would like to thank my husband, Brandon. Without your constant love and support I could not have finished the work I set out to do. I may not be happy all day every day, but you make me happy every day just knowing you are there for me.

TABLE OF CONTENTS

LIST OF TABLES

LIST OF FIGURES

LIST OF APPENDIX TABLES

CHAPTER 1. INTRODUCTION

The automotive industry, the single largest consumer of polyamides, is becoming a proponent of greater utilization of biobased materials [1]. This effort makes the addition of biobased fillers in engineering thermoplastics attractive for applications such as under-the-hood shrouds. The incorporation of biobased fillers into the most consumed plastics can truly help offset the use of petroleum, while maintaining, if not improving, the mechanical integrity of manufactured parts. Furthermore with the right pretreatment, the incorporation of biobased fillers into engineering thermoplastics, traditionally higher cost materials, the price of final goods could be significantly reduced.

Over the last decade the use of biobased materials as fillers in thermoplastics has seen a remarkable increase. The low cost to density ratio coupled with improved mechanical properties and processing conditions, have led to the increased acceptance of natural fibers as replacements for traditional synthetic fibers [2]–[7]. It is well known from previous work that adding natural fiber reinforcements to commodity polyolefin matrices (i.e. polyethylene, polypropylene, etc.) will in general increase the elastic modulus, decrease the tensile strength, increase the flexural performance, and decrease the impact resistance of the material. By adding reinforcements to the unfilled matrix, these rigid impurities in the material prevent the polymer chains from sliding past one another, thus causing an increase in modulus, a decrease in tensile strength, and induced brittle failure. The filler can be considered as impurities in the biocomposite because of a lack in interfacial bonding between the filler and matrix. The lack of interfacial bonding comes from the mismatch in polarities between the matrix and filler; the matrix generally being hydrophobic and the filler being hydrophilic. However, these imperfections are the cause of increased elastic

modulus by impeding the molecular chain movement within the polymer. They are also the cause of increased flexural performance and decreased impact resistance. In polyolefin matrices it has been determined the use of a compatibilizer can aid in improving the interfacial bond between filler and matrix. While the focus has thus far been on producing biobased composites out of commodity polyolefins or bio-derived resins, little work has been done in the realm of engineering thermoplastics [2], [3], [5]–[8].

1.1. Polyamide Composites

For many years the increased rigidity, good resistance to creep, improved wear resistance, and increased heat deflection temperatures of polyamide composites have made them appealing to replace metals in a vast array of applications. Due to the increased processing temperatures of polyamides only thermally stable fillers such as fiberglass, carbon fibers, and minerals have been used. Of all the fillers used in polyamide composites, fiberglass is the most common. It was estimated in 2003 that 200,000 tons of glass filled polyamides were used every year [9], [10].

The fastest growing use of polyamides is accredited to the automotive industry. Since the discovery of polyamides in 1939 the automotive industry has used it to replace weight expensive metals parts, with an immediate implementation for self-lubricating bearings after its introduction at that year's World's Fair. Initially designers limited the use of polyamides to non-critical components due to a lack of information on how polyamides performed in harsh environmental conditions [1], [11].

The 1960s brought about an increased use of polyamides in cars, with an average of 0.4 pounds of polyamide per vehicle. The introduction of glass and mineral filled polyamides around 1968 changed the mindset of designers, who began designing polyamide radiator and fuel system

components. An enhanced understanding of the high temperature performance and chemical resistance of polyamides along with government regulations for pollution control, pushed the consumption of polyamides and polyamide composites even higher in the 1970s. An average of 2 pounds of polyamide was in every car. It was not until the 1980s that polyamides and their composites were really trusted for high performance components, such as air intake manifolds, and were consistently used across all lines of vehicles. The polyamide and polyamide composite content of cars jumped to an average of 8.8 pounds by 1995, including general acceptance of polyamide air and cam manifolds, and the United States automotive industry alone consumed 212 million pounds polyamides. This wide acceptance of polyamides in vehicle design made it the largest used engineering thermoplastic in the automotive industry. By 2000 every car contained on average 11.06 pounds of polyamides and polyamide composites under-the-hood alone; 30 times more than in 1960 when polyamide automotive parts were introduced [1], [11].

1.2. Polyamide Biocomposite Production

For engineering thermoplastics, the increased processing temperatures cause degradation of the natural fiber. This degradation is the breakdown of hemicellulose (220 - 320 °C), fats, residual waxes, etc. leaving behind the cellulose and lignin that do not fully degrade at these temperatures [12]. While the natural fiber does not degrade completely, volatiles deposited on the fiber surface are enough to hinder mechanical performance of the composite. One method of preventing the degradation of biobased fillers is to decrease the amount of time the filler is exposed to the increased temperatures. There have been several attempts at creating nylon biocomposites in which the biobased fillers were introduced in a manner that minimized the exposure time. Compression molding with a 2.5 minute cycle time to minimize the degradation

of the filler and an extrusion process that introduces filler down-stream just before the die are all methods of reducing filler degradation [2], [4].

The introduction of Curauá fibers, the leaves from a tropical fruit much like the pineapple, during a twin screw extrusion process was shown to be successful in reinforcing polyamide 6 when the fibers were introduced just before the die. An intermeshing co-rotating screw was used for this work and a temperature profile from feeder to die of 215, 220, 225, 230 °C was used. A fiber loading of 20 wt% was achieved during this extrusion process, however, the tensile and flexural properties fell short of the traditional glass or talc filled polyamide 6 (PA6) composites. Table 1.1 shows mechanical properties of the 20 wt% filled polyamide composites. The tensile strength of the Curauá filled polyamide displays an 18% drop below the traditional glass filled polyamide. However the Curauá filler does show improved tensile strength over the talc composite. Thus the Curauá filled polyamide biocomposites are viable replacements for certain applications where glass or talc filled composites are currently used [4].

Table 1.1: Tensile, Flexural, and Density Comparison of 20 wt% Curauá, Glass, and Talc Filled Polyamide 6 Composites [4]

Filler	Tensile Strength (MPa)	Tensile Modulus (GPa)	Flexural Strength (MPa)	Flexural Modulus (GPa)	Impact Toughness (kJ/m^2)	Density (g/cm^3) ±0.01
PA6	63 ± 1	1.3 ± 0.1	95 ± 1	2.2 ± 0.1	10 ± 1	1.13
Curauá	83 ± 3	5.1 ± 0.4	116 ± 2	3.7 ± 0.1	9 ± 2	1.18
Talc	73 ± 1	6.7 ± 06	114 ± 2	4.4 ± 0.1	9 ± 2	1.27
Glass	101 ± 1	6.5 ± 0.5	160 ± 5	5.0 ± 0.1	7 ± 1	1.27

A second method of limiting natural fiber exposure during processing is to utilize compression molding. Polyamide 6 fibers and wood fibers were combined and pressed into rectangular plaques using 50 kN of force at a temperature of 230 °C. The composite plaques were held under pressure at temperature for 2.5 minutes. Filler loadings of 2.5, 5, 7.5, and 10 wt% were achieved using the compression molding process. Table 1.2 summarizes the tensile

properties measured from the compression molded specimens. It can be seen from the table that the incorporation of wood fiber into the polyamide matrix increased the tensile modulus by as much as 42% over the unfilled polyamide 6. The tensile strength also showed improvement with added wood fiber by as much as 53% [2].

Table 1.2: Tensile Properties of Compression Molded Polyamide Wood Composites [2]

Wt%	Tensile Strength (MPa)	Tensile Modulus (GPa)
0	30	1.9
2.5	46	3
5	40	2.6
7.5	31	2.4
10	34	2.7

In both the Curauá and wood fiber studies, the biocomposites produced showed improvements on both tensile and flexural properties. In a polyolefin biocomposite the tensile strength generally decreases due to the poor fiber-matrix interactions. For a polyamide based biocomposite the interfacial bond between fiber and matrix is stronger. Polyamides are more hydrophilic as compared to polyolefins which make their inherent compatibility with very hydrophilic biomass better. Without the need of an added compatibilizer to strengthen the fiber-matrix bond polyamide biocomposites are more economically appealing than polyolefin biocomposites [2], [4].

While the cost savings of replacing an expensive plastic such as polyamide with inexpensive fillers is appealing, moisture uptake is a concern. The hydrophilic nature of polyamide, while good for aiding in fiber-matrix bonding, is detrimental to maintaining mechanical integrity in harsh environmental conditions. Moisture is absorbed through the amorphous regions of polyamides and begins to modify the structure. Interchain hydrogen bonds begin to weaken as a result of absorbed moisture. This weakening of bonds allows increased chain movement in the polymer, thus decreasing glass transition temperature and decreasing

mechanical integrity. Figure 1.1 shows the chemical structure of polyamide 6 and 6,6. The interaction of water molecules and polyamides occurs between the carbon oxygen double bonds and nitrogen hydrogen bonds where hydrogen bonding occurs between polymer chains. This hydrogen bond is what limits the chain movement in dry polyamides. Figure 1.2 shows the interaction of water molecules in more detail, the red circles indicate the water molecules that have weakened the chain to chain hydrogen bonding [13]. For a greater acceptance of polyamide biocomposites, the issues of fiber degradation and moisture absorption need to be addressed.

1.3. Chemically and Thermally Modified Fillers

Chemical modification of wood dates back to 1928 and is simply defined as covalently bonding molecules to reactive sites along the cell wall polymers of wood. While there is an array of chemicals suitable for chemical modification of wood fibers, the acetylation process using acetic anhydride is the most common. In 1928 the first acetylation of pine wood was performed with acetic anhydride and sulphuric acid catalyst to isolate lignin. The acetylation of beach wood later in 1928 showed that through the isolation of lignin the hemicellulose present in the wood could be removed. Then in 1946 it was discovered that the acetylation of wood could prevent swelling during moisture absorption [14].

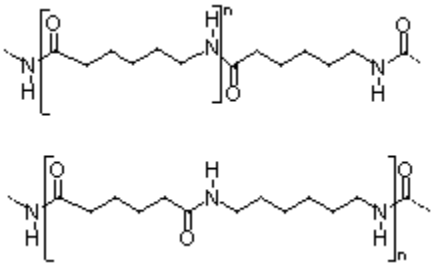

Figure 1.1: Chemical structure of polyamide 6 (top) and polyamide 6,6 (bottom).

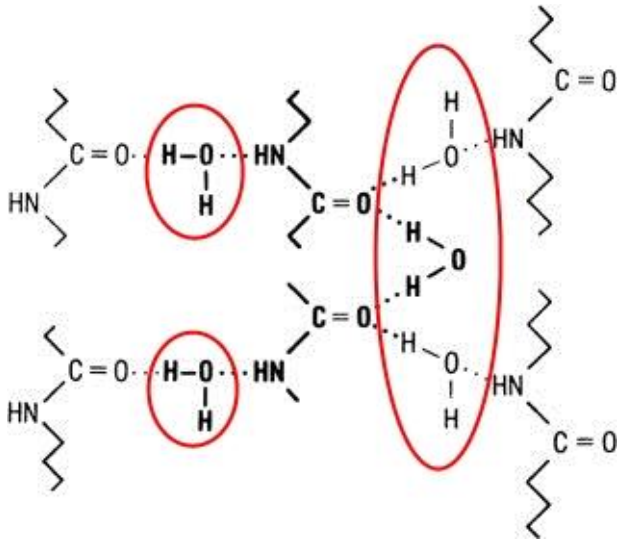

Figure 1.2: The interaction of water in polyamides [13].

While the acetylation of wood has been well studied over the years the process can also be applied to many biobased fibers. Acetylation is a chemical reaction that replaces one hydroxyl group in the biobased fiber molecule with an acetyl group from acetic anhydride. Figure 1.3 shows the chemical reaction between natural fibers and acetic anhydride. The acetylation process is very simple; fibers are washed in acetic anhydride while heat is applied and then dried before being processed into biocomposites. As Figure 1.3 shows, the by-product of acetylation with acetic anhydride is acetic acid, a flammable irritant that has harmful vapors [14]–[18]. The addition of acetylated fiber has shown to improve the dimensional stability, hydrophobicity, and interfacial shear strength in polymer matrix biocomposites [15]–[18].

Figure 1.3: The chemical reaction that occurs during acetylation of natural fibers using acetic anhydride [18].

While acetylation will sufficiently modify the surface of natural fibers to improve mechanical performance over untreated fibers, the use of harsh chemicals can be undesirable. A more recent process known as thermal modification has shown to be promising at eliminating the need for harsh chemicals while maintaining the desired improvements of fiber modification. Thermal modification much like the acetylation process is done at elevated temperatures, around 200 °C for several hours, but in an atmosphere low in oxygen content. At 140 °C the degradation of natural fibers begins to be significant when exposure times are lengthy. In an atmosphere low in oxygen the hemicellulose, and to a small extent the amorphous cellulose, begins to break down. It is not until the temperatures reach 230 °C that the amorphous cellulose decomposition becomes significant. Due to the low temperature of thermal modification the thermally stable crystalline cellulose will not see any structural changes. When added to polymer matrices, thermally modified fibers have been shown to improve the dimensional stability, hydrophobicity, and interfacial shear strength over untreated fibers [16], [17], [19]. However, as thermal modification is only conducted at 200 °C, well below the process temperatures of most engineering thermoplastics, a more aggressive method such as torrefaction must be employed before natural fibers can be introduced into engineering thermoplastics.

1.4. Torrefaction

Torrefaction, traditionally an alternative method of producing energy, is a decomposition and densification process conducted in an inert atmosphere at elevated temperatures. Torrefaction converts low molecular weight constituents within biomass to syngas and carbon. Three distinct phases are created during the torrefaction process: a solid carbonized mass, an acidic liquid phase, and syngas. One advantage of the solid by-product of torrefaction over untreated biomass, for the energy sector, is the production of a more homogeneous, dry

lignocellulosic material high in energy content. Another advantage is the ability to store torrefied biomass for extended lengths of time without any concern of bacterial growth or biodegradation due to environmental exposure. The ability to store torrefied biomass for extended periods of time stems from the increased hydrophobicity of the fiber. Although torrefaction of biomass has been studied extensively over the last several years, the exact chemical reactions occurring during the process are still unclear. It has been shown that the breakdown of hydroxyl groups on cellulose microfibrils is the cause of increased hydrophobicity [12], [20]–[25].

The solid by-product of torrefaction can be used in the traditional gasification or co-firing processes for electricity production, but its heating value is lower than that of traditional coal. However, it also has the potential to be used in biocomposite production with high temperature thermoplastics such as polyamide. The increased hydrophobicity being a potential solution for the moisture absorption issues discussed earlier with polyamide biocomposites. The syngas produced during torrefaction can potentially be burned to power the next torrefaction process making it self-sustaining after the initial torrefaction run.

As discussed with thermally modified fillers, natural fibers begin to significantly degrade at 140 °C when exposure times are lengthy. The major difference between thermal modification and torrefaction is temperature range. Torrefaction is traditionally done in the range of 225-300 °C in an inert atmosphere for several hours. The length and temperature chosen for the process will determine the degree of torrefaction of the fibers. As with the thermal modification the hemicellulose, fats, waxes, and other low degradation point constituents within the fibers are converted to syngas and carbon yielding a biomass consisting of mostly crystalline cellulose, degrading between 300–375 °C, and lignin, degrading slowly over 250–500 °C [24], [25]. In the mild degradation during thermal modification the amorphous cellulose saw minor structural

changes; whereas torrefaction will degrade the amorphous cellulose to a higher degree and begin to mildly degrade the crystalline cellulose.

Figure 1.4 depicts the various reactions leading to degradation and conversion of the three main constituents within biomass; hemicellulose, lignin, and cellulose. There are four main reactions that occur within the individual constituents, while each occurs at different temperatures for each constituent the reactions are very similar. There is also one reaction that only occurs in the lignin present in the biomass. Reaction A is the physical drying of the biomass, this occurs at temperatures well below the processing temperature. Reaction B, only seen in the lignin, is the relaxation of the polymer chains. This relaxation is what aids in the densification process of torrefied biomass as the softened lignin acts as a binder. As the temperature increases reaction C begins to take place. There are two parts to reaction C, the depolymerization of the constituent and the condensing of the shortened polymer chains into a solid by-product. As temperatures climb beyond reaction C, reaction D begins to take over. Reaction D brings limited devolatilization and carbonization of intact polymer chains within the constituent and the solid by-product formed in reaction C. As the temperatures of the torrefaction approach reaction E extensive devolatilization and carbonization of the polymer chains and solid by-products of all previous reactions occurs. The transition from reaction to reaction is slow and occurs over a range of temperatures which can make prediction of by-products difficult for processes occurring at transition points. At 300 °C (torrefaction temperature targeted in this work) it can be seen from Figure 1.4 that the hemicellulose will see extensive devolatilization and carbonization. The lignin will begin to see more extensive devolatilization and carbonization. However, the reaction occurring within cellulose is in the transition between limited and extensive devolatilization and carbonization, so it is not as easily predicted [26].

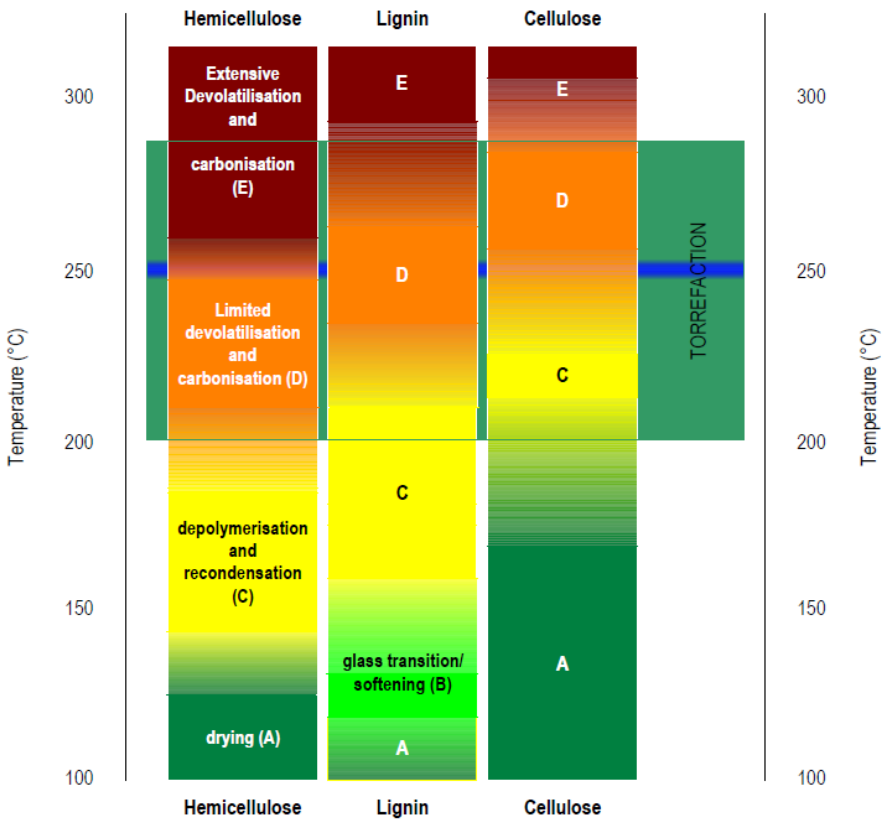

Figure 1.4: Reactions caused by torrefaction at varying temperatures [26].

As the temperature at which torrefaction is conducted increases, the amount of solid char produced from the various reactions also increases as seen in Figure 1.5. Part A of Figure 1.5 shows the chemical characteristics of the components within natural fiber and part B shows the components of the solid torrefaction by-product or char. There are four distinct char regions depending on the torrefaction temperature. Transition char results from the mildest torrefaction. In this region the lignin begins to depolymerize, the amorphous cellulose undergoes significant degradation, crystalline cellulose begins to undergo molecular changes, and char begins to form. The next degree of torrefaction yields amorphous char. In this region the amorphous cellulose and lignin are completely converted and very little crystalline cellulose remains intact. The most severe degrees of torrefaction occurring above approximately 400 °C have converted all forms of cellulose and lignin to syngas and carbon. At these temperatures turbostatic crystallites form and

continue to grow with increased temperature, but the char does not reach the order or crystallinity of graphite [21]. As crystalline cellulose is the component within natural fibers that reinforces biocomposites, maximizing the survival of this component during torrefaction is critical to producing viable filler for polyamide biocomposites. For this reason the bulk of this work will focus on the production of transition char; more specifically the production of transition char that contains little to no intact hemicellulose.

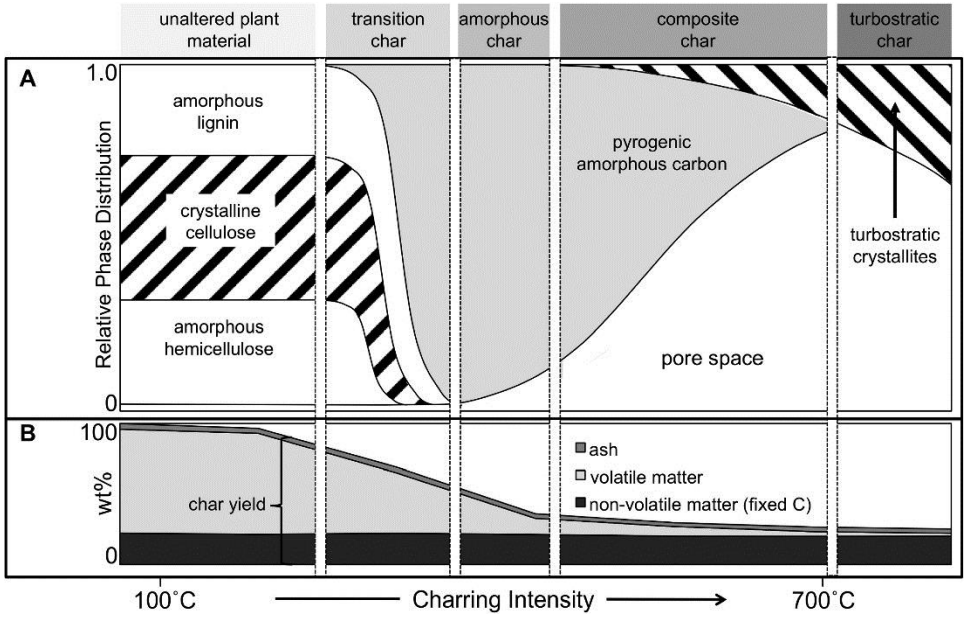

Figure 1.5: Char characteristics and constituent break down at varying temperatures of torrefaction measured by thermal gravimetric analysis [21].

Knowing which of the constituents present in a biomass feed stock will undergo some conversion to syngas and carbon during torrefaction will estimate how much mass loss is expected during the process. Calculating the percent yield of a torrefaction process will indicate a rough estimate of the degree of torrefaction. This first requires knowing the break down by mass percentage of the various constituents present in biomass feedstock. There are many ways of determining the constituent makeup of a biomass feedstock, for this work wet chemical analysis was employed. As lignin and cellulose are the primary constituents remaining after

torrefaction, the total of their mass content will estimate how much of the biomass weight should remain after a successful process. Several other methods of grading the degree of torrefaction are studied in this work.

1.5. Microwave Torrefaction

One of the appealing qualities of adding natural fiber fillers to polyolefins is the ability to offset petroleum usage with renewable resources while the cost to produce a final composite remains relatively unchanged. For engineering thermoplastics the added preprocessing of the filler adds a substantial energy input increasing the cost to produce a final part. On a lab scale, the average high temperature gas sealed oven runs at 8 kilowatts of power, while the maximum power for a scientific microwave controlled oven with an output power of 1200 watts is 3.7 kilowatts. If it is assumed that the microwave and the conventional oven need to run for the same length of time to complete a torrefaction run the microwave would save 54% of the required energy for one run. With the average cost of electricity being $0.12 per kilowatt hour, according to the United States Energy Information Administration, it costs $7.68 to run a conventional oven for 8 hours compared to $3.55 for the same length of time in a microwave. Aside from the fact that it takes 54% less energy to run a microwave over the conventional oven, it takes less time to complete a torrefaction run. One of the overall goals of this work is to determine exactly how much less time it will take to complete a successful torrefaction run in a microwave.

Torrefaction for the energy sector using conventional ovens has been well established and studied for several years. However, the use of microwaves to reduce energy input and reduce processing times has seen little work thus far. Several attempts at microwave torrefaction or carbonization have been made using focused microwave devices such as the one shown in Figure 1.6. The biggest drawback to a focused microwave device is the limited specimen sizes. With the

average sample size on the milligram scale these focused microwave devices are impractical for an industrial setting. There is speculation that the small scale focused microwave devices could be scaled up to an industrial scale but there are several potential issues with the larger scale. On the smaller scale the focused microwave devices produce even heating and homogeneous solid by-product, both of which could be potential issues when scaled up. One possible solution to uneven heating and nonhomogeneous output is to add a microwave absorbing phase to the biomass to aid in the production of heat. While the focused microwave systems are appealing for the reduced energy input and processing times, the return on investment has been a deterrent for industry to make the switch from conventional heating methods [27]–[31].

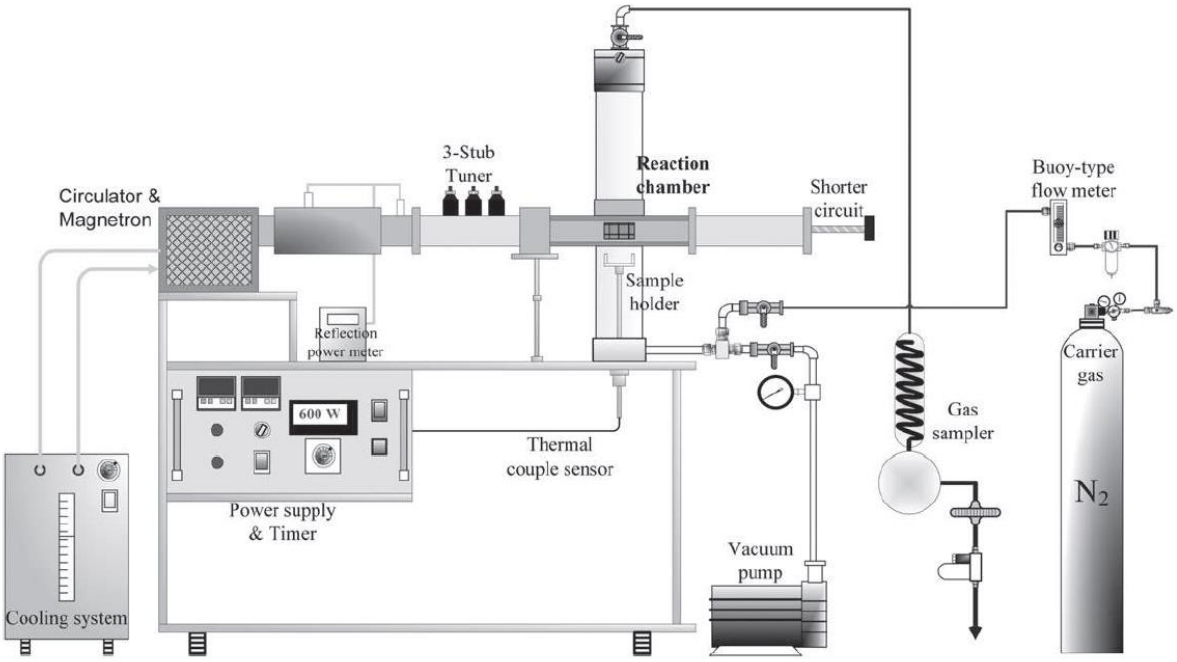

Figure 1.6: An example focused microwave device used for thermal treatment of various samples [31].

A muffle furnace microwave oven like the Milestone Pyro Ashing System depicted in Figure 1.7 could be the solution that both utilizes the rapid heating from microwaves yet produces larger quantities of homogeneous torrefied biomass. The silicon carbide plate at the top

of the heating chamber absorbs the microwaves, the metal then heats up, and radiantly heats the furnace chamber preventing hotspots that lead to uneven torrefaction. As this work focuses on reducing the time required for torrefaction using microwaves the Pyro system will be utilized both as a traditional temperature controlled furnace and a traditional power output controlled microwave to determine the ideal torrefaction process.

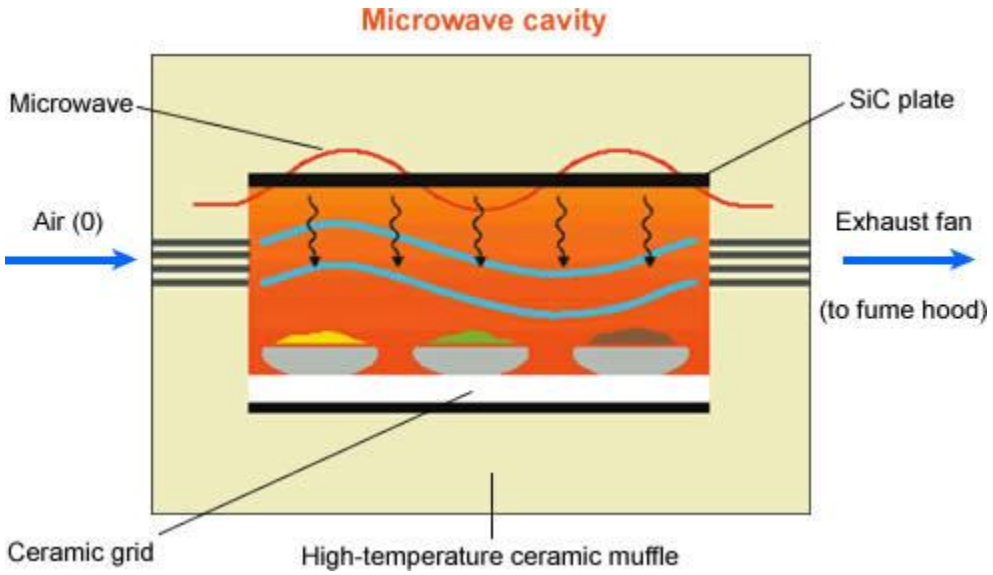

Figure 1.7: Depiction of the Milestone Pyro Ashing System used in this work [33].

1.6. Torrefied Biomass Filled Biocomposites

Leading up to this work the use of conventional oven torrefaction was studied as a means of producing fillers for polyamide biocomposites [32]. The conventional method of heating proved to produce biocomposites that were viable replacement where neat polyamides are currently utilized. By converting the hemicellulose, fats, waxes, et cetera that degrade at a lower temperatures, a biomass filler was created that could withstand the increased processing temperatures of PA6. Polyamide 6,6 (PA66) blends were also produced but the processing temperatures still proved to be too detrimental to the filler. The lack of a consistent and uniform torrefaction process lead to voids within the PA66 biocomposites as seen in Figure 1.8.

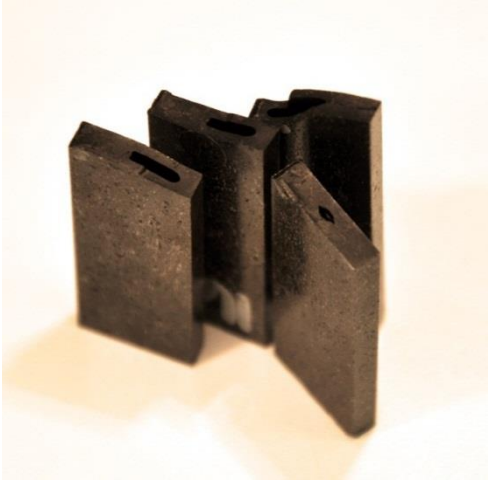

Figure 1.8: Voids observed in PA66 biocomposites.

Sunflower hulls were expected to have a yield of 62.6%; the total mass content of the dry untreated hulls accredited to cellulose and lignin as shown in Table 3.2. For flax shive the yield was expected to be 61.3%. Figure 1.9 shows the sunflower hulls prior to and after the torrefaction process took place. The color of the torrefied sunflower hulls (TSFH) is of note, the darker fibers are indicative of a higher degree of torrefaction, however the lighter brown fibers indicate a milder or incomplete torrefaction. Figure 1.10 shows the difference in untreated flax shive and torrefied flax shive (TFS). With the variation in colors it was concluded that the lab scale torrefaction used in this work was not a uniform and complete process. This is due to the equipment available; a more uniform consistent process would be needed to validate the use of torrefied biomass on a commercial scale.

The small lab scale process employed here limited the size of a single torrefaction batch to approximately 200 g of untreated biomass, which only yields approximately 120 g of torrefied biomass. For this reason the torrefaction for all the biocomposite grades was done prior to any composite processing so the multiple batches needed could be mixed together. This helped

ensure that any differences among torrefaction batches did not affect the mechanical performance of the biocomposites.

Figure 1.9: The difference between untreated sunflower hulls (left) and TSFH (right).

Figure 1.10: The differences between untreated flax shive (left) and TFS (right).

SEM images taken of the untreated and torrefied fibers can be seen in Figure 1.11. Images A and C show the untreated flax shive and sunflower hull respectively. Images B and C are of the TFS and TSFH respectively. For both fiber types the torrefaction process has increased the surface porosity, which aids in matrix diffusion of the fiber surface. This diffusion aids in increased fiber matrix interaction ultimately leading to improved material strengths.

PA6 based biocomposites were successfully produced using both the TFS and TSFH. Table 1.3 lists the tensile and flexural properties measured for the PA6 biocomposites. Here it can be observed that the tensile strengths of the biocomposites are within 70% of the unfilled matrix with slightly decreasing strengths with increasing filler loadings. As would be expected

with the addition of fillers the elastic modulus displays an increasing trend with increased filler loading, with an average increase of 150% over the unfilled matrix. The flexural strength remained within 94% of the unfilled matrix on average, an unexpected phenomenon with the addition of filler. The flexural modulus however did follow an expected trend, displaying an average of 154% increase over the unfilled matrix. The uneven torrefaction of the biomass discussed earlier is believed to have led to a plasticization effect from under-torrefied fibers. These under-torrefied fibers continued to degrade in the presence of oxygen during the composite processing allowing the polymer chains to move more freely than would be expected from a rigid filler. A more uniform torrefaction process as is expected from the microwave processing will help alleviate this plasticization effect. Table 1.4 shows the impact performance of the PA6 biocomposites. The impact toughness shows a decreasing trend with increased filler content as would be expected with the addition of a rigid filler [32].

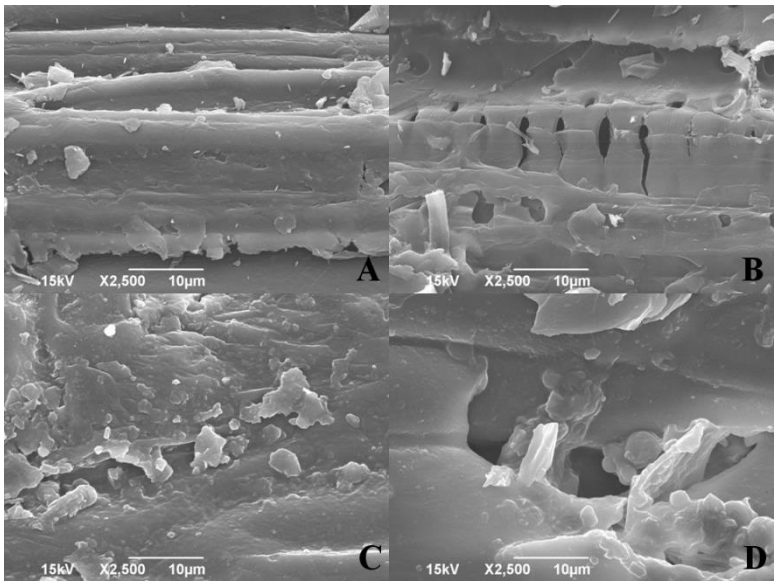

Figure 1.11: SEM images of untorrefied flax shive (A), torrefied flax shive (B), untorrefied sunflower hull (C), and torrefied sunflower hull (D).

Table 1.3: Tensile and Flexural Properties of PA6 Biocomposites

	Tensile Strength (MPa)	Elastic Modulus (GPa)	Flexural Strength (MPa)	Flexural Modulus (GPa)
Unfilled PA6	69.1 ± 0.5	2.8 ± 0.1	94.0 ± 1.2	2.2 ± 0.0
10% TFS PA6	46.5 ± 2.7	3.4 ± 0.1	82.2 ± 1.3	2.1 ± 0.1
20% TFS PA6	51.2 ± 2.9	4.0 ± 0.1	84.5 ± 4.6	2.5 ± 0.0
30% TFS PA6	40.3 ± 5.8	4.2 ± 0.1	90.1 ± 7.5	3.4 ± 0.1
10% TSFH PA6	52.6 ± 2.5	3.2 ± 0.1	93.9 ± 6.8	2.5 ± 0.1
20% TSFH PA6	51.2 ± 4.4	3.4 ± 0.1	90.7 ± 7.3	3.0 ± 0.2
30% TSFH PA6	48.9 ± 3.3	4.0 ± 0.1	89.0 ± 8.1	3.4 ± 0.1

Table 1.4: Impact Performance of PA6 Biocomposites

	Impact Toughness (kJ/m^2)
Unfilled PA6	3.7 ± 0.6
10% TFS PA6	2.5 ± 0.2
20% TFS PA6	1.8 ± 0.5
30% TFS PA6	1.4 ± 0.2
10% TSFH PA6	2.8 ± 0.2
20% TSFH PA6	2.3 ± 0.3
30% TSFH PA6	2.2 ± 0.2

From this previous study [32], it was shown that torrefaction is a viable option for the pretreatment of biomass for engineered thermoplastics compounding. However, many questions were raised in the process. In order to understand more fully how added biomass interacts with a polymer matrix, the chemical and microstructural changes from torrefaction to the fiber surface need to be study. It is understood what constituents will undergo conversion during torrefaction, however the degree to which they are converted is not well understood. The inability to produce PA66 biocomposites points to the need to better understand the degree of torrefaction and how it affects the mechanical properties of biocomposites.

CHAPTER 2. OBJECTIVES

While the offset of petroleum usage is a significant driving factor in the green movement, from an industrial point of view the economics need to line up as well. For a polyolefin matrix such as polypropylene the idea of adding a low cost filler is appealing from an economic stand point. However, due to the weak interfacial bonds between polyolefin matrices and natural fibers the addition of a compatibilizer is necessary to maintain comparable mechanical properties to the unfilled matrix. A compatibilizer such as maleic anhydride drives the price per pound of the biocomposite closer that of the unfilled matrix, eliminating the advantage of adding the low cost natural fiber.

For engineering thermoplastics the addition of biomass filler is not viable until costly pre-processing of the fiber has been done. Whether this pre-processing comes in the form of chemical or thermal treatment the economics are not appealing enough to encourage industry to make the switch from synthetic fillers or unfilled matrices. As previous work has shown the use of torrefied biomass as fillers in polyamide matrices is a promising renewable replacement [32]. However, the torrefaction method is costly from an energy stand point. Eight hours at temperatures of 300 °C or more adds a significant cost to the once low cost filler. By utilizing microwave heating the cost of treating the biomass fillers will be decreased. On top of the lower energy input the time required for processing will also be decreased to less than an hour at temperature. The overall goal of this work is to produce a homogeneous higher degree torrefied biomass using microwave energy and develop an understanding of how torrefaction effects the chemical and microstructural makeup of the biomass. This study also works to develop an

understanding of how the addition of torrefied biomass effects the mechanical properties of engineered thermoplastic biocomposites.

2.1. Experimental Goals

- Develop a viable microwave torrefaction process which converts low melting point constituents present in biomass to carbon and syngas, producing a homogeneous thermally stable solid by-product.
- Characterize the chemical and microstructural makeup of torrefied biomass.
- Produce torrefied biomass filled polyamide biocomposites which are viable drop-in replacements anywhere polyamides are currently used.
- Characterize the thermo-mechanical performance of polyamide based biocomposites.

2.2. Analytical Goals

- Determine the effect of time, temperature, microwave power level, particle size, and sample mass on the efficiency of microwave torrefaction.
- Determine the conversion process of torrefaction.
- Develop predictive models for torrefaction yield and 90% stability temperatures.
- Determine which biomass constituents remain intact after the torrefaction process.
- Determine how the addition of torrefied biomass enhances or hinders the mechanical performance of polyamide based biocomposites.

2.3. Intended Outcomes

By introducing a fully torrefied natural fiber into engineering thermoplastics:

- The tensile strength of the unfilled matrix should be relatively maintained in the composite while increasing the elastic modulus
- The flexural strength and modulus should also see increases with increased filler content, as the higher degree of torrefaction will alleviate the plasticization effect seen in previous work
- As is expected with the addition of rigid fillers the impact toughness of the biocomposites will likely decrease from the unfilled matrix
- With the increased hydrophobicity of the torrefied filler the once problematic moisture uptake of polyamides can be lessened, allowing the biocomposites to maintain more mechanical integrity under harsh environmental conditions than the unfilled matrix
- The increased thermal stability of torrefied fillers will aid in increasing the heat deflection temperature of the biocomposites, this will allow for increased working temperatures in final parts
- A reduction of petroleum usage by as much as 30% can be achieved

CHAPTER 3. MATERIALS AND PROCESSING

Materials for this work were chosen based on the current industrial demand and local supply chains. The polymers used are some of the most widely used materials in commercial production which provides a broad application base for the biocomposites produced in this work. Natural fibers were chosen based on the local agricultural waste streams from commodity processors alleviating costly shipping. As the cost of materials is of concern for industrial acceptance it was important to utilize low cost locally available resources wherever possible.

3.1. Polyamide

Due to its abundant usage in commercial applications, PA66 was used for this work. PA66 was obtained from PolyOne, Avon Lake, Ohio. Ultramid 1000-11 NF 2001 manufactured by BASF Corporation, a general purpose homopolymer, was chosen for the PA66. Table 3.1 shows the published material properties for the polyamide.

Table 3.1: Material Properties for the PA66 Used in this Work

	Melting Temperature (°C)	Density (g/cm^3)	Elastic Modulus (GPa)	Tensile Strength (MPa)	Flexural Modulus (GPa)	Flexural Strength (MPa)	Impact Toughness (J/m)
PA66	536 - 581	1.14	3.0	83.0	2.9	117.0	53.0

3.2. Biomass

For this work three biomasses were chosen based on the available agricultural waste streams in the Fargo, North Dakota area. As North Dakota is one of the leading growers of sunflowers in the country, there is a natural waste stream from commodity processors in the area processing the seeds of the sunflower into consumer goods. During commodity processing, the seeds of the sunflower are removed from the flower and roasted for human consumption,

packaged for bird or pet feed, or the protective hull is removed so the seed can be processed into oil, butter, roasted for consumption, etc. The hulls or shells of the seeds removed during the commodity processing have very low nutritional value; hulls can be substituted at no more than 20% of the feed for livestock. As the demand of hulls for the purpose of livestock feed is low, the waste stream is abundant and inexpensive [34]. The hulls for this work were provided by Red River Commodities, Fargo, North Dakota.

The second biomass chosen for this work is flax shive. Flax shive, unlike the outer protective nature of the sunflower hull, comes from the central woody core of the flax stalk. Figure 3.1 shows a scanning electron microscopy image of a flax stem. The arrows point to the cuticle or protective outer layer of the flax stem. The area labeled F is the bast fiber which makes up flax fiber, underneath this is the cellulosic woody core of the stem, labeled area C, where shive comes from. Flax shive is a byproduct of flax fiber production. Flax straw left on the field after flax seeds are harvested goes through a decortication process to remove flax fiber. By-products of decortication are then passed through sieves to remove any short fibers or seeds remaining and to sort out the various sizes of shive. The larger shive fractions are typically used as bedding for horses and the smaller fractions are used for biofuels and composite manufacturing. The flax shive used in this work was obtained from Flax Stalk Natural Fiber Solutions a subsidiary of Schweitzer-Mauduit International, Winkler, Manitoba, Canada.

The third biomass chosen for this work was hemp hurd. Much like flax shive hemp hurd comes from the woody core of the hemp stalk. Figure 3.2 shows a cross section of hemp stalk. The outer rings of the stalk are made up of the outer protective layer of stalk and the bast fiber used in the production of hemp fiber. The inner most ring of the hemp stalk is the woody core or hurd. The hurd is a by-product of the hemp fiber production process. During the fiber production

process the hurd is shattered into small pieces. Predominantly the hurd has been used as bedding for animals due to its absorbent nature and low dust production. Hurd has been shown to absorb four times its weight in fluid. More recently the combination of hurd, hemp fiber, and lime has become popular as a building material for above grade construction [35]–[38]. The hemp hurd used in this work was obtained from Hemp Technologies Global, Asheville, North Carolina.

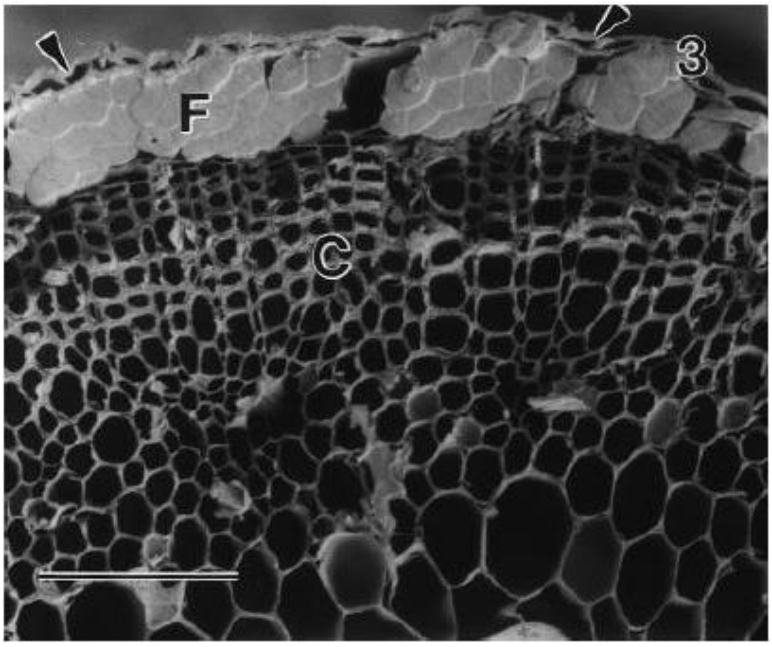

Figure 3.1: SEM image of a flax stem [39].

Wet chemical analysis was performed by the Animal Sciences Department at North Dakota State University to determine the constituent makeup of the sunflower hulls, flax shive, and hemp hurd. AOAC standard 930.15 was used in dry matter determination, AOAC standard 920.39 was used to determine crude fat, and AOAC standard 2001.11 was used for the determination of crude protein. The USDA Agricultural Handbook No. 379 was followed for the analysis of neutral detergent fiber, acid detergent fiber, and acid detergent lignin. The constituent breakdown of the fibers used in this work can be seen in Table 3.2.

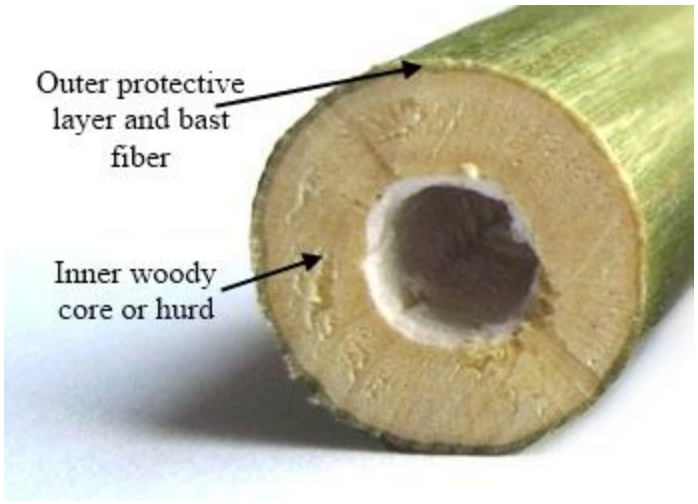

Figure 3.2: Cross section of hemp stalk [35].

Table 3.2: Constituent Breakdown for the Biomasses Used in this Study, All Numbers Are Weight Percentage.

Biomass	Lignin	Cellulose	Hemi-cellulose	Moisture	Ash	Starch	Calcium	Phosphorus	Crude Fat	Crude Protein
Sunflower Hull	22.4	39.8	15.1	7.1	2.7	0.6	0.3	0.17	7.0	5.3
Flax Shive	21.1	40.2	16.8	5.2	2.8	0.7	0.2	0.01	0.3	2.3
Hemp Hurd	14.4	56.7	21.2	2.5	2.5	0.4	0.4	0.1	0.3	2.2

3.3. Microwave Torrefaction Parameters

To develop a viable method of microwave torrefaction three test matrices were evaluated. The first matrix looks at the effects of particle size and sample mass on the efficiency of torrefaction. For this matrix torrefaction time will be held constant at 30 minutes at a temperature of 350 °C. Table 3.3 depicts the 3^{2-1} factorial experimental design for this matrix. The numbers inside the following experimental design tables are the randomized run orders generated by Minitab. The effects of the variables in each experimental design will be evaluated using a standard two-factor analysis of variance (ANOVA).

After the evaluation of the particle size and sample mass experiment, the most efficient combination of particle size and sample mass was used for the final two matrices. One matrix examines the effects of the power level on the torrefaction process, this matrix allows the temperature within the chamber to rise freely while the power output is controlled. Another focuses on how varying temperature effects the degree of torrefaction. The best process was then used to produce larger batches of torrefied filler and compounded into PA66 biocomposites.

Table 3.3: 3^{2-1} Experimental Design for Particle Size and Sample Mass Optimization

		Sample Mass	
		50 g	100 g
Particle Size	As-Received	4	5
	≤ 750 µm	3	6
	≤ 200 µm	2	1

Table 3.4 depicts the 4^{2-1} factorial experimental design intended to determine the effects of power level and temperature on the torrefaction of biomass. While torrefaction is largely a temperature dependent process, one advantage of using a microwave oven is the ability to rapidly heat the chamber. The heating rate can be controlled by controlling the power output level of the magnetron. The idea behind utilizing microwaves for torrefaction is to reduce processing time while providing an even heating which inherently reduces production costs of the final part. Using the microwave as it is intended, by controlling the power output of the magnetron allowing the chamber to heat freely speeds up the torrefaction process, and at the same time provides a higher degree of torrefaction than that of a temperature controlled process. Temperatures were monitored throughout the power controlled processes only to ensure no damage was done to the microwave which has a maximum processing temperature of 1000 °C.

Table 3.5 depicts the 3^2 factorial experimental design intended to determine the effects of temperature and time on the torrefaction process. As discussed in the previous work section

several issues arose in the conventional heating that will alleviated with a microwave heating process using a scientific microwave. One issue is the uneven torrefaction of a single batch of fiber that lead to a plasticization effect in the final biocomposite parts. The other larger issue was the inability to produce PA66 biocomposites due to incomplete torrefaction. The temperature and time experimental design explores torrefaction at the previously studied 300 °C and two higher temperatures too. By exploring higher torrefaction temperatures the torrefied fibers have a higher degree of torrefaction allowing for higher processing temperature during final part production.

Table 3.4: 4^{2-1} Factorial Experimental Design for Power Controlled Microwave Torrefaction

		Power Level			
		300 W	400 W	500 W	600 W
Time	20 min	11	5	2	12
	30 min	8	1	3	6
	40 min	7	10	4	9

Table 3.5: 3^2 Factorial Experimental Design for Temperature Controlled Microwave Torrefaction

		Temperature		
		300 °C	350 °C	400 °C
Time	10 min	1	5	4
	20 min	8	3	9
	30 min	7	6	2

As the last two experimental designs indicate 21 runs of microwave torrefaction were conducted to determine the ideal process to produce large quantities of torrefied biomass for composite production. These 21 runs were conducted using flax shive and the best process for each matrix was then used to process sunflower hulls and hemp hurd.

Prior to analyzing any of the test matrices several experiments were conducted to determine the best crucibles and nitrogen flow for torrefaction. Alumina combustion boats, stainless steel bowls, and Pyrex petri dishes were all tested in the microwave. Both the alumina combustion boats and the stainless steel bowls placed the fibers too close to the silicon carbide

plate in the microwave causing the top fibers to heat rapidly enough to combust. Pyrex petri dishes were chosen for the remainder of this work. Various flow rates of nitrogen were also studied, it was determined that 9440 sccm of nitrogen was the ideal flow rate for this system. The biomass was not stirred during the torrefaction process. Figure 3.3 shows a typical heating curve for microwave torrefaction.

3.4. Twin Screw Extrusion

Multiple 50 g batches of TSFH, TFS, and torrefied hemp hurd (THH) were produced using as-received biomass at a torrefaction temperature of 400 °C for 30 minutes using at most 500 W of power. The TFS batches had an average yield of 33.2%, THH batches had an average yield of 30.8%, and TSFH batches had an average yield of 31.4%. The torrefied biomass was then compounded into PA66 based biocomposites at a fiber loading of 30 wt%. As the density of the torrefied biomass is unknown, producing biocomposites based on fiber volume fraction is challenging, therefore all the composite work done in this study is based on weight percentage. A Leistritz Micro-18/GL-40D, co-rotating twin-screw extruder was used for the melt compounding. All torrefied fillers and polymer matrices were dried overnight at 80 °C in a convection oven prior to processing. The polymer matrix, PA66, was first dry blended with the torrefied biomass based on weight percentage. A temperature profile of: 236, 252, 258, 269, 280, 274, 269, 269 °C starting at the feeding zone and ending with the metering zone was used for extrusion. The extruded biocomposites were water cooled, pelletized, and dried overnight at 80 °C in a convention oven prior to injection molding.

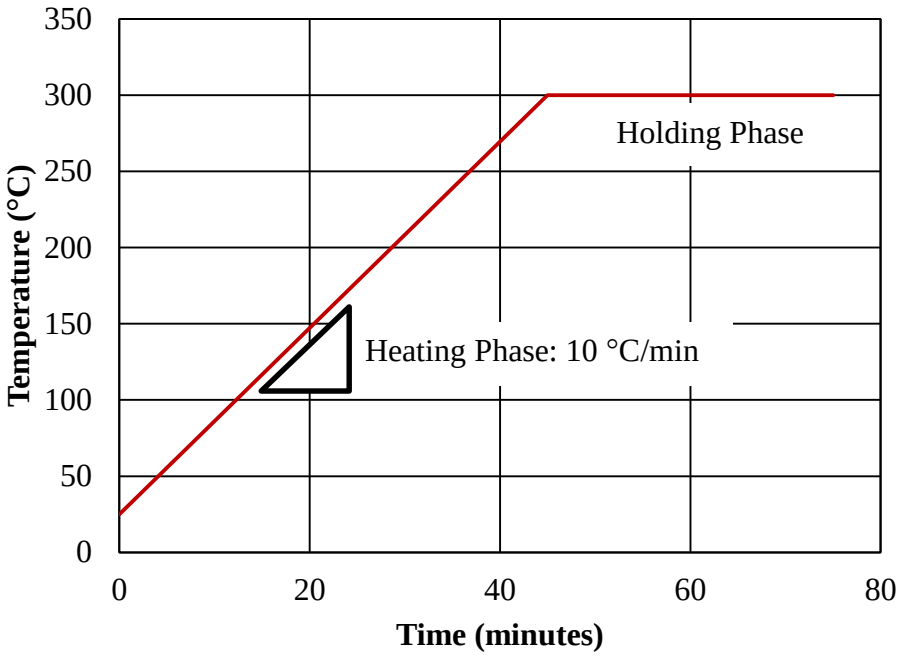

Figure 3.3: Typical heating profile for microwave torrefaction.

3.5. Injection Molding

The pelletized biocomposites were dried at 80 °C overnight in a convection oven prior to injection molding. A Technoplas, Inc. Model Sim-5080 injection molder was used for injection molding. The Technoplas molder has a single screw with four heating zones plus the injection nozzle. Temperatures for these zones from feeding zone to nozzle were: 271, 282, 293, 299, 304 °C for the PA66 used in this work. Geometries of the final specimens were dog bones and rectangular bars approximately 3.2 mm thick based on ASTM standards. For this work a single extrusion batch was used to produce all injection molded specimens therefore this work focused on the intra-analysis of mechanical properties. Further studies would be needed to understand the inter-comparison among multiple batches of composite material and reliability of mechanical performance.

3.6. Specimen Preparation

As stated in ASTM International testing standards the injection molded specimens were conditioned prior to mechanical testing. The specimens were placed in a Boekel dricycler for a minimum of 48 hours before testing was conducted. The specimens were then stored in the dricycler until all specimens were tested to ensure proper conditioned moisture content and temperature.

CHAPTER 4. EXPERIMENTAL PROCEDURES

The ultimate goal of this work is to produce homogeneous high degree torrefied biomass for utilization in engineering thermoplastic biocomposites by way of microwave heating. Three test matrices were used to determine the effectiveness of time, temperature, power level, particle size, and sample mass on the efficiency of microwave torrefaction. This chapter will look at how the torrefied biomass and their biocomposites were evaluated.

4.1. Characterization Methods for Torrefied Biomass

One of the biggest challenges with torrefaction is establishing the degree to which it has been torrefied without performing the torrefaction in a thermogravimetric analyzer. For wide acceptance of torrefied biomass filler in engineering thermoplastics large batches need to be produced with small samples taken for quality control. Part of this work was to establish a method for determining the degree of torrefaction beyond just mass retention.

4.1.1. Fourier Transform Infrared Spectroscopy

Fourier transform infrared spectroscopy (FTIR) was used to examine the changes in chemical bonding within the biomass. By analyzing both the untreated biomasses and the torrefied biomasses the FTIR spectra indicates how the torrefaction process has removed or changed various chemical bonds within the biomass, this will indicate on a qualitative basis what level of torrefaction is reached. A Nicolet 6700 FTIR spectrometer equipped with germanium crystal was used to scan each sample 32 times between wavelengths of 4000 and 650 cm^{-1}.

4.1.2. Thermogravimetric Analysis

Thermogravimetric analysis (TGA) was used to analyze the degradation of torrefied biomasses. The rate and temperatures at which the torrefied biomasses degrade indicates the extent of torrefaction or if low molecular weight polymers still remain within the filler. The TGA curve was also used to indicate the maximum processing temperature allowed before significant degradation of the filler begins. A TA Instruments Q500 TGA was used to analyze the torrefied biomass. A temperature ramp rate of 10 °C per minute from room temperature to 400 °C under an oxygen rich environment was used to simulate an environment much like that seen in traditional extrusion and injection molding processes. Three samples were tested for each of the untreated fibers and the large batched of torrefied biomass used in the composite production.

4.1.3. Scanning Electron Microscopy

Scanning electing microscopy (SEM) was used to analyze the surface quality of torrefied fibers and compare them to the untreated fibers. As the torrefaction converts low molecular weight constituents within the fibers to carbon and syngas pores begin to form on the fiber surface. A JEOL JSM-6940LV SEM with an accelerating voltage of 15kV was used to capture images of the fiber surfaces, which were coated in gold prior to analysis, to qualitatively compare fiber surface porosity. The SEM was also used to analyze elemental make up by energy dispersive x-ray spectroscopy (EDS). Based on the elements present in the fiber along with the constituent makeup a correlation was developed to determine degree of torrefaction which can be applied to any torrefied biomass.

4.1.4. Water Absorption and Desorption

Water sorption and desorption of untorrefied and torrefied fibers was measured using a Surface Measurement Systems Dynamic Vapor Sorption (DVS) Advantage instrument. Small samples of each fiber, approximately 10 mg, were placed in a temperature controlled chamber at 25 °C while a mixture of dry air and water vapor was introduced into the chamber to achieve a set relative humidity. The mass of each sample was monitored continuously, once the change in mass per minute fell below 0.005 mg/min the fiber and chamber were considered to be in equilibrium for the set relative humidity. Measurements were taken from 0% to 90% relative humidity in increments of 10% for the sorption curve and 90% to 0% relative humidity in increments of 10% for the desorption curve. The total sorption and desorption cycle was repeated twice for a single sample of each fiber type. All DVS testing was provided by the Composites Innovation Centre, Winnipeg, Manitoba, Canada.

4.2. Polyamide Biocomposite Characterization Methods

One of the goals for this study is to characterize the effects on thermo-mechanical properties of adding torrefied biomass to polyamide matrices. This section outlines the full mechanical and thermo-mechanical tests used for this characterization. Unless otherwise noted, all testing was conducted under laboratory standard temperature and humidity.

4.2.1. Elastic Modulus and Tensile Strength

Tensile modulus and strength were evaluated according to ASTM standard D638, standard test method for tensile properties of plastics. An Instron Model 5567 load frame equipped with a 30 kN load cell was used for all tensile testing. An MTS model 632.35B-200 extensometer was used to record strain during the first portion of the testing. Once the specimen

reached 15% elongation, the test was paused while the extensometer was removed. Testing then continued until failure occurred or the load peaked and necking began. For each grade of material, five specimens were tested at a cross head rate of 5 mm/min. Tensile modulus was calculated using the extensometer readings and tensile strength was recorded as the maximum stress achieved.

4.2.2. Flexural Modulus and Strength

Flexural modulus and strength were determined according to ASTM standard D790, standard test methods for flexural properties of unreinforced and reinforced plastics and electrical insulating materials. The Instron load frame described above was also used for all flexural testing. For each grade of material, five specimens were tested using 3.2 mm diameter loading and support pins. Flexural strength was recorded as the maximum stress achieved unless the strain at maximum stress was greater than 5%. If a specimen displayed more than 5% strain the flexural strength was recorded as the stress at 5% strain. Flexural modulus was calculated from extension readings.

4.2.3. Impact Toughness

ASTM standard D256, standard test methods for determining the Izod pendulum impact resistance of plastics, was used to evaluate the impact toughness of the biocomposites. A pendulum weight of 4.497 N was used, following procedure A. Each specimen was notched with a 2.54 mm notch prior to testing using a Veekay Testlab Veekay Notch Cutter. A total of six specimens were tested for each grade of material. Impact toughness was calculated using the energy absorbed by the specimen and the area at the notch region. In accordance with the ASTM

standard any specimen with a crack propagation less than 90% of the width of the specimen were considered a non-failure.

4.2.4. Immersion Density

The densities of the materials being studied were determined using a Mettler Toledo 33360 immersion density kit. All testing was conducted at room temperature in isopropyl alcohol to avoid any uptake of liquid during the testing. The density for each specimen (ρ) was calculated using the following equation:

$$\rho = \left(\frac{m_{dry}}{m_{dry} - m_{immersed}}\right) * \rho_{fluid}$$

where m_{dry} is the dry mass of the specimen prior to immersion, $m_{immersed}$ is the mass of the specimen when immersed in the fluid, and ρ_{fluid} is the density of the fluid. The value for ρ_{fluid} was taken from tabulated densities of 100% pure isopropyl alcohol at various temperatures. Six specimens were used to determine the density of each grade of material.

4.2.5. Moisture Uptake

An Arizona Instruments Computrac 4000XL Moisture Analyzer was used to determine the moisture uptake of the materials. Specimens were soaked in distilled water for 24, 72, and 168 hour intervals. Adsorbed moisture was removed by towel drying the specimens prior to analysis. Each specimen was heated to 210 °C and while maintaining this temperature, mass loss was recorded. Once the mass loss slowed to 0.015% moisture/minute, the analysis was complete and the total mass loss measured was recorded as the total moisture absorbed. A total of three specimens were analyzed for each material grade at each soak length. To reduce the error from retesting specimens, a new specimen was used for each test.

4.2.6. Dynamic Mechanical Analysis

A TA Instruments Q-800 Dynamic Mechanical Analyzer (DMA) was used to determine the glass transition temperature of the materials. These tests were conducted according to ASTM standard D7028, standard test method for glass transition temperature of polymer matrix composites by dynamic mechanical analysis. Using a dual cantilever fixture, specimens were subjected to an amplitude of 20 µm at a frequency of 20 Hz while the temperature was raised at 3 °C/min up to 200 °C. The glass transition temperature was recorded as the temperature at the peak of the tangent delta curve. Storage modulus was also studied. Figure 4.1 shows an example curve used to determine the glass transition temperature and storage modulus. A total of four specimens were tested for each material grade.

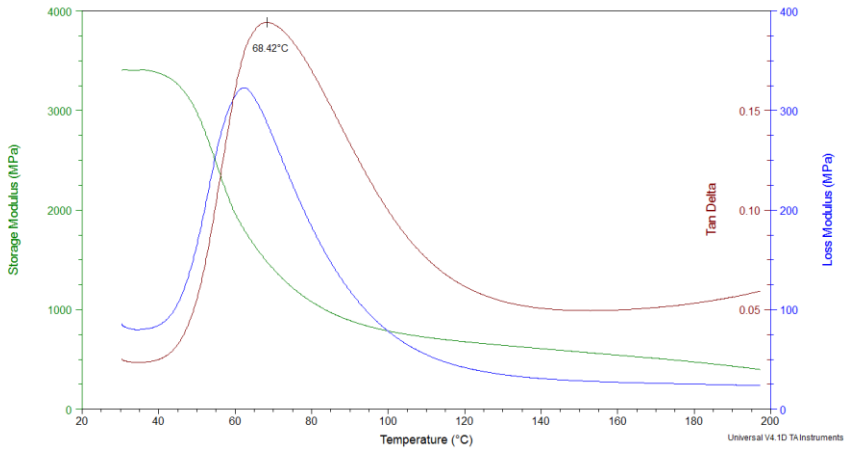

Figure 4.1: Example of a graph used to determine glass transition temperature.

4.2.7. Heat Deflection Temperature

A modified ASTM standard D648, standard test method for deflection temperature of plastics under flexural load in the edgewise position, was used to determine the heat deflection temperature of the materials. The ASTM standard was modified to use the TA Q-800 DMA with a three-point bending fixture installed. Specimens were subjected to a constant stress of 1.82

MPa while the temperature was increased at 3 °C/min up to 200 °C. Due to the limited specimen size using the DMA, the specified deflection in D648 was converted to a strain based on the standard dimensions. This strain of 0.121 % was then used to determine at what deflection in the smaller DMA samples the standard strain was achieved. The temperature at which the determined deflection occurred was taken as the heat deflection temperature. A total of four specimens were tested for each material grade.

4.2.8. Coefficient of Linear Thermal Expansion

ASTM standard E831, standard test method for linear thermal expansion of solid materials by thermomechanical analysis, was used as a guide to determine the linear thermal expansion of the materials. Using the above described DMA equipped with a film/fiber tension fixture, specimens were heated at 3 °C/min up to 200 °C. Using a strain versus temperature plot the slope of the linear region prior to the glass transition temperature is recorded as the coefficient of linear thermal expansion. Figure 4.2 shows an example of the strain versus temperature graph. A total of four specimens were tested for each material grade.

4.2.9. Differential Scanning Calorimetry

A TA Instruments Q1000 Differential Scanning Calorimeter (DSC) was used to determine the percent crystallinity of the materials. The melting and crystallization temperatures were also determined through DSC testing. Three samples of each material grade were tested during DSC analysis. The DSC analysis consisted of a heating portion where the temperature with in the DSC chamber was raised at 5 °C/minute up to 300 °C and a cooling portion where the chamber was cooled at 5 °C/minute down to 25 °C. Aluminum hermetic pans were used for all DSC testing. Figure 4.3 shows an example graph used in determinging the percent crystallinity,

melting temperature, and crystallization temperature. A standard heat of 255.8 J/g and a sigmoidal horizontal baseline were used in the calculation of percent crystallinity. The melting temperature was taken as the peak of the endothermic spike. The crystallization temperature was taken as the peak of the exothermic peak. Glass transition temperature was taken as the inflection point of the heating curve between room temperature and the crystallization temperature. Genreally while analyzing the crystalization of a composite, the weight of the filler is removed from the mass of the sample because it has no effect on the heat flow. As torrefied biomass can still under go some conversion within the temperature range of DSC analysis, each of the torrefied biomasses were also analyzed to determine their effect on the biocompoiste curves. Figure 4.4 shows the cooling curves for each of the torrefied biomasses. This figure shows that in the range of crystallization, 225 - 240 °C, the fibers are endothermic which indicates they do have an effect on the heat flow of the biocomposites. Therefore, all biocomposite DSC analysis the weight of the fiber has been included in the smaple mass.

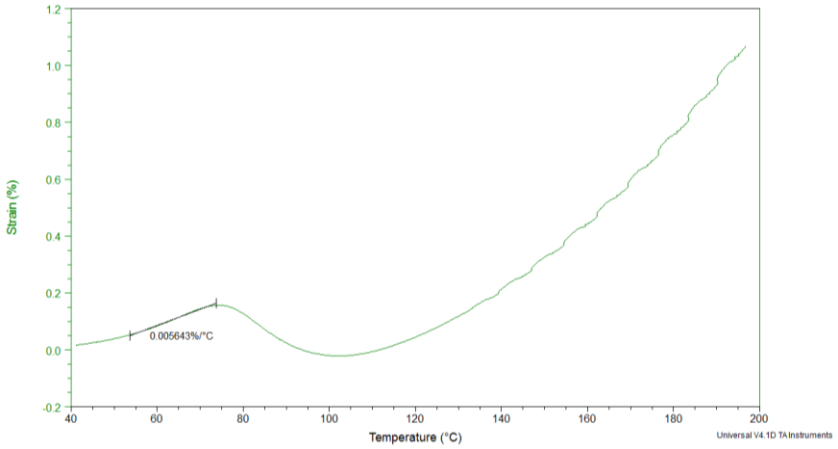

Figure 4.2: Example of a graph used to determine coefficient of linear thermal expansion.

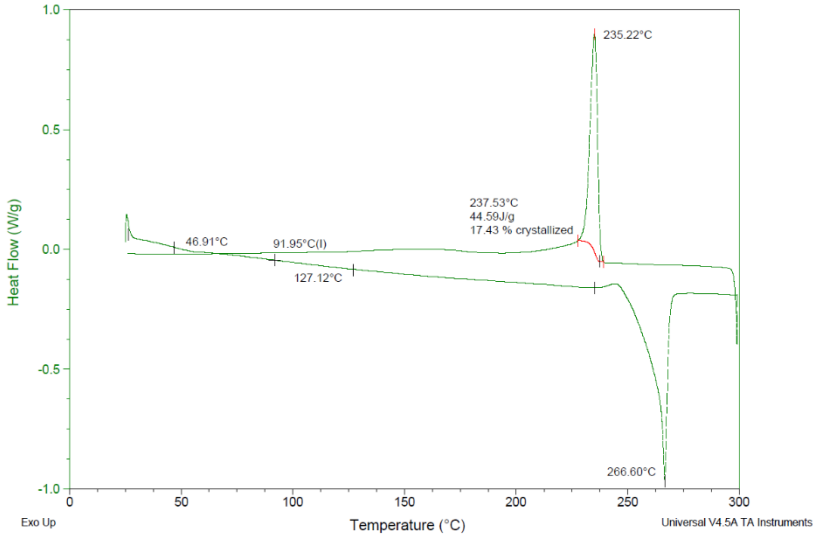

Figure 4.3: Example of a graph used to determine percent crystallinity, melting temperature, glass transition temperature, and crystallization temperature.

4.2.10. Melt Flow Index

According to ASTM standard D1238, standard test method for melt flow rates of thermoplastics by extrusion plastometer, melt flow index (MFI) was measured for the materials. A Tinius Olsen Model MP600 melt flow indexer with a 225 g mass was used for this testing. Procedure A with a travel distance of 2.25 cm and a set temperature of 270 °C was used to capture the MFI. For each grade of material three samples were measured.

4.2.11. Microscopy

Optical microscopy was used to analyze the void content of the molded specimens. Small specimens of the material were cast in vinyl ester resin and polished with sandpaper prior to microscopy. Images captured with a Zeiss Axiovert 40 MAT microscope equipped with a ProgRes C10 camera were used to evaluate void content.

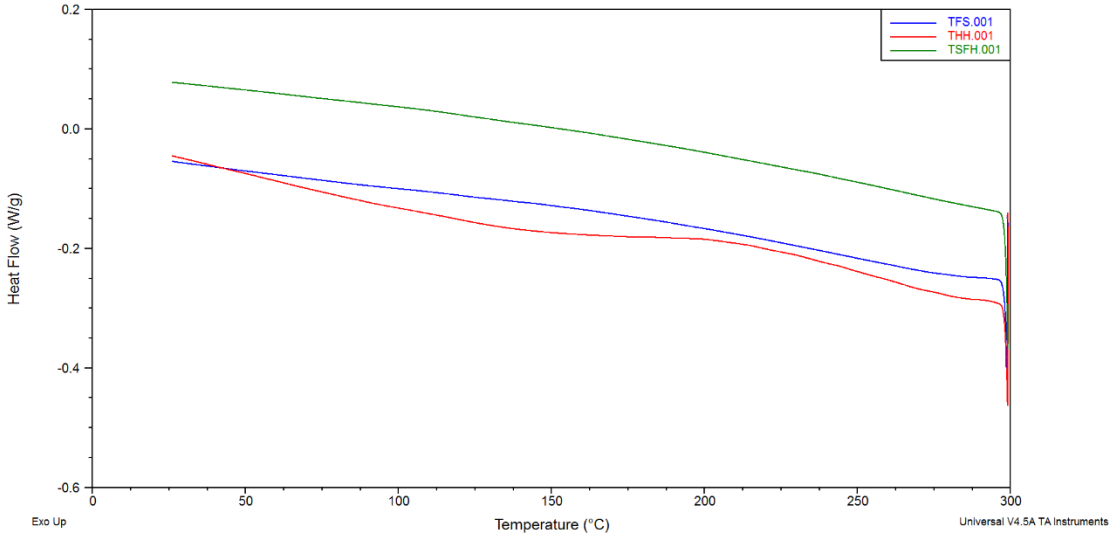

Figure 4.4: Differential scanning calorimetry cooling curves of torrefied biomass.

CHAPTER 5. RESULTS AND DISCUSSION

5.1. Analysis of Torrefied Biomass

To determine the ideal torrefaction conditions for the Milestone Pyro Ashing System used in this work three test matrices, consisting of 27 different torrefaction runs, as described earlier were studied. In the following section various parameters are analyzed to determine how they affect the outcomes of torrefaction. The remaining sections then look at the full characterization of TFS, TSFH, and THH.

5.1.1. Analysis of Variance

A standard two-factor ANOVA analysis was used to test the null hypothesis that mean yields of torrefaction, 90% stability temperatures, or the mass lost per degree raised were equal when factors such as particle size, sample mass, temperature, power level, and time were varied. Table 5.1 depicts a typical two-factor full factorial design. In this table a represents the number of levels for factor A, b represents the number of levels for factor B, and n represents the number of data points collected in each cell of the design. Also in the table $y_{i..}$ represents the sum of data points at the i^{th} level of factor A, $y_{.j.}$ represents the sum of the observations at the j^{th} level of factor B, $y_{ij.}$ represents the sum of all the observations in the ij^{th} cell of the design, and $y_{...}$ denotes the sum of all observations in the experimental design. These sums are then used to determine the sums of squares, mean square errors and the test statistics (F_0) for each of the factors and their interaction as seen in Table 5.2. Where:

$$y_{i..} = \sum_{j=1}^{b}\sum_{k=1}^{n} y_{ijk} \quad i = 1, 2, \dots, a$$

$$y_{\cdot j\cdot} = \sum_{i=1}^{a}\sum_{k=1}^{n} y_{ijk} \quad j = 1, 2, \dots, b$$

$$y_{ij\cdot} = \sum_{k=1}^{n} y_{ijk} \quad i = 1, 2, \dots, a;\ j = 1, 2, \dots, b$$

$$y_{\dots} = \sum_{i=1}^{a}\sum_{j=1}^{b}\sum_{k=1}^{n} y_{ijk}$$

$$SS_A = \frac{1}{bn}\sum_{i=1}^{a} y_{i\cdot\cdot}^2 - \frac{y_{\dots}^2}{abn}$$

$$SS_B = \frac{1}{an}\sum_{j=1}^{b} y_{\cdot j\cdot}^2 - \frac{y_{\dots}^2}{abn}$$

$$SS_{AB} = \frac{1}{n}\sum_{i=1}^{a}\sum_{j=1}^{b} y_{ij\cdot}^2 - \frac{y_{\dots}^2}{abn} - SS_A - SS_B$$

$$SS_E = SS_T - SS_A - SS_B - SS_{AB}$$

$$SS_T = \sum_{i=1}^{a}\sum_{j=1}^{b}\sum_{k=1}^{n} y_{ijk}^2 - \frac{y_{\dots}^2}{abn}$$

To determine if the source of variation has an impact on the

Table 5.1: General Two-Factor Full Factorial Experimental Design

		Factor B			
		1	2	…	b
Factor A	1	$y_{111}, y_{112}, \dots, y_{11n}$	$y_{121}, y_{122}, \dots, y_{12n}$		$y_{1b1}, y_{1b2}, \dots, y_{1bn}$
	2	$y_{211}, y_{212}, \dots, y_{21n}$	$y_{221}, y_{222}, \dots, y_{22n}$		$y_{2b1}, y_{2b2}, \dots, y_{2bn}$
	⋮				
	a	$y_{a11}, y_{a12}, \dots, y_{a1n}$	$y_{a21}, y_{a22}, \dots, y_{a2n}$		$y_{ab1}, y_{ab2}, \dots, y_{abn}$

For this work only one replicate of each experimental cell was conducted, thus n = 1. A significance level of 0.05 was used in determining the significance of effects from the factors and their interactions. If F_0 for any source of variation was greater than F_{α,v_1,v_2}, where α is the

significance level, υ_1 is the degrees of freedom for the numerator of F_0, and υ_2 is the degrees of freedom for the denominator of F_0 the source of variation was concluded to have an impact on the average yield of torrefaction [40].

Table 5.2: Two-Factor ANOVA Analysis

Source of Variation	Sum of Squares	Degrees of Freedom	Mean Squares	F_0
Factor A	SS_A	$a-1$	$MS_A = \frac{SS_A}{a-1}$	$F_0 = \frac{MS_A}{MS_E}$
Factor B	SS_B	$b-1$	$MS_B = \frac{SS_B}{b-1}$	$F_0 = \frac{MS_B}{MS_E}$
Error	SS_E	$ab(n-1)$	$MS_E = \frac{SS_E}{ab(n-1)}$	
Total	SS_T	$abn-1$		

The first test matrix studied for this work focused on the effects of particle size and sample mass on the mean yield and 90% stability temperature of TFS. Table 5.3 shows the ANOVA analysis for the effects of particle size and sample mass on the torrefaction yield. From the table it can be seen that F_0 for both the particle size effect and sample mass effect is lower than the F values proving the null hypothesis true; mean torrefaction yields are equal with varying particles sizes and sample masses. Table 5.4 shows the ANOVA analysis for the effects of particle size and sample mass on the 90% stability temperature of the TFS. This table again shows that both F_0 values are below the F factors proving the null hypothesis true; 90% stability temperatures are equal with varying particles sizes and sample masses. With both factors proving to have no effect on yield or stability temperature of the TFS, as-received fiber was used for the remainder of this work to avoided any added costs from fiber grinding and the largest possible sample mass of 50 g was used in all remaining torrefaction runs for efficient use of time.

The second test matrix studied in this work looked at the effects of torrefaction time and microwave power output on the yield, 90% stability temperature, and mass lost per degree raised of TFS. Table 5.5 shows the ANOVA analysis for the effects of torrefaction time and microwave

power on the torrefaction yield of TFS. It can be seen from the table that both factors have higher F_0 values than F factors, proving the null hypothesis false. Torrefaction time and microwave power have an effect on the torrefaction yield. Table 5.6 shows the ANOVA analysis for the effects of torrefaction time and microwave power on the 90% stability temperature of TFS. Again this table shows that both factors have higher F_0 values than F factors, proving the null hypothesis false. Both factors have an effect on the 90% stability temperature of TFS. For this test matrix the microwave was allowed to heat freely for a given length of time at each power level, it is more useful to look at the amount of mass lost per degree raised to fully understand how time and power level effect torrefaction outcomes. Table 5.7 shows the ANOVA analysis for amount of mass lost per degree raised. From this table it can be seen that time and power level have lower F_0 values than F factors, thus neither time or power level have an effect on mass lost per degree raised. Since power level does not have an effect on the amount of mass lost per degree raised, a heating rate of 10 °C/minute was targeted for the remainder of this work. Table 5.8 shows the heating rates measured at various microwave power outputs, to achieve the 10 °C/minute target, a power setting of 500 W was chosen for the remainder of this work.

Table 5.3: Two-Factor ANOVA Analysis of Yield versus Particle Size and Mass

Source of Variation	Sum of Squares	Degrees of Freedom	Mean Squares	F_0	F
Particle Size	1.293	2	0.647	1.59	19.00
Mass	0.807	1	0.807	1.98	18.51
Error	0.813	2	0.407		
Total	2.913	5			

Table 5.4: Two-Factor ANOVA Analysis of Stability Temperature versus Particle Size and Mass

Source of Variation	Sum of Squares	Degrees of Freedom	Mean Squares	F_0	F
Particle Size	426.733	2	213.366	2.03	19.00
Mass	0.522	1	0.522	0.00	18.51
Error	210.462	2	105.231		
Total	637.717	5			

Table 5.5: Two-Factor ANOVA Analysis of Yield versus Time and Power

Source of Variation	Sum of Squares	Degrees of Freedom	Mean Squares	F_0	F
Time	2077.52	2	1038.76	10.02	5.14
Power	2535.95	2	845.32	8.15	4.76
Error	622.05	5	103.68		
Total	5235.52	11			

Table 5.6: Two-Factor ANOVA Analysis of Stability Temperature versus Time and Power

Source of Variation	Sum of Squares	Degrees of Freedom	Mean Squares	F_0	F
Time	3254.53	2	1627.27	14.23	5.14
Power	3873.51	2	1291.17	11.29	4.76
Error	686.22	5	114.37		
Total	7814.26	11			

Table 5.7: Two-Factor ANOVA Analysis of % Mass Lost/°C versus Time and Power

Source of Variation	Sum of Squares	Degrees of Freedom	Mean Squares	F_0	F
Time	13.786	2	6.893	3.14	5.14
Power	7.142	3	2.381	1.08	4.76
Error	13.180	6	2.197		
Total	34.107	11			

The final test matrix studied in this work was to determine the most effective time and temperature for torrefaction. Table 5.9 shows the ANOVA analysis for the effects of torrefaction hold time and torrefaction temperature on the torrefaction yield of TFS. From this table it can be seen that both torrefaction hold time and temperature have larger F_0 values than F factors; thus the null hypothesis is false both factors have an effect on the torrefaction yield. Table 5.10 shows the ANOVA analysis for the effects of torrefaction hold time and torrefaction temperature on the 90% stability temperature of TFS. This table again shows that hold time has no effect on stability temperature while torrefaction temperature does. Based on both ANOVA analyses a goal of a stability temperature of at least 280 °C a hold time of 30 minutes with a torrefaction temperature of 400 °C was chosen as the ideal torrefaction conditions for the microwave used in this work.

Based on the results of all three test matrices and their respective ANOVA analyses the ideal torrefaction conditions for the Milestone Pyro Ashing System used for this work were set.

For the production of biocomposites filled with TFS, THH, and TSFH as-received fiber was torrefied in 50 g batches at 400 °C with a hold time of 30 minutes using a microwave power output of 500 W. All torrefaction yields, 90% stability temperatures, and mass lost per degree raised for the three test matrices discussed can be found in the appendix.

Table 5.8: Heating Rates for Various Microwave Power Levels

Power Output (W)	Start Temp (°C)	Stop Temp (°C)	Time (min)	Heating Rate (°C/min)
200	35	300	132.000	2.008
400	24	300	45.083	6.122
600	40	300	21.850	11.899
800	40	300	16.833	15.446
1000	24	300	15.583	17.711
1200	22	300	13.750	20.218

Table 5.9: Two-Factor ANOVA Analysis of Yield versus Time and Temperature

Source of Variation	Sum of Squares	Degrees of Freedom	Mean Squares	F_0	F
Time	26.462	2	13.231	7.12	6.94
Temperature	242.249	2	121.124	65.20	6.94
Error	7.431	4	1.858		
Total	276.142	8			

Table 5.10: Two-Factor ANOVA Analysis of Stability Temperature versus Time and Temperature

Source of Variation	Sum of Squares	Degrees of Freedom	Mean Squares	F_0	F
Time	574.34	2	287.17	2.80	6.94
Temperature	3121.35	2	1560.68	15.23	6.94
Error	409.91	4	102.48		
Total	4105.61	8			

5.1.2. Fourier Transform Infrared Spectroscopy

FTIR analysis was used in this work to provide a qualitative comparison of the differences in chemical bonds present in untreated and torrefied biomass. Figure 5.1 shows the individual spectra for flax shive (FS) and TFS, Figure 5.2 shows the spectra for hemp hurd (HH) and THH, and Figure 5.3 shows the spectra for sunflower hulls (SFH) and TSFH. All three biomasses contain the same individual constituents in varying quantities. The varying quantities

appear through FTIR spectra in differing peak intensities. With the goal of torrefaction being the conversion of low weight constituents, the FTIR spectra of torrefied biomass will show the loss or weakening of intensities corresponding to these constituents. As was discussed before the majority of the conversion process comes from the breakdown of cellulose, hemicellulose, and lignin, which is the focus of the FTIR spectra analysis.

Each of the untorrefied spectra display common peaks all seen within the spectra of the individual constituents. The broad peaks seen in the spectra of untreated biomass around 3,300 cm^{-1} correspond to the O-H stretching of acids and methanol. This OH stretching band coupled with a peak near 1700 cm^{-1}, the C=O stretching band, indicates the presence of carboxylic acids. The medium peak seen between 2900 cm^{-1} and 2700 cm^{-1} indicates the $O\text{-}H_n$ stretching of aliphatic or aromatic alkyls. The medium peaks between around 1632 cm^{-1} is associated with C=C stretching within benzene rings. A pair of weak peaks seen at 1613 cm^{-1} and 1450 cm^{-1} also comes from the stretching of C=C bonds; these peaks are indicative of skeletal stretching of aromatic rings. Between 1510 cm^{-1} and 1560 cm^{-1} a medium intensity peak shows the C=O stretching with in ketones and carbonyl groups. Medium peaks between 1470 cm^{-1} and 1430 cm^{-1} indicates the bending of $O\text{-}CH_3$ within aromatic methyl groups. The bending of O-H from acids appears as a strong peak between 1440 cm^{-1} and 1400 cm^{-1}. Stretching of the C-O-C bonds appears as a strong peak between 1300 cm^{-1} and 1000 cm^{-1} from the presence of ethers. Strong peaks near 1215 cm^{-1} come from the stretching of C-O bonds within phenols. The strong peaks at 1170 cm^{-1} correspond to the stretching vibration of the C-O-C bonds within the pyranose rings. The medium peaks found between 900 cm^{-1} to 700 cm^{-1} is due to the out of plane bending of aromatic C-H [41–43].

Figure 5.4 shows the 1:1 subtraction of untreated spectra from the torrefied spectra to show the changes in chemical structure due to torrefaction. Between 3300 cm^{-1} and 1750 cm^{-1} torrefaction removed most of the peaks. This indicates the conversion of acids, methanol, and aliphatic or aromatic alkyls. The peaks seen around 2300 cm^{-1} are the fingerprint of the germanium crystal used during FTIR and are thus insignificant in this work. The increased intensities near 1632 cm^{-1}, 1613 cm^{-1}, and 1450 cm^{-1} indicate the increased number of C=C bonds due to torrefaction, an expected outcome of a carbonization process. The small increases in peak intensities between 1560 cm^{-1} and 1170 cm^{-1} due to torrefaction stems more from the higher concentration of the given bonds from the breaking or conversion of other chemical bonds within the feedstock. The largest change seen from torrefaction is the decreased peak intensity between 1300 cm^{-1} and 650 cm^{-1} indicating the breaking of C-O, C-O-C, and C-H bonds.

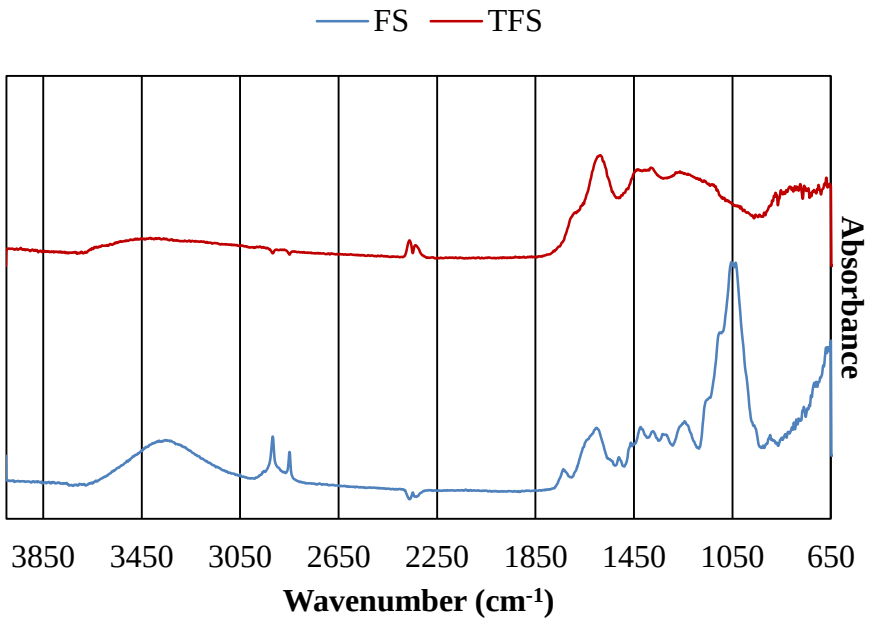

Figure 5.1: FTIR spectrum for untorrefied flax shive and torrefied flax shive.

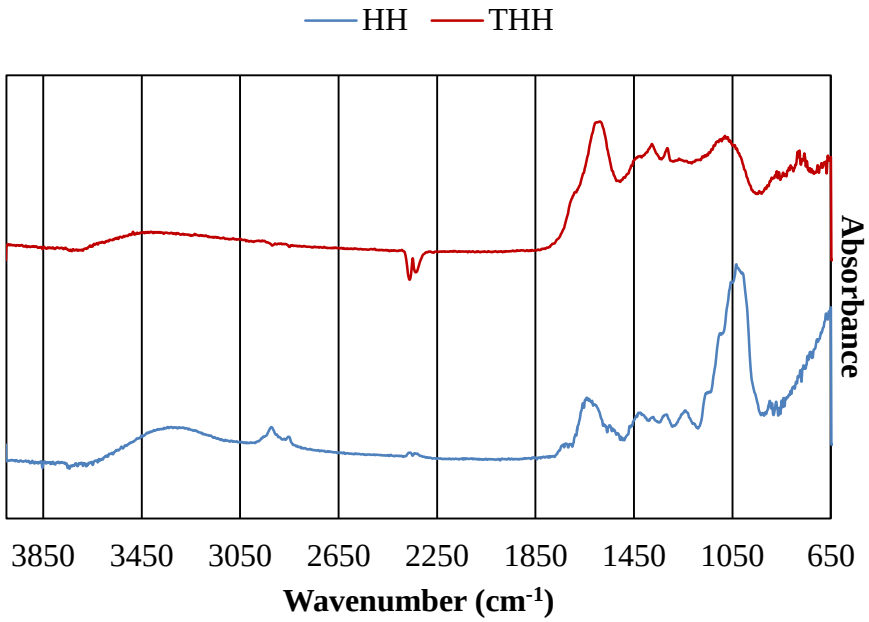

Figure 5.2: FTIR spectrum for untorrefied hemp hurd and torrefied hemp hurd.

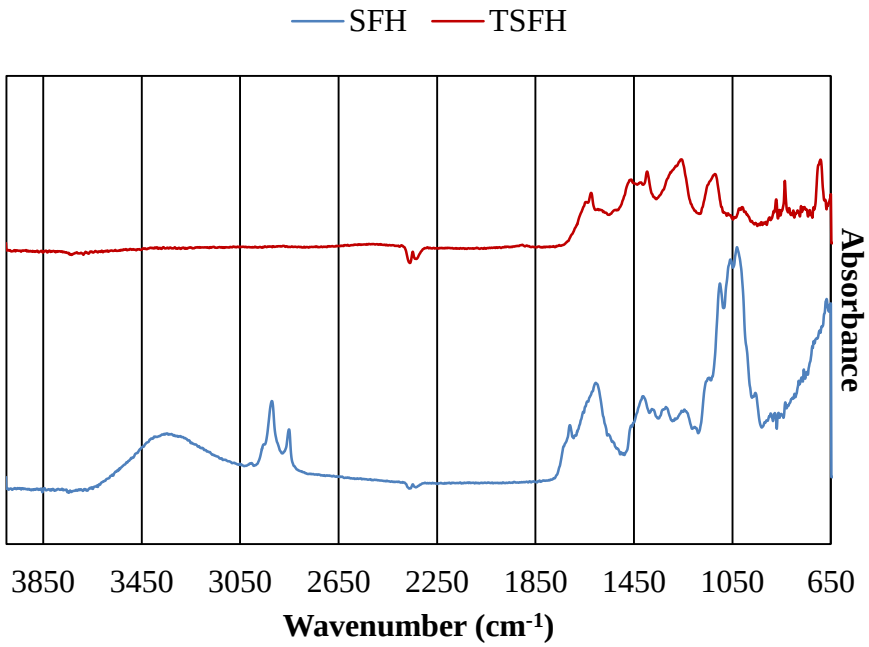

Figure 5.3: FTIR spectrum for untorrefied sunflower hull and torrefied sunflower hull.

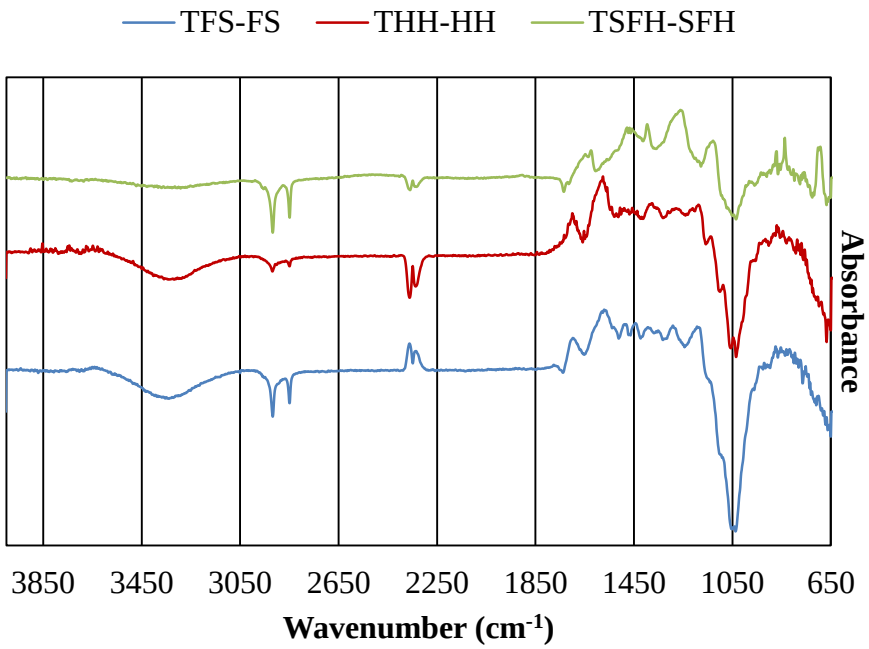

Figure 5.4: FTIR spectrum differences by subtraction of untorrefied biomass spectrum from the torrefied biomass spectrum.

The large change in peak intensities centered around 1050 cm^{-1} indicates there is little to no undecomposed cellulose, hemicellulose, or lignin left within the torrefied biomass. With little to no intact cellulose or lignin left, the torrefied biomass is approaching the chemical composition of carbon black, meaning the torrefaction has been taken beyond the intended outcomes for this work. In the discussion of Figure 1.5 it was stated that the goal for this work was to produce transition char containing some intact cellulose and lignin. Given the results of the FTIR analysis it is likely that the torrefaction in this work has produced late stage transition or amorphous char containing mostly pyrogenic amorphous carbon [21].

5.1.3. Thermogravimetric Analysis

By analyzing the changes in mass of a sample with respect to temperature through TGA the conversion of individual constituents within biomass can are observed. Figure 5.5 shows the TGA curves for FS and TFS, Figure 5.6 shows the curves for HH and THH, and Figure 5.7

shows the curves for SFH and TSFH. The various phases of torrefaction are exhibited within the first derivative of mass curves of the untreated biomass. The small peaks in mass loss between room temperature and 170 °C is due to fiber drying. The increase in mass loss beginning around 200 °C is associated with the conversion of hemicellulose, this conversion peaks near 270 °C. Cellulose conversion is associated with the increased mass loss around 350 °C to 370 °C. The continued mass lass above 370 °C is associated with the continued conversion of cellulose along with the conversion of lignin. Based upon the phases of torrefaction the TGA curves of TFS, THH, and TSFH indicate that small amounts of lignin and cellulose may still exist within the torrefied biomass. This points to the production of very late stage transition char bordering on the amorphous char discussed earlier.

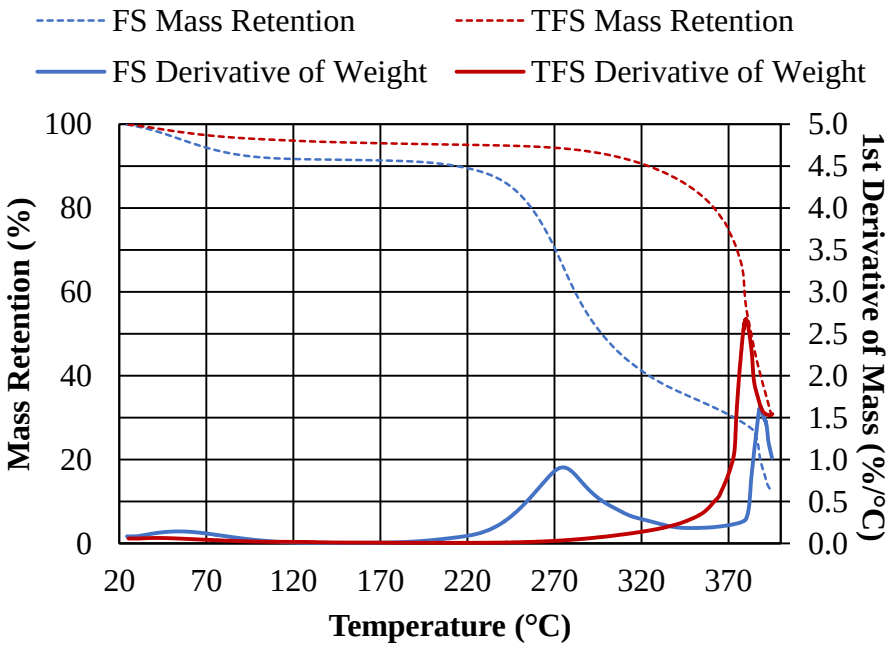

Figure 5.5: TGA curves from untorrefied and torrefied flax shive.

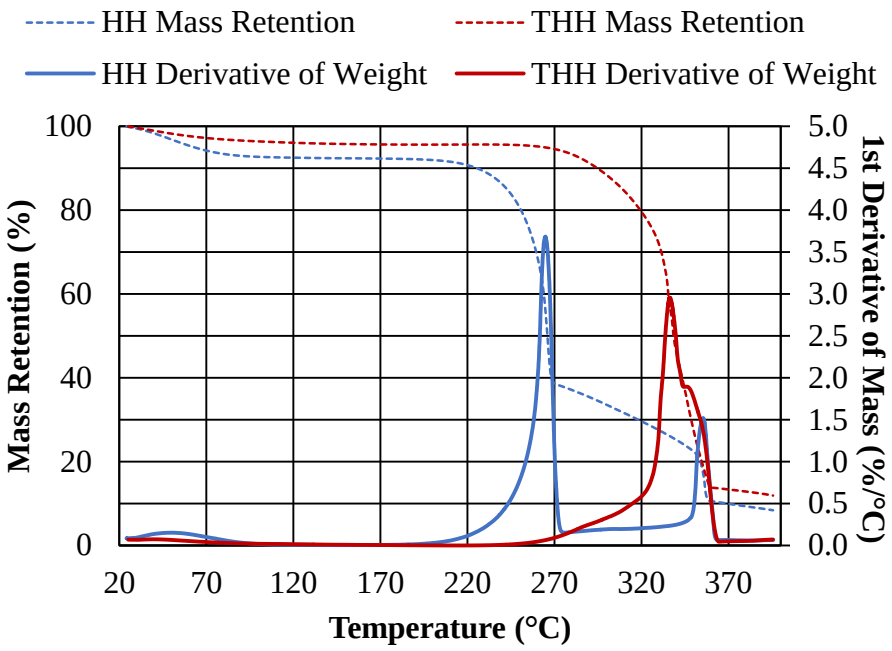

Figure 5.6: TGA curves from untorrefied and torrefied hemp hurd.

One of the advantages to the torrefaction process is the increased thermal stability of biomass. With the goal of viable high temperature biocomposites in mind it is important to understand how thermally stable the torrefied biomass is. Figure 5.8 shows the 90% stability temperature for the torrefied and untorrefied biomasses. All three torrefied biomasses clearly show an increased thermal stability over the untorrefied biomass. Prior to torrefaction FS, HH, and SFH displayed very similar stability temperatures near 220 °C. After torrefaction TFS displayed the highest stability temperature at 325 °C, followed by TSFH at 318 °C, and THH at 296 °C. In order for a viable polyamide biocomposite to be produced a target stability temperature of 280 °C was set, all three torrefied biomass fulfilled that requirement.

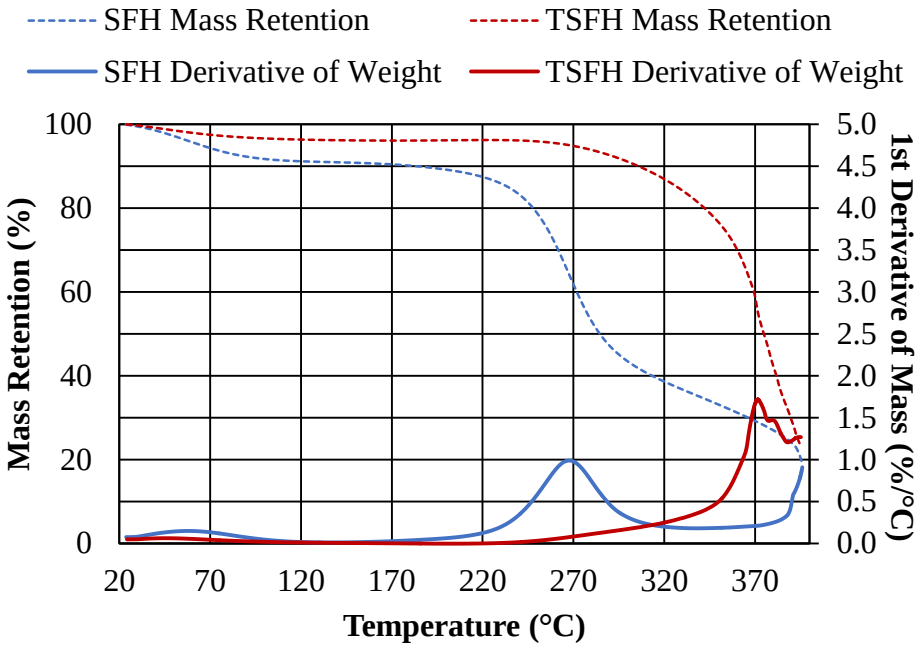

Figure 5.7: TGA curves from untorrefied and torrefied sunflower hulls.

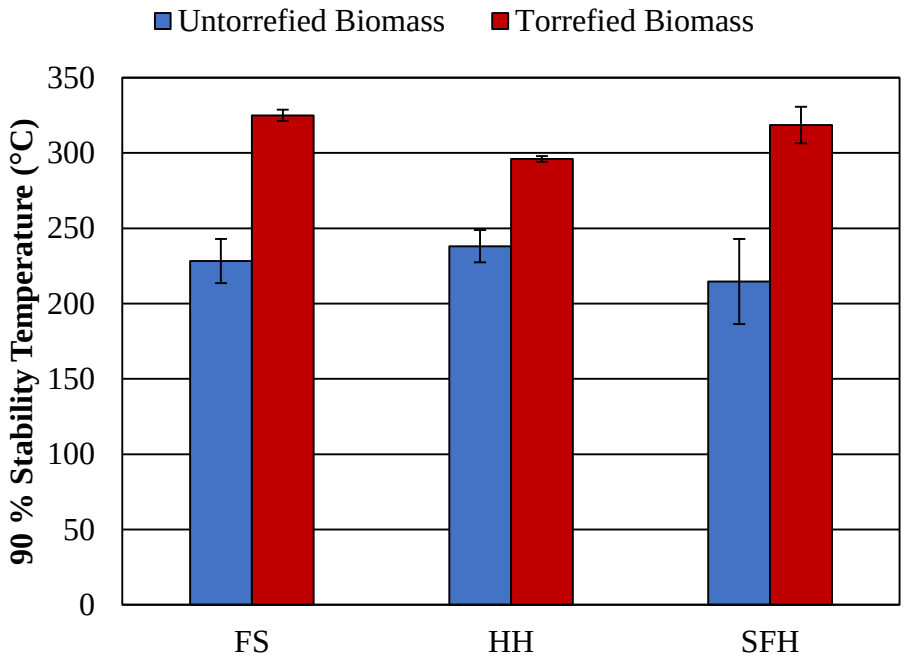

Figure 5.8: 90% mass retention stability temperatures for untorrefied and torrefied biomass.

5.1.4. Scanning Electron Microscopy

The physical appearance of torrefied biomass can also indicate the extent of torrefaction. For this work SEM was used to analyze the fiber surfaces of torrefied and untorrefied biomass. Figure 5.9, Figure 5.10, and Figure 5.11 show the SEM images for FS, HH, and SFH feedstock respectively. The top row of each image shows the SEM images of untreated fiber, the bottom rows all show the images of torrefied fiber. The SEM images of untorrefied biomass for the most part all show intact clean surfaces with one exception; in Figure 5.10 small microbial bodies can be seen on the surface of HH. The SEM images of the torrefied biomass all display at first what appears to be very dirty surfaces; however a closer look reveals clean surfaces full of pores. The torrefied surfaces are so clean the structure of the plant cells is visible. Again according to Figure 1.5 late transition char and amorphous char both contain increasing amounts of pore space; the presence of pores on the torrefied biomass surfaces further points to a product falling on the line of transition and amorphous char.

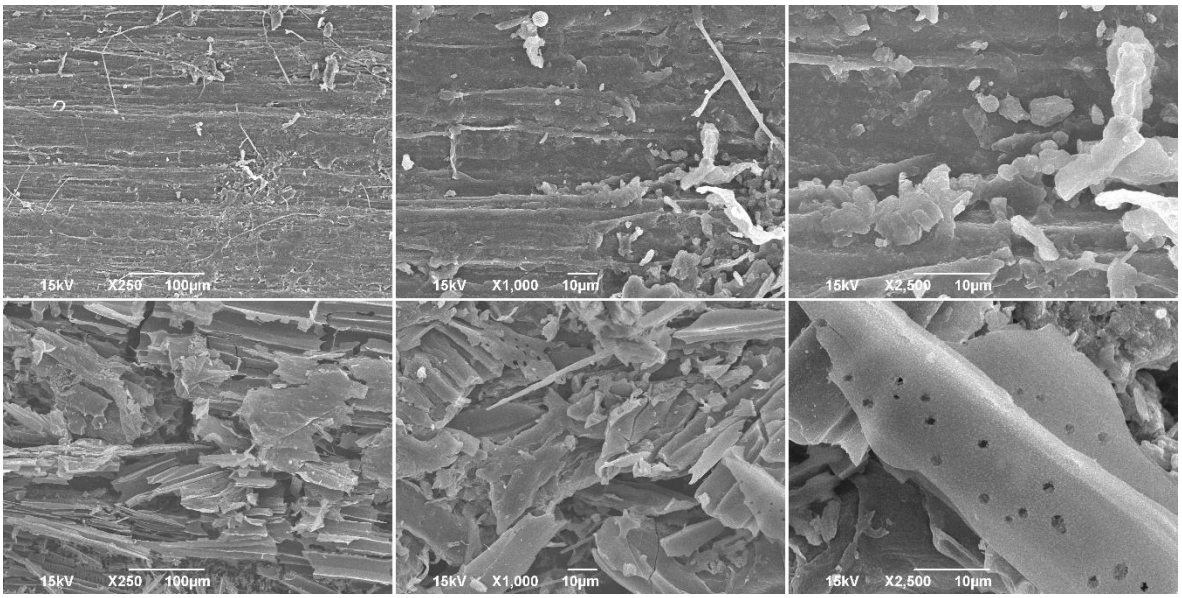

Figure 5.9: SEM images of untorrefied (top row) and torrefied flax shive (bottom row).

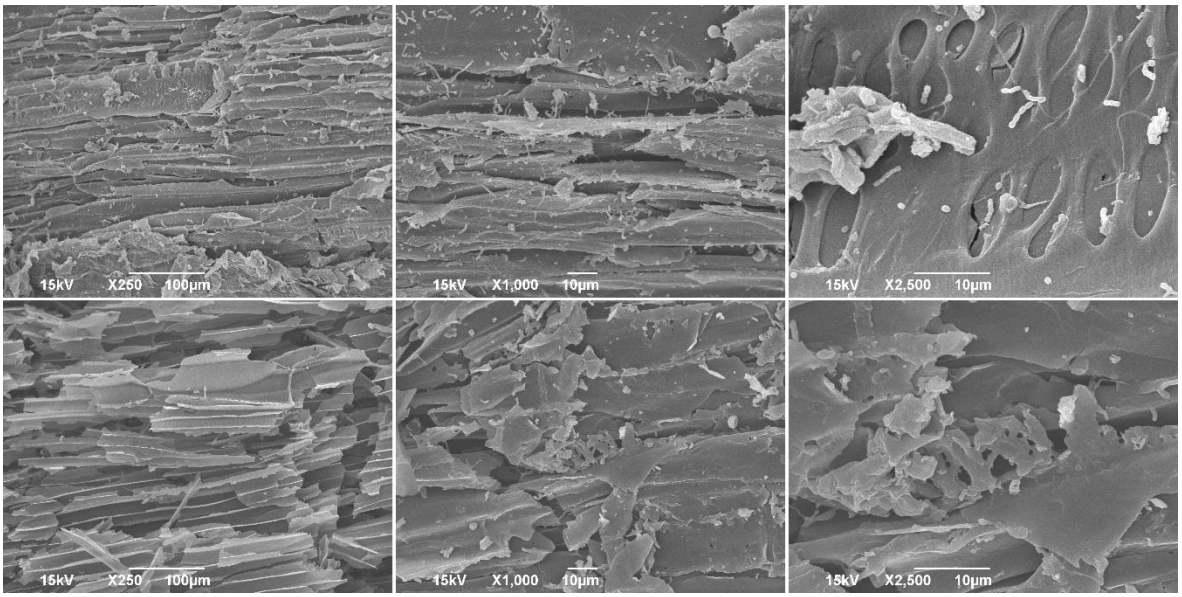

Figure 5.10: SEM images of untorrefied (top row) and torrefied (bottom row) hemp hurd.

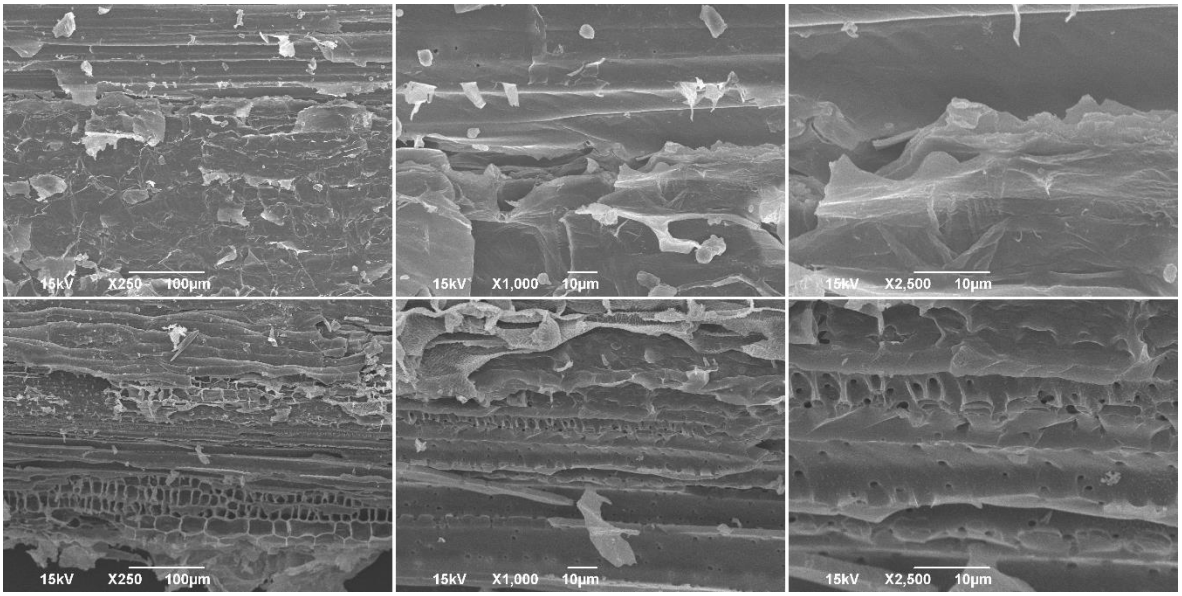

Figure 5.11: SEM images of untorrefied (top row) and torrefied (bottom row) sunflower hulls.

5.1.5. Energy Dispersive X-Ray Spectroscopy

Elemental analysis through EDS provides one more indicator of to what extent the torrefaction of biomass has reached. Figure 5.12 shows the carbon and oxygen content of torrefied and untorrefied biomass along with the carbon to oxygen ratio. Prior to torrefaction the carbon to oxygen ratio of FS is 1.86 after torrefaction this ratio more than doubles to 4.16. For

HH the carbon to oxygen ratio nearly doubles with torrefaction from 2.54 to 4.39. The carbon to oxygen ration increases the most for SFH nearly tripling from 1.95 to 5.73. The increased carbon content and carbon to oxygen ratio is indicative of a carbonization process that has significantly converted plant matter constituents. All of the fiber analysis combined in this work point to the production of very late transition char, and for the goal of producing viable biocomposites this means the torrefaction has gone too far. Having over-torrefied biomass will impact the mechanical properties of the biocomposites negatively; this is discussed in subsequent sections.

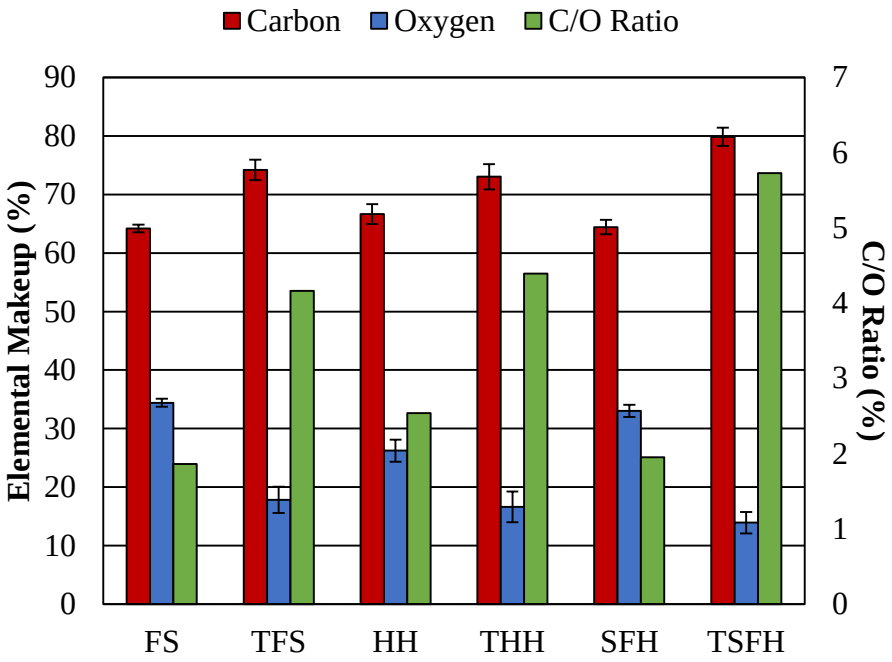

Figure 5.12: Carbon and oxygen make up of untorrefied and torrefied biomass from EDS.

5.1.6. Water Absorption and Desorption

Another advantage to torrefied biomass is its increased hydrophobicity. In the application of biocomposites this means the ability to decrease the moisture uptake of the biocomposite compared to the unfilled polymer. One focus of this work was the ability to measure the increased hydrophobicity of the torrefied fibers. The first method used to measure the moisture

uptake of fibers allowed samples of fiber to soak in distilled water for given periods of time. The fiber was then allowed to air dry for one hour to remove any adsorbed moisture before analysis in the moisture analyzer described in section 4.2.5. This method proved unreliable with results exhibiting a random pattern. This led to the use of a DVS system to measure the moisture sorption and desorption.

Figure 5.13 shows the two DVS sorption and desorption curves for FS and TFS. From this graph it can be seen that TFS absorbs 45% less moisture than FS at 90% relative humidity. Figure 5.14 shows the sorption and desorption cycles for HH and THH. This graph shows that THH absorbs 31% less moisture than HH at 90% relative humidity. Figure 5.15 shows the sorption and desorption curves for SFH and TSFH. This graph shows that TSFH absorb 50% less moisture than SFH at 90% relative humidity. For all three fiber feedstocks the graphs show that at all relative humidity levels the torrefied biomass absorbs less moisture than the untreated fiber. The increased hydrophobicity of torrefied biomass stems from the breakdown of low energy bonds seen in the FTIR analysis discussed earlier. The increased concentration of high energy bonds such as C=C and C=O leaves fewer sites available for water molecules to bond to the fibers, thus decreasing the moisture absorption.

One more insight into the degree of torrefaction can be the moisture absorption. Figure 5.16 shows the sorption curves for the torrefied biomasses only. All three biomass feedstocks display similar sorption rates at each relative humidity with the exception of THH at 90% relative humidity. The increased absorption of THH may be an indication that it has a lower degree of torrefaction than TFS or TSFH. If the FTIR, TGA, and SEM results are revisited, it can be seen that THH does have a lower degree of torrefaction. From Figure 5.2, the FTIR spectra for THH, it can be seen that the weak broad peak centered around 3300 cm^{-1} is stronger in THH

than in the analysis of TFS or TSFH. From the TGA analysis of THH in Figure 5.6 is can be seen that the peak of mass loss occurs at approximately 330 °C, 40 °C below either TSFH or TFS. Finally from the SEM images of THH seen in Figure 5.10 fewer pores are seen than in the images of the other two torrefied biomasses. This lower degree of torrefaction for THH could be a result of either constituent makeup or fiber structure. Both SFH and FS have higher amounts of lignin, the most thermally stable constituent with in the biomass as seen in Table 3.2. The HH particles are significantly thicker than SFH or FS preventing heat from penetrate the fiber as quickly.

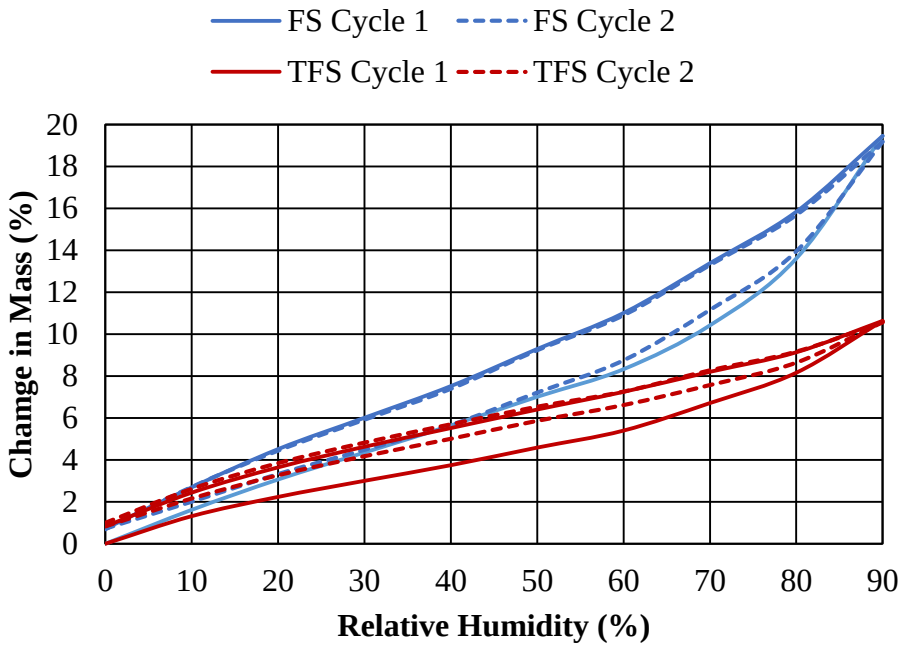

Figure 5.13: Moisture sorption and desorption of untorrefied and torrefied flax shive.

In a similar manner it can be concluded that TSFH had the highest degree of torrefaction. The FTIR spectra of TFS, seen in Figure 5.1 shows a more intense peak at 3300 cm^{-1} than TSFH. Fewer pores than TSFH can be seen in the SEM images of TFS in Figure 5.9. The TGA analysis of TSFH and TFS both indicate the peak mass loss of the torrefied biomass to be around 370 °C. Finally from Figure 5.16 is can be seen that TSFH has the lowest affinity to moisture.

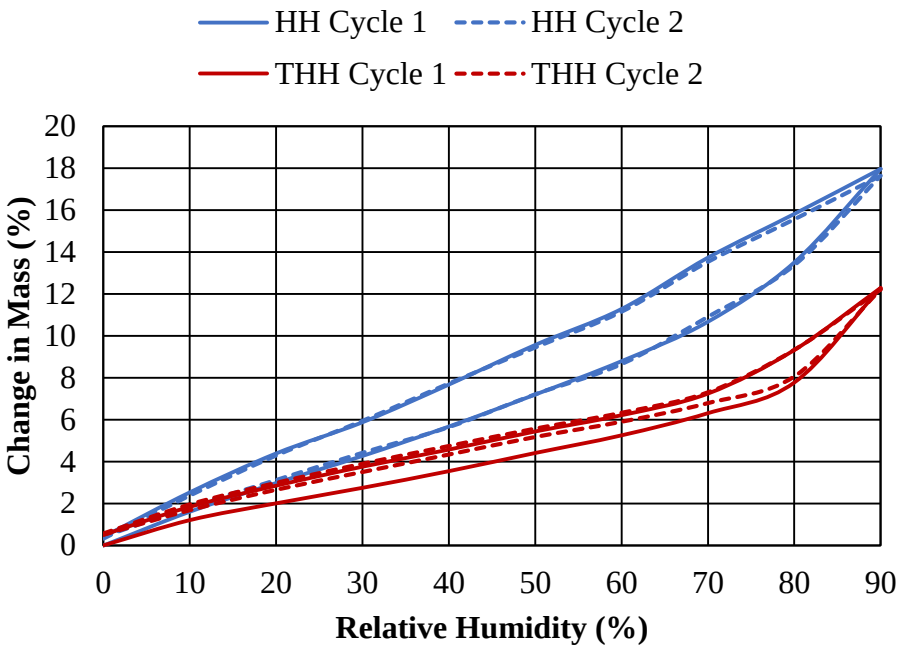

Figure 5.14: Moisture sorption and desorption of untorrefied and torrefied hemp hurd.

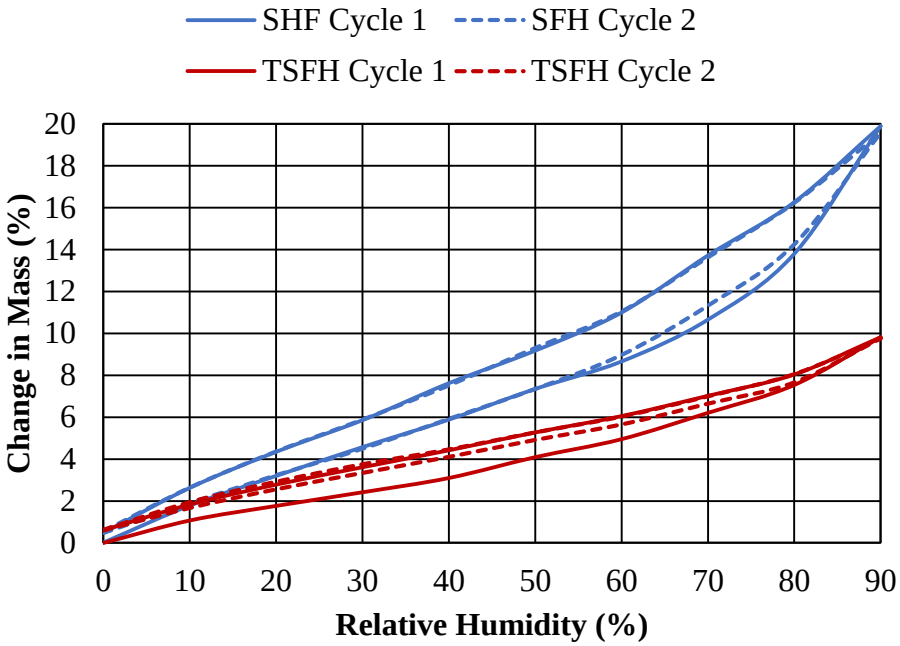

Figure 5.15: Moisture sorption and desorption of untorrefied and torrefied sunflower hulls.

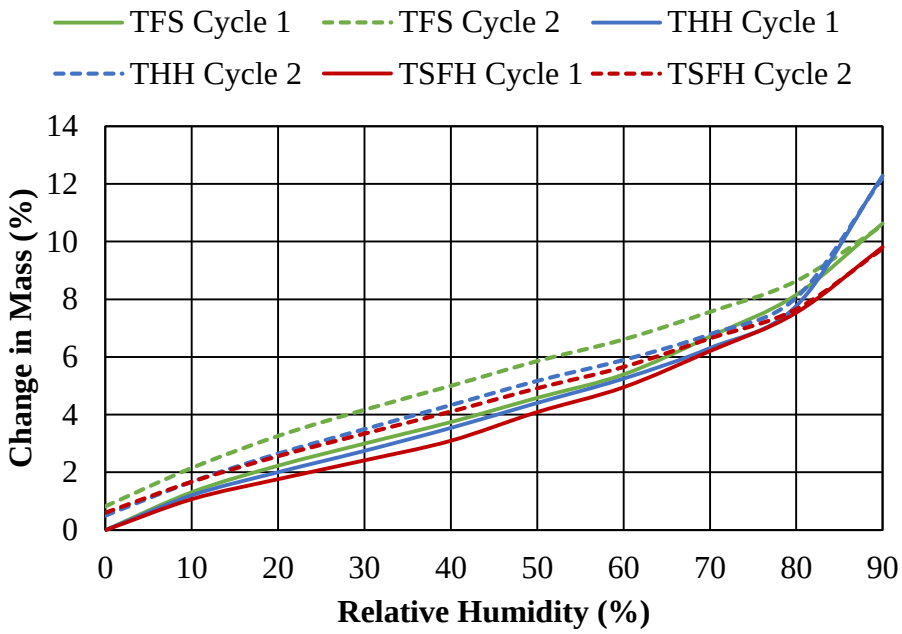

Figure 5.16: Moisture sorption of torrefied biomass.

5.1.7. Yield and Stability Temperature Predictive Modeling

In order to make torrefaction of biomass a viable option for use as industrial biocomposite fillers, there is a need for predictability and tailoring of the torrefaction process for individual applications. From the ANOVA analysis torrefaction parameters it is known that torrefaction temperature and hold time have the most significant effect on yield and stability temperature of the torrefied product. Regardless of torrefaction time, biomass will undergo some conversion from the heating process. Through TGA analysis of cellulose, hemicellulose (extracted from birchwood), and lignin the surviving mass percentage for each major constituent is known to be approximately quadratic with torrefaction temperature [41]. The following equations determine what percentage of each of the major constituents will survive the heating portion of torrefaction, where T is the torrefaction temperature, cellremain is the surviving

percentage of cellulose, hemiremain is the surviving percentage of hemicellulose, and ligremain is the surviving percentage of lignin:

$$cellremain = 99.6902 + 0.0157 * T - 0.0001 * T^2$$

$$hemiremain = 100.9762 - 0.0376 * T - 0.0001 * T^2$$

$$ligremain = 102.6530 - 0.1073 * T$$

By multiplying the percentage of each constituent present in a given biomass by the surviving percentage and adding up the results a predicted torrefaction yield from heating alone can be calculated. This prediction can be seen in the following equation, where cell is the starting mass percentage of cellulose, hemi is the starting mass percentage of hemicellulose, and lig is the starting percentage of lignin:

$$yield_{heating} = \frac{cell * cellremain}{100} + \frac{hemi * hemiremain}{100} + \frac{lig * ligremain}{100}$$

Torrefaction consists of two phases; the heating phase which brings the torrefaction chamber and biomass up to temperature, and a hold phase which keeps the chamber and biomass at the torrefaction temperature for a certain length of time. While the heating phase accounts for a large portion of the conversion process associated with torrefaction the hold time contributes for the remainder of the mass loss. Figure 5.17 shows a plot of the difference in the predicted yield due to heating and the actual yield from the time and temperature test matrix studied earlier with respect to hold time. From the Figure it can be seen that the difference between the predicted and actual yields is linear with respect to hold time. It can also be seen that the linear relationship changes with torrefaction temperature. Figure 5.18 shows the plot of linear regression coefficients versus torrefaction temperature. This Figure shows that both linear regression coefficients follow a quadratic relationship with torrefaction temperature. By first calculating the linear regression coefficients, a_0 and a_1, with these equations:

$$a_0 = 0.038 + 0.02 * T + 0.0001 * T^2$$

$$a_1 = -0.0015 + 0.0028 * T + 0.000006 * T^2$$

then applying the following equation, where t is torrefaction hold time, the mass loss due to hold time is calculated.

$$yield_{time} = a_0 + a_1 * t$$

This change in mass due to hold time is subtracted from the expected yield due to heating to calculate the expected final yield due to torrefaction of any biomass at any given temperature and torrefaction time.

$$yield = yield_{heat} - yield_{time}$$

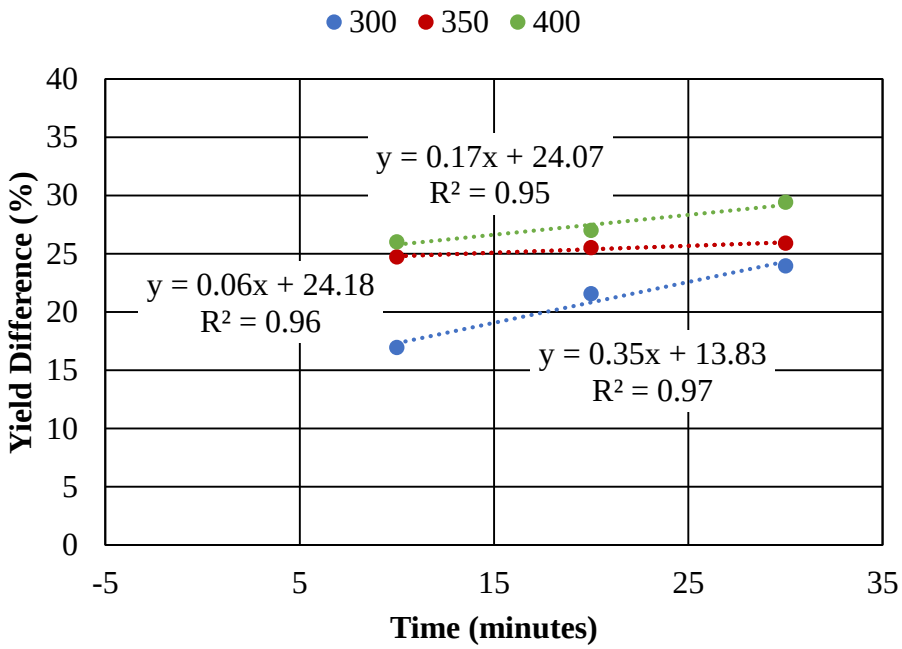

Figure 5.17: Linear regression of torrefaction yield versus hold time.

The torrefaction yield model was based on the test matrices discussed previously that studied the effects of various torrefaction parameters on TFS. As expected the model predicts the final torrefaction yield of TFS well, but the model needs to also predict the yields for any biomass that may be chosen for a given application. Figure 5.19 shows the comparison of

predicted and actual yields for the multiple batch production of TFS, THH, and TSFH. The yield prediction for both TFS and TSFH falls within 3% of the average torrefaction yield, well within the standard deviation of the process. The prediction of THH yield is where the model deviates from the experimental data. The HH used in this work was tested and found to contain approximately 10% moisture at the time of torrefaction, higher than the 2.5% when the biomass was tested using wet chemical analysis. The increased moisture content is likely one significant source of this deviation from the model and indicates the need for accurate values for the constituent makeup of each biomass.

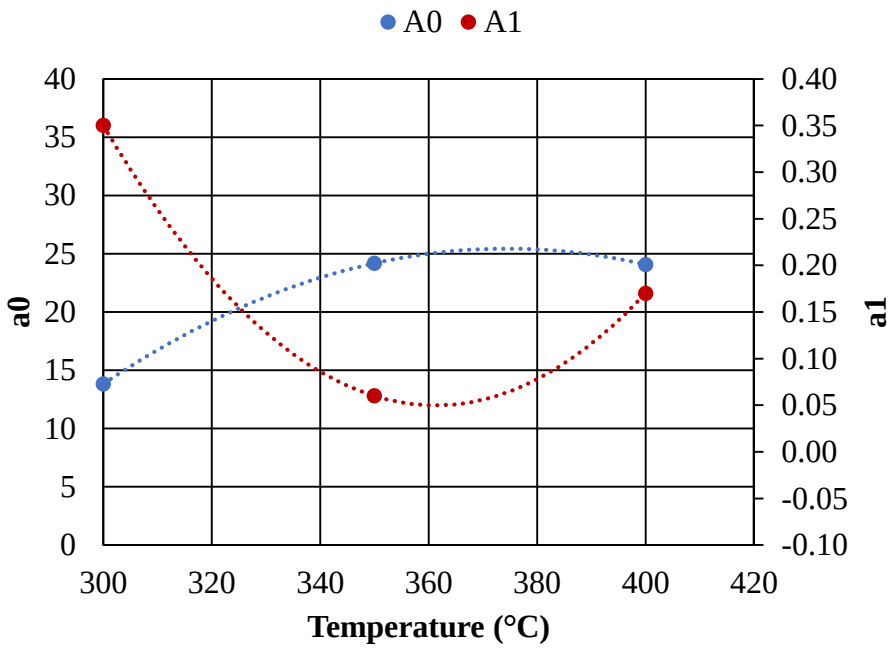

Figure 5.18: Quadratic relationship of linear regression coefficients versus torrefaction temperature.

Beyond the need to predict the efficiency of torrefaction for large scale biocomposite production the thermal stability of the torrefied fiber also needs to be predicted. The processing temperatures of the base polymer will dictate how far the torrefaction needs to be taken to ensure degradation during biocomposite processing is limited. From the test matrices of TFS studied

earlier it is known that temperature has the largest effect on the 90% stability temperature of TFS. As the torrefaction temperature is already accounted for in the yield prediction model, it was concluded that the stability temperature can be predicted based off the already described prediction model. Figure 5.20 shows a plot of all the actual torrefaction yields and 90% stability temperatures from the three test matrices studied in this work. This figure shows that the stability temperature has a cubic relationship to the torrefaction yield, x in the equation seen in the figure.

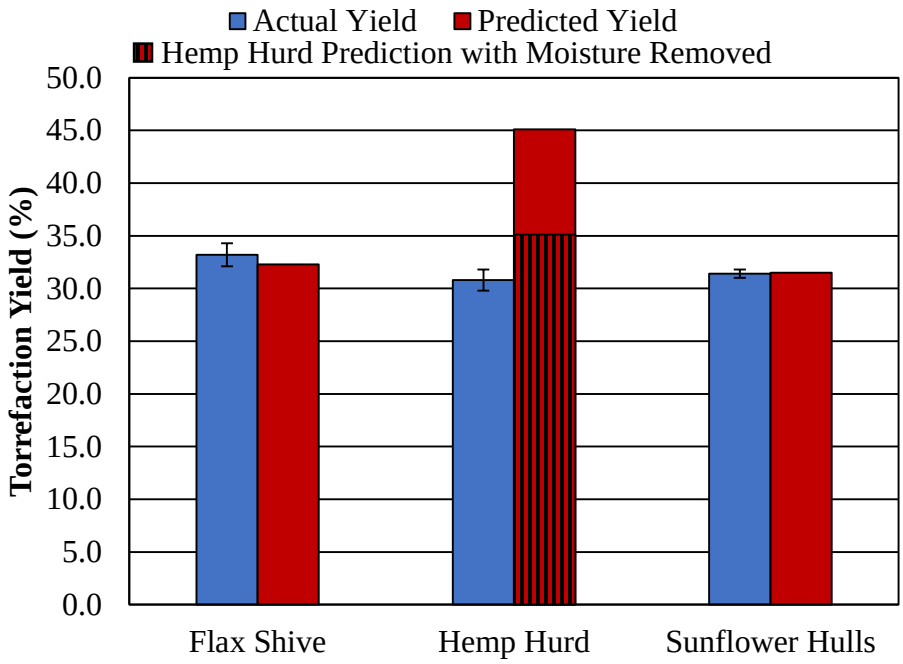

Figure 5.19: Actual and predicted torrefaction yields of various biomass from microwave induced torrefaction.

Similar to the yield model the stability model was based off the work studying TFS and must be verified for other biomass feedstocks. Figure 5.21 shows the comparisons of measured stability temperatures and predicted stability temperatures for various torrefied fibers. From the figure it can be seen that the model predicts the stability temperature of TFS, THH, and TSFH within 6% of the experimental average. The prediction of the THH stability temperature is low likely due to the discrepancy in the yield model from inaccurate constituent data. The over

prediction of the TSFH stability may stem from the increased presence of residual surviving oils within the feedstock.

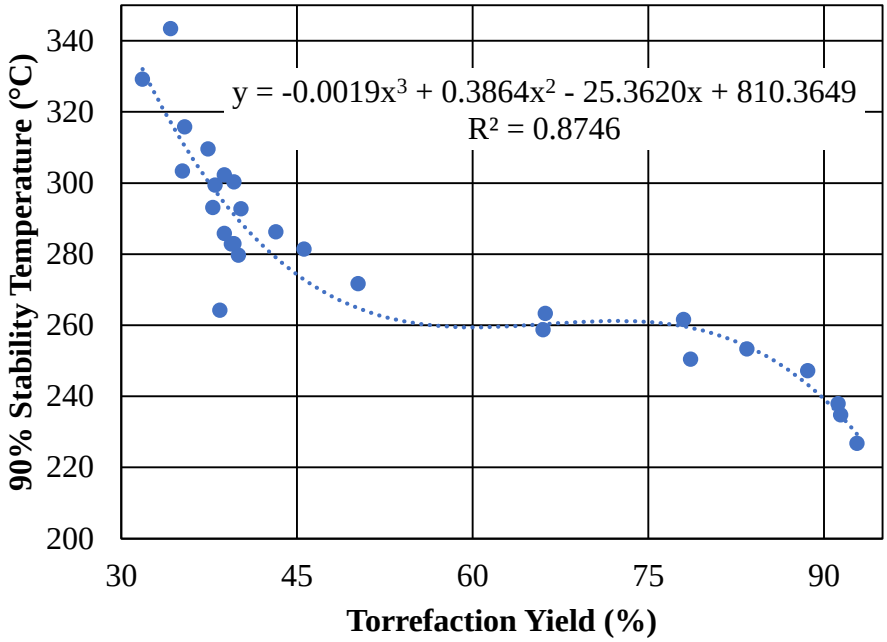

Figure 5.20: Cubic Regression of Stability Temperature versus Torrefaction Yield

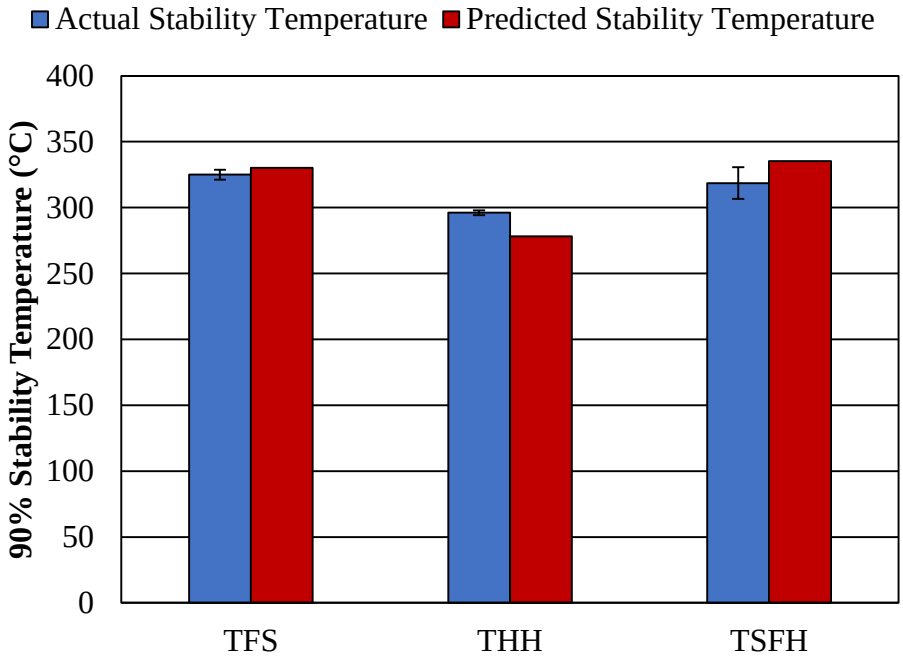

Figure 5.21: Actual and predicted stability temperatures of various torrefied biomass.

In the yield model only cellulose, hemicellulose, and lignin are used in the calculations, there are conversions of other constituents occurring within the biomass as well which have been assumed to be negligible due to the low starting concentrations of each constituent. The low starting concentrations can be seen in Table 3.2. The conversion of oils may play a larger role in the torrefaction of SFH than has been accounted for. Repeating the analysis of the test matrices using SFH and HH as feedstocks would provide a little more insight into how the presence of oils, torrefaction temperature, and hold time effect yield and stability temperature. All of the data used in the formulation of these models can be seen in the appendix along with the MATLAB code of the model.

5.2. Characterization of Polyamide Biocomposites

In order to validate torrefied biomass filled biocomposites as drop-in replacements for current parts made of virgin or glass filled polymer, the changes to mechanical properties need to be fully understood. The addition of torrefied biomass with a stability temperature at or above the processing temperatures of the base polymer should result in biocomposites with comparable mechanical properties to the unfilled matrix. The following sections discuss how the biocomposites compare to the unfilled matrix and why the improvements or shortcomings occur.

5.2.1. Elastic Modulus and Tensile Strength

From previous work the addition TFS and TSFH to PA6 was shown to maintain 70% of the ultimate tensile strength of the unfilled matrix while increasing the elastic modulus by 150%. This work also showed that due to uneven torrefaction a plasticization effect from the degradation of under-torrefied fibers was causing lower mechanical properties than were expected [32]. Figure 5.22 shows the comparison of tensile strengths and elastic moduli for

PA66 biocomposites filled with 30 wt% TFS, THH, and TSFH. From this figure it can be seen that the addition of microwave torrefied biomass produced PA66 based biocomposites that maintain at least 60% of the tensile strength of the neat matrix while increasing the elastic modulus by as much as 121% over unfilled PA66.

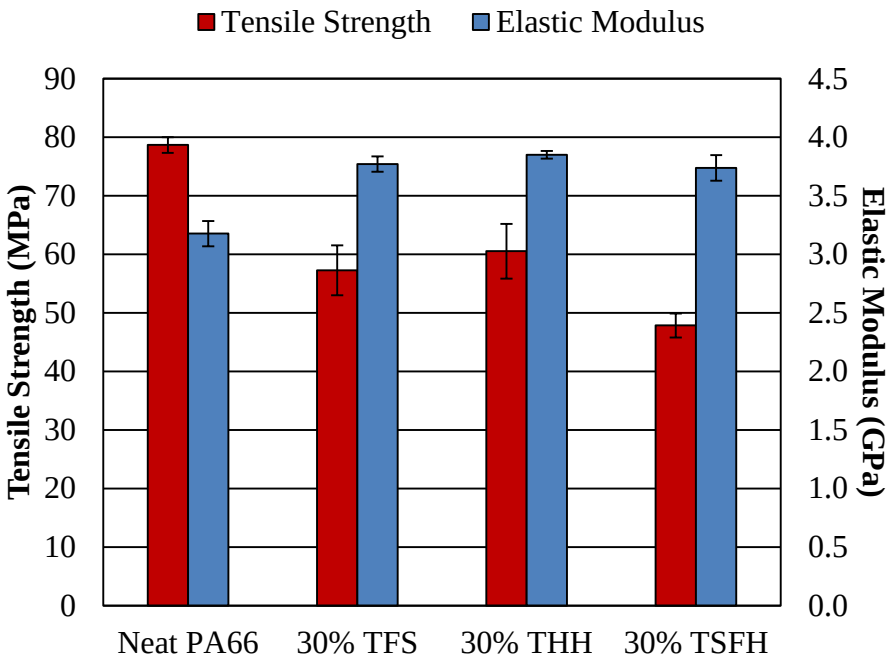

Figure 5.22: Tensile properties of neat PA66 and torrefied biomass filled PA66.

While the overall tensile properties are promising, it is important to look at the results from individual biomass feedstocks alongside the study of the degree of torrefaction. From the discussion on the degree of torrefaction for TFS, THH, and TSFH in previous sections, it was concluded that THH had the lowest degree of torrefaction. From Figure 5.22 it can be seen that the THH biocomposites had the highest tensile strength and elastic modulus among the fiber filled composites. The TSFH filled biocomposites displayed the lowest tensile properties, yet TSFH had the highest degree of torrefaction. These results lead to the hypothesis that there is an inverse relationship between the degree of torrefaction and tensile properties. However, there are more parameters affecting the tensile properties than just the degree of torrefaction. Particle size,

presence of voids within the final parts, and crystallinity are all potential causes for differences in mechanical properties and will be discussed in subsequent sections.

5.2.2. Flexural Modulus and Strength

The addition of TFS and TSFH to PA6 in previous work was shown to maintain flexural strengths within 94% and increase flexural moduli by 154% over the unfilled matrix. The decrease in flexural strength was shown to be due to the plasticization effect of under-torrefied fibers degrading further during biocomposite production [32]. Figure 5.23 show the flexural strengths and moduli of 30 wt% filled PA66 biocomposites compared to the unfilled matrix. This figure shows that the addition of microwave torrefied biomass has mixed results. All three biocomposites displayed similar if not slightly improved flexural moduli, however there is some sacrifice in flexural strength.

It is once again easier to analyze the results of flexural testing alongside the degree of torrefaction discussion. The lower degree of torrefaction associated with THH and TSFH, produced very similar results. Biocomposites filled with TFS showed to have the highest flexural strength and modulus. The TSFH biocomposites displayed a very slightly increased flexural modulus, however, the flexural strength of these composites was the lowest of the three fiber types. In terms of flexural strength there again appears to be an inverse relationship between degree of torrefaction and flexural properties, but much like the tensile discussion there are many more parameters affecting the flexural results.

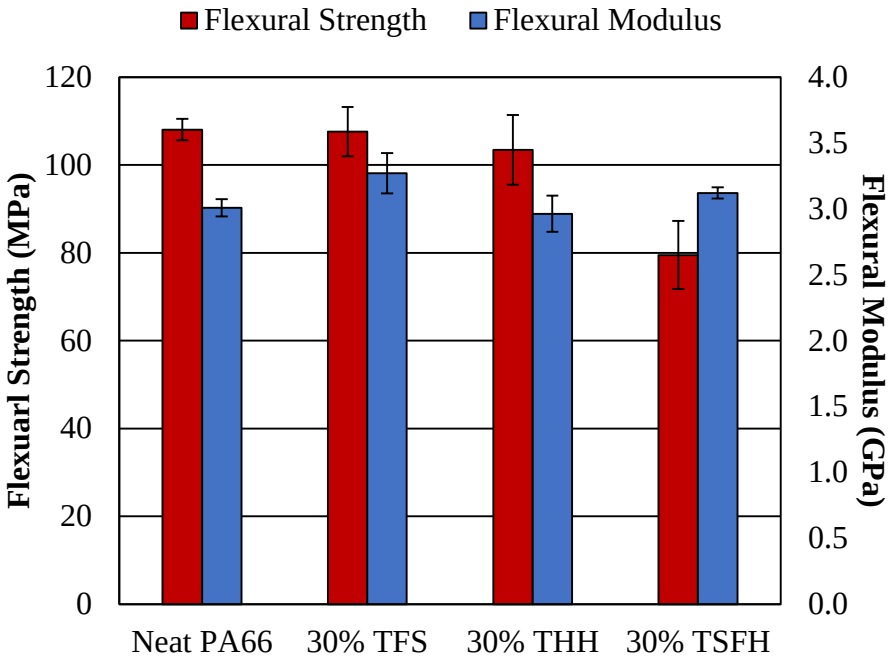

Figure 5.23: Flexural properties of neat PA66 and torrefied biomass filled PA66.

5.2.3. Impact Toughness

One of the areas that biocomposites have fallen short of neat matrices is in impact properties. The addition of rigid fillers restricts the movement of polymer chains preventing the absorption of energy during an impact event. Figure 5.24 shows the impact toughness of the unfilled PA66 and the 30 wt% torrefied fiber filled biocomposites. This figure shows the expected trend of decreased impact toughness with added rigid fillers. The addition of TFS to PA66 decreased the impact toughness of PA66 by approximately 28%, which was the smallest drop-in impact toughness of all the biocomposites. The addition of THH dropped the impact toughness by approximately 40% and TSFH dropped the impact toughness by approximately 53%. If the degree of torrefaction between THH and TFS is assumed to be equivalent, there appears to be an inverse relationship between decreased impact toughness and increased degree of torrefaction. There is a more interesting trend that appears in the impact toughness results

though, decreasing fiber size appears to increase the impact toughness. In this work no fiber fractionation occurred before the biocomposite production, meaning as-received fiber was torrefied and directly introduced into the extrusion process. The fiber size of FS was the smallest and TSFH had the largest fiber size. The size of fiber going into the biocomposite production process was not studied in this work, but it is an interesting result that merits further investigation.

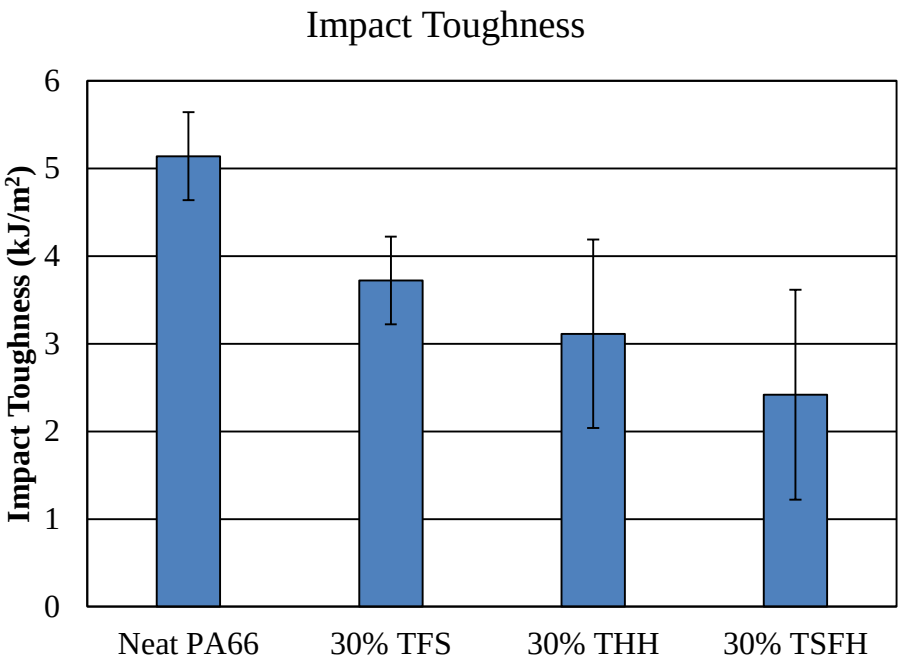

Figure 5.24: Impact toughness of neat PA66 and torrefied biomass filled PA66.

5.2.4. Immersion Density

With the ever increasing push to go green especially in the transportation industries, the weight of parts is critical. The current standard for polyamide composites is fiberglass. The addition of fiberglass with an average density of 2.5 g/cm^3 into a polyamide matrix with an approximate density of 1.1 g/cm^3 the weight of a composite part will be higher than that of one made from unfilled polymer. While it is hard to get around increasing the weight of a part by

switching from unfilled polymer to composite material due to the higher density of fillers; it is possible to save some weight within a composite part by switching from fiberglass to less dense biomass based fillers. Figure 5.25 shows the immersion densities of the unfilled PA66 and the 30 wt% filled biocomposites. This figure shows that all three biomass feedstocks displayed similar densities, all approximately 4% higher than the neat PA66. If these composites were filled with fiberglass at the same 30 wt% loading the density would increase even further to approximately 1.5 g/cm^3, 16% higher than the unfilled matrix.

5.2.5. Moisture Uptake

One of the largest advantages to torrefaction is the increased hydrophobicity of biomass. This is advantageous for the storage of biomass as it hinders the growth of bacteria which generally is due to moisture and temperature within the storage environment. Figure 5.26 shows the moisture uptake of the unfilled PA66 and the three biocomposites at three different soak lengths; 24, 48, and 72 hours. At all soak lengths the biocomposites absorbed more moisture than the unfilled PA66. This was an unexpected result that could ultimately be explained through the degree of crystallinity discussed in a subsequent section. Another interesting trend seen among the biocomposites is the decreased moisture uptake of the TFS composite. The particle size of TFS was smaller than either TSFH or THH. By decreasing the particle size of the torrefied biomass prior to composite processing it is possible that the moisture uptake could be further reduced. The results of moisture testing were not as promising as those seen in previous work [32], however with some modifications of the biocomposite recipe it is believed that the decreased moisture uptake seen in previous work could be achieved.

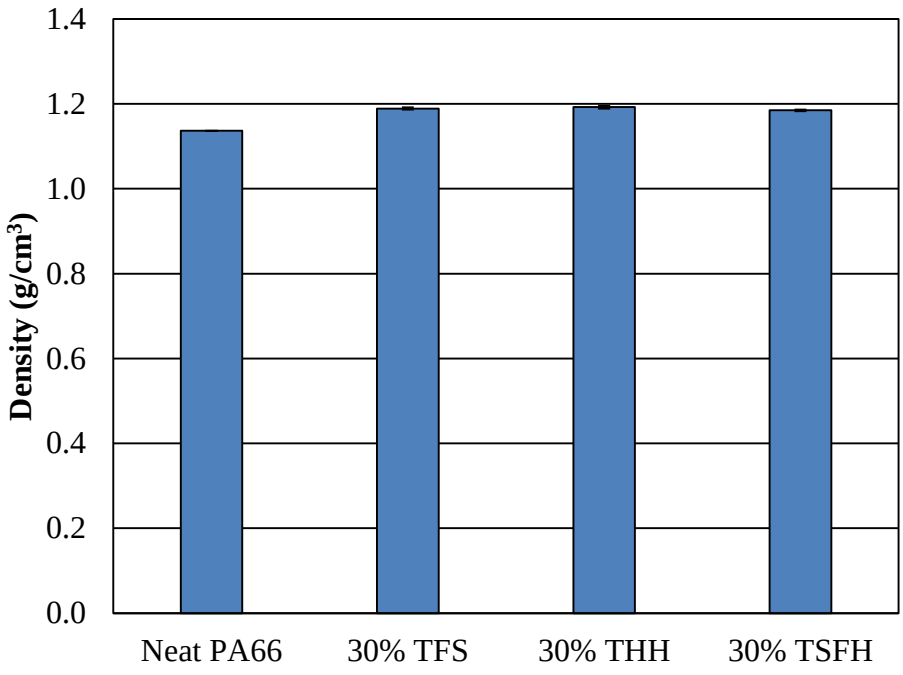

Figure 5.25: Density of neat PA66 and torrefied biomass filled PA66.

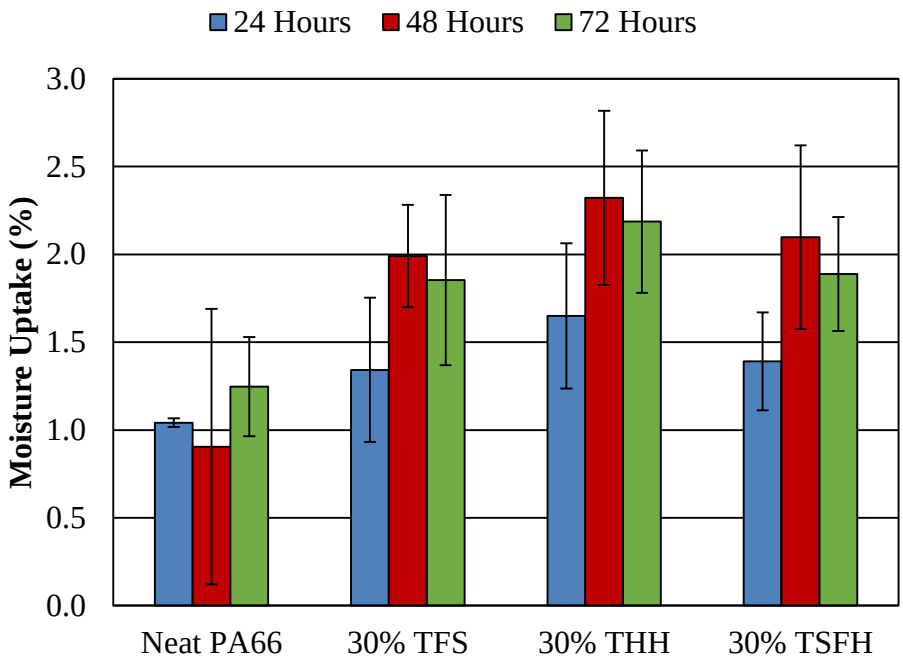

Figure 5.26: Moisture absorption of neat PA66 and torrefied biomass filled PA66.

5.2.6. Dynamic Mechanical Analysis

In previous work done with TFS and TSFH filled PA6 biocomposites, the effects of under-torrefied biomass showed to have a plasticization effect [32]. This plasticization affected several mechanical properties along with the glass transition temperature. The TSFH biocomposites which were believed to contain increased amounts of unconverted oils displayed decreased glass transition temperatures. Figure 5.27 shows the glass transition temperatures of PA66 biocomposites filled with microwave torrefied biomass. The figure shows a slight increase, three to four degrees on average, in the glass transition temperature over the unfilled PA66 for the biocomposites. The increase in glass transition temperature is small, but does indicate that a more complete conversion of low weight constituents was achieved through microwave torrefaction.

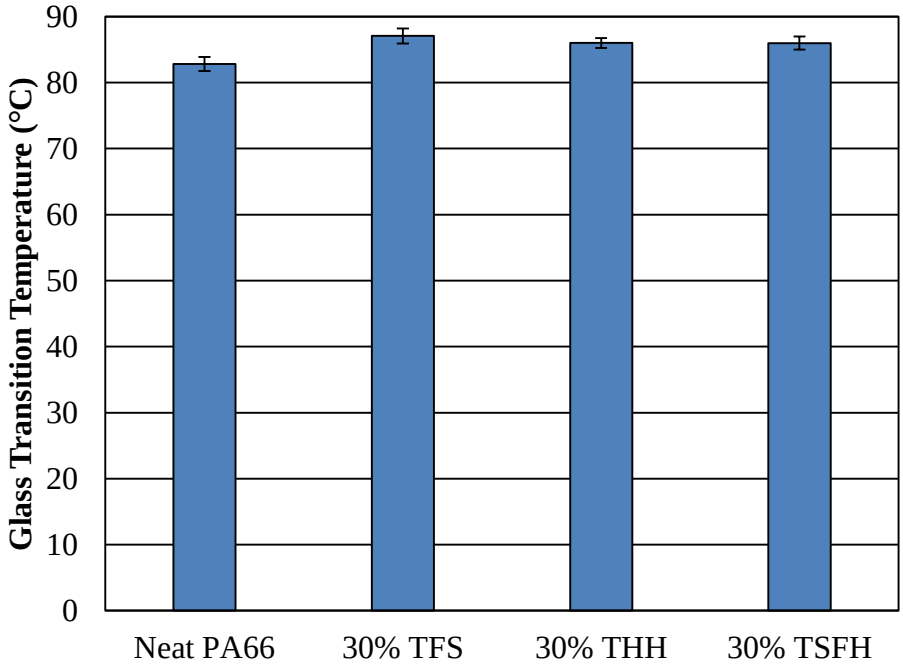

Figure 5.27: Glass transition temperature of neat PA66 and torrefied biomass filled PA66 from dynamic mechanical analysis.

The glass transition temperatures discussed above were determined from the peak of the tangent delta curve. Figure 5.28 shows the tangent delta curves for each of the specimens tested. The discrepancy between the unfilled PA66 and biocomposites is one more indicator of a more complete conversion from microwave torrefaction. In the previous work utilizing conventionally torrefied biomass the differences in the tangent delta curves were very minimal, one more indication that a plasticization effect was limiting the increased elastic behavior often seen in composite materials [32]. In the present work, there is a distinct shift in the tangent delta values with the added filler indicating increased elastic behavior over the unfilled PA66. However, width at half height of the tangent delta curves were all equivalent.

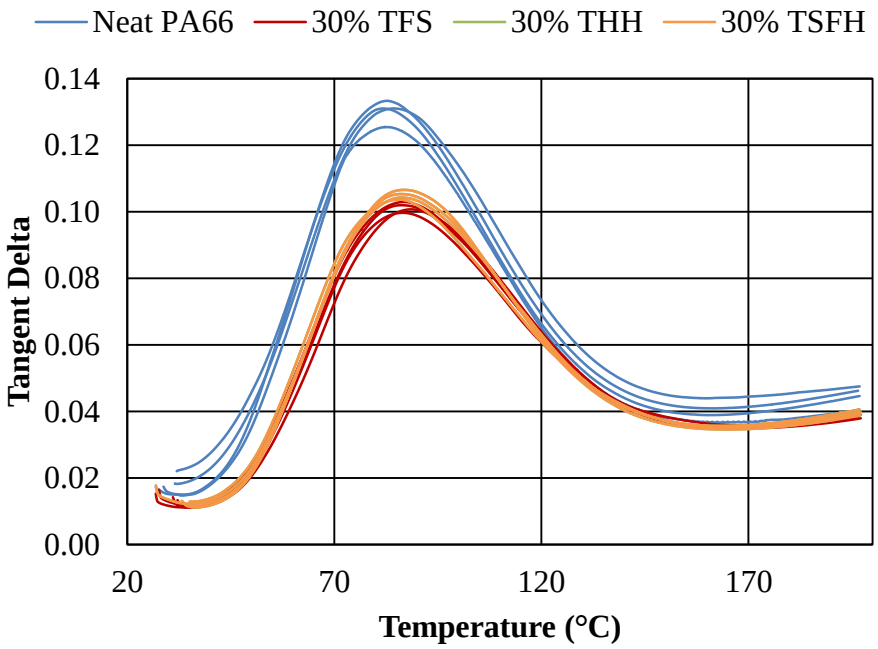

Figure 5.28: Tangent Delta of neat PA66 and torrefied biomass filled PA66.

Aside from the glass transition temperature of the materials, DMA analysis was also used to study the effects of the added torrefied fiber on storage and loss modulus. Figures 5.29 and 5.30 show the storage and loss modulus curves respectively for each of the samples tested. The increased storage modulus form the addition of torrefied biomass is one more indicator that the

elastic behavior of the biocomposites is higher than the unfilled PA66 matrix. The loss modulus of the unfilled PA66 displayed higher values for the loss modulus than the biocomposites at temperatures below the glass transition temperature and lower than the biocomposites at higher temperatures. Part of this work was to determine how the various biomass feedstocks vary the properties of the biocomposites as well. Unlike the variation seen within the tensile, flexural, and impact results; the DMA analysis showed very similar results between each of the biocomposites for glass transition temperature, storage, and loss moduli.

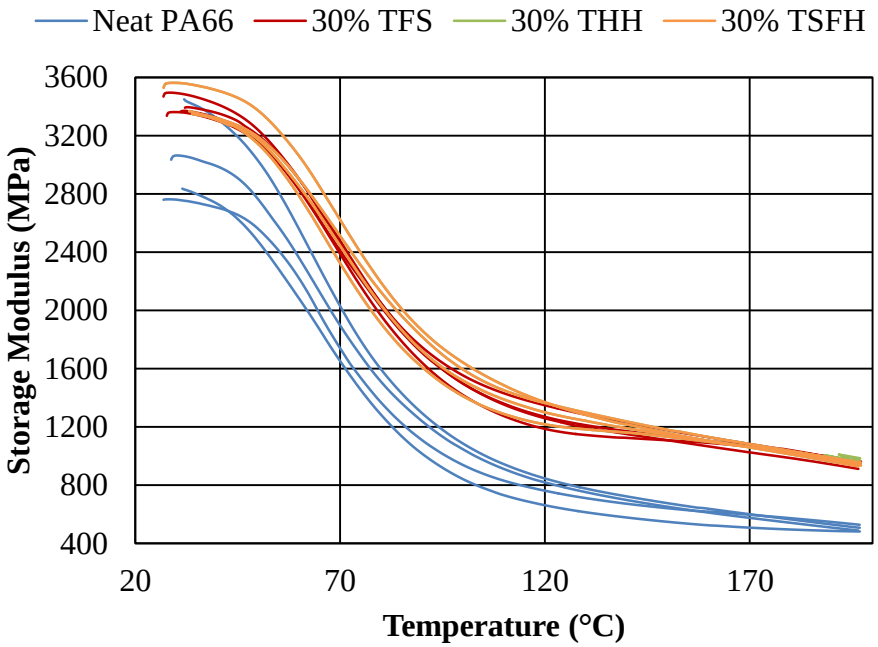

Figure 5.29: Storage Modulus of neat PA66 and torrefied biomass filled PA66.

5.2.7. Heat Deflection Temperature

The additional thermal stability of torrefied biomass makes them attractive for use in high temperature environments. One of the important parameters that determines the viability of a material for a given application is the heat deflection temperature, the temperature at which the material begins to soften and loose strength. For the automotive industry this is a critical property

for any part within the engine bay, which sees elevated temperatures. Figure 5.31 shows the heat deflection temperatures measured for the unfilled PA66 and each of the torrefied biomass filled biocomposites. For each of the biocomposites the addition of torrefied biomass increased the heat deflection temperatures over the neat matrix. Within previous discussions decreased crystallinity was discussed as a potential reason for decreased strength and increased moisture absorption of the biocomposites from the unfilled matrix. A lower crystallinity would generally lead to a decreased heat deflection temperature however, the addition of rigid fibers prevents the movement of polymer chains which leads to the increased elastic behavior and flexural properties of composites. For heat deflection temperature the added fiber means an increased amount of energy needed to start sliding the polymer chains past the inserted rigid fiber with much higher softening temperatures.

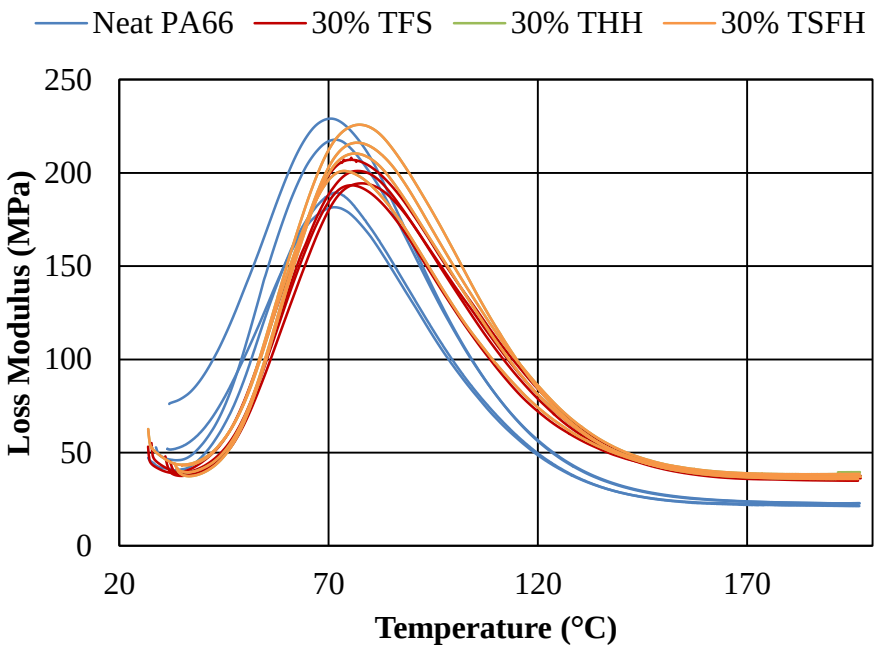

Figure 5.30: Loss Modulus of neat PA66 and torrefied biomass filled PA66.

The overall trend is promising for the application of torrefied biomass fillers in high temperature applications. It is also important to understand how the degree of torrefaction could

affect the heat deflection temperature. Once again revisiting the degree of torrefaction discussion will shed some light on how the degree of torrefaction affects the heat deflection temperature. From the discussion of degree of torrefaction is was concluded that TSFH had the highest degree of torrefaction, from the figure TSFH filled PA66 had the highest heat deflection temperature. Similarly, THH was shown to have the lowest degree of torrefaction which resulted in the lowest heat deflection temperature within the biocomposites. This leads to the belief that heat deflection temperature is directly related to the degree of torrefaction; an increased degree of torrefaction will yield an increased heat deflection temperature.

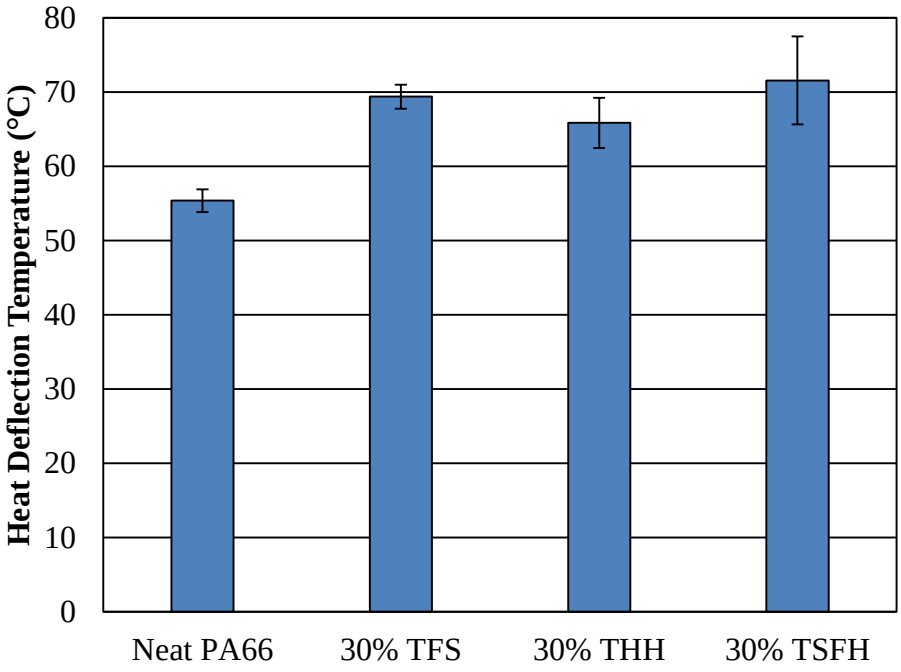

Figure 5.31: Heat deflection temperature of neat PA66 and torrefied biomass filled PA66.

5.2.8. Coefficient of Linear Thermal Expansion

The coefficient of linear thermal expansion is an important material property when it comes to the designing the molds used for final part production. Fully understanding how the material will expand or shrink during the manufacturing process is necessary to ensure proper

tolerances are met within final parts. Figure 5.32 shows the coefficients of linear thermal expansion as measured from DMA film tension analysis for the unfilled PA66 and torrefied biomass filled biocomposites. From the graph it can be seen that the addition of torrefied biomass to PA66 has decreased the coefficient of linear thermal expansion. This was an expected outcome as the insertion of rigid fillers to the polymer matrix prevents polymer chains from sliding past one another resisting expansion at elevated temperatures. Once again the effects of the various biomass feedstocks are of interest when looking at the coefficient of linear thermal expansion. Recalling the degree of torrefaction discussion, THH showed the lowest degree of torrefaction. From the figure among the biocomposites the THH filled PA66 did display the highest coefficient of linear thermal expansion. The highest degree of torrefaction was assigned to TSFH which displayed the lowest coefficient of linear thermal expansion. However, taking into account the variation in the results there is no discernable difference between the three biocomposites, which indicates the addition of the rigid fiber has more effect on the coefficient of linear thermal expansion than the degree of torrefaction.

5.2.9. Differential Scanning Calorimetry

From the tensile, flexural, impact, and moisture testing discussed above some discrepancies from the expected results of adding torrefied biomass to thermoplastic matrices presented themselves. The expectations of increased tensile and flexural performance over the neat matrix with minimal change in impact performance stemmed from previous work done on TFS and TSFH filled PA6 biocomposites [32]. In this previous work it was believed that the addition of torrefied biomass provided an increased number of nucleation sites which increased the crystallinity of the biocomposites over the unfilled PA6. Unfortunately this belief does not hold true for torrefied biomass filled PA66 biocomposites. Figure 5.33 shows the percent

crystallinity measured through DSC analysis for the unfilled PA66 and torrefied biomass biocomposites. The figure shows a clear decrease in crystallinity with the addition of torrefied biomass to PA66. The obvious explanation for this shortcoming is the relatively high degree of crystallinity found in unfilled PA66 to start with; adding rigid fillers to this PA66 matrix prevents the formation of large crystalline regions in the biocomposites. It is also possible that the torrefaction process has deposited low molecular weight compounds on the surface of the fibers, lowering the degree of crystallinity of the composites.

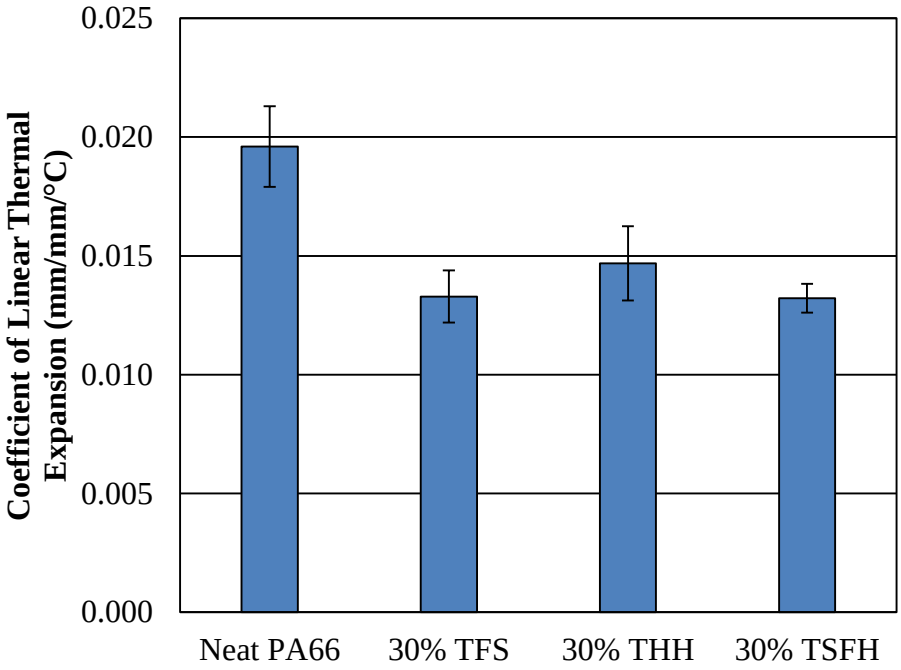

Figure 5.32: Coefficient of linear thermal expansion of neat PA66 and torrefied biomass filled PA66.

From the previous work on TFS and TSFH filled PA6 is was seen that the fillers enabled lower processing temperatures during extrusion and injection molding [32]. It was originally believed the addition of torrefied biomass decreased the melting temperature of the biocomposites from the neat matrix. However, Figure 5.33 shows a very different story for the PA66 biocomposites. This figure shows that the melting temperature is unaffected by the

addition of torrefied biomass, with very minor decreases in crystallization temperatures with added filler. This indicates the changes in processing parameters are only due to the restriction of polymer chain movement by the rigid filler. Figure 5.34 also shows the glass transition temperature measured from DSC analysis. The values shown in this graph are similar to those measured from DMA analysis. This indicates that the DMA testing did capture the glass transition temperature.

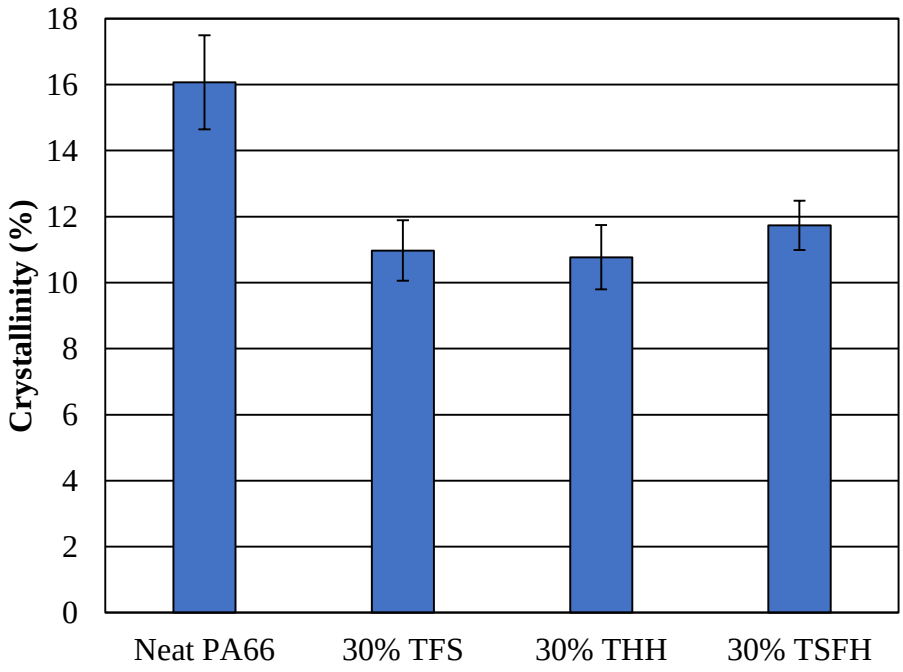

Figure 5.33: Percent crystallinity of neat PA66 and torrefied biomass filled PA66.

A representative curve for neat PA66 and the torrefied biomass filled PA66 biocomposites can be seen in Figure 5.35. The slightly lower crystallization temperatures plotted in Figure 5.34 can also be seen in the shift of the crystallization peaks in Figure 5.35. This figure also shows a distinct widening of the crystallization peaks with the added filler, indicating a slower rate of crystallization. Figure 5.36 shows the widths at half height of the crystallization peaks. This figure again shows a distinct slowing trend of crystallization with the addition of

torrefied biomass to PA66. The slower crystallization and decreased crystallinity of the biocomposites does point to the possibility that low weight compounds have been deposited on the surface of the fibers during torrefaction. Due to the slower crystallization times of the biocomposites the conditions during injection molding may need to be modified from the neat matrix to promote more crystallization.

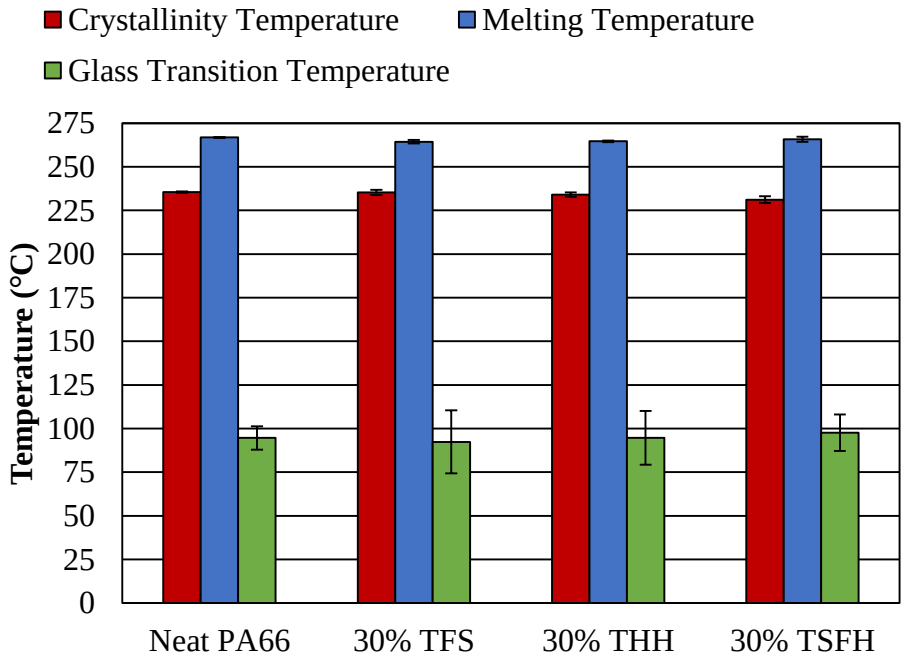

Figure 5.34: Crystallinity and melting temperatures from DSC of neat PA66 and torrefied biomass filled PA66.

5.2.10. Melt Flow Index

One of the other material properties of interest for manufacturers is the melt flow index. The melt flow index is a measure of how much molten material flows through an orifice in a given amount of time. This proves useful when predicting how long the molding process will take for final part geometries. A lower melt flow index can mean more difficulties during the molding process, longer fill times, and higher pressures to ensure proper flow of the material through a mold. Figure 5.37 shows the measured melt flow indexes of the unfilled PA66 and the

torrefied biomass filled biocomposites. The addition of torrefied biomass has decreased the melt flow index of PA66 by over 90%. The restricted movement of polymer chains that causes changes in mechanical performance of composites is the same phenomena that causes decreased melt flow indexes.

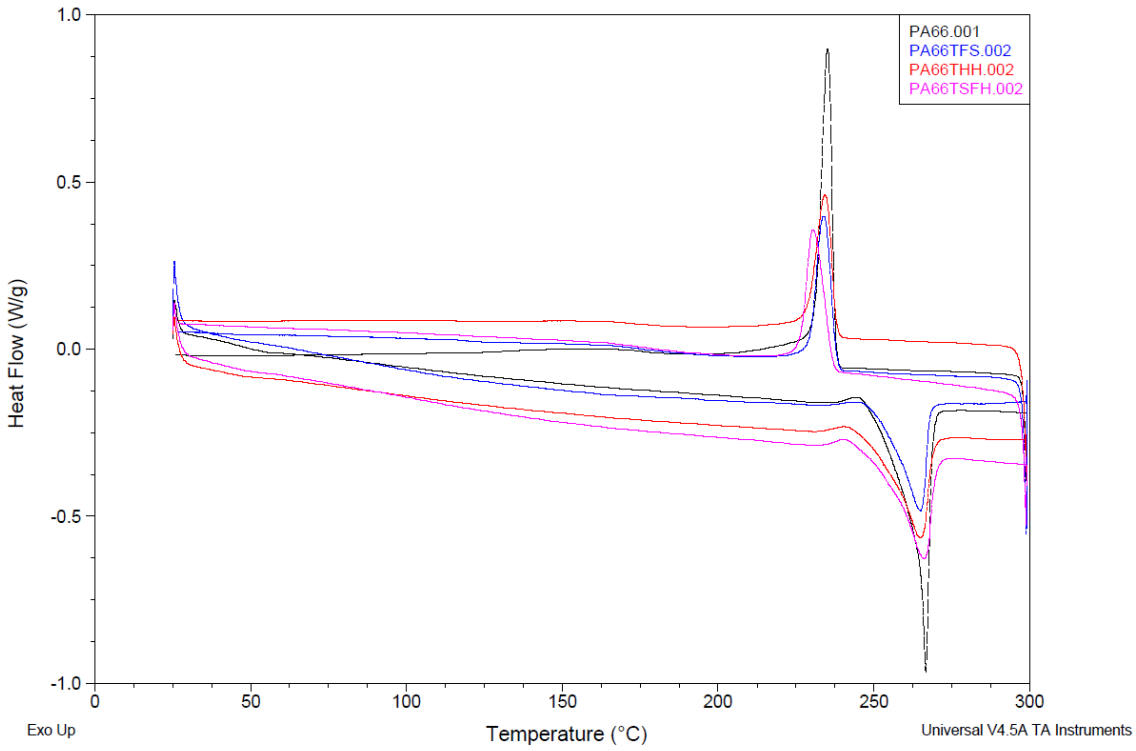

Figure 5.35: Differential scanning calorimetry curves for neat PA66 and torrefied biomass filled PA66.

Like many of the other material properties already discussed, the effect of degree of torrefaction on the melt flow index is of interest. Figure 5.38 shows zoomed in graph of the measured melt flow indexes of the biocomposites. Here a clear increasing trend can be seen between melt flow index and increased degree of torrefaction. As the degree of torrefaction increases, the structure of the torrefied biomass approaches that of carbon black. With an increased carbon structure the added filler begins to act like a lubricant for the polymer chains,

while still displaying some effects of a rigid particle. One aspect of biocomposites not studied in this work is the particulate size going into the extrusion process. With all parameters being the same smaller particles should also increase the melt flow index of the biocomposite. Some further work could validate this believe about the effects of particle size on the processability of biocomposites.

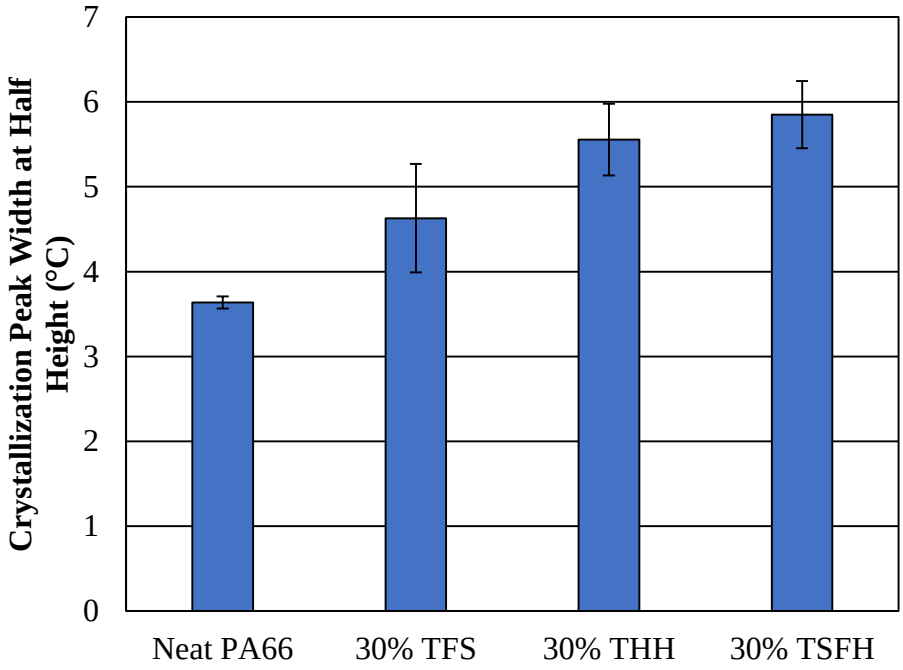

Figure 5.36: The width at half height of the crystallization peak from DSC for neat PA66 and torrefied biomass filled PA66.

5.2.11. Microscopy

The last material aspect studied in this work was how well the torrefied biomass distributed in the polymer matrix. Figures 5.39, 5.40, and 5.41 show the optical microscopy images taken of each of the three biocomposites. In each of the figures the top image is of TFS filled PA66, the middle image is of THH filled PA66, and the bottom image is of TSFH filled PA66. Figure 5.39 shows each of the biocomposites at 10X, Figure 5.40 shows the biocomposites at 20X, and Figure 5.41 shows the biocomposites at 50X. All three figures show

that the torrefied biomasses have dispersed well within the PA66 matrices. There are a wide range of particle sizes in each of the biocomposites, however as discussed earlier TSFH displayed the largest particle sizes of the three feedstocks. The particle sizes of the TFS and THH biocomposites were very similar.

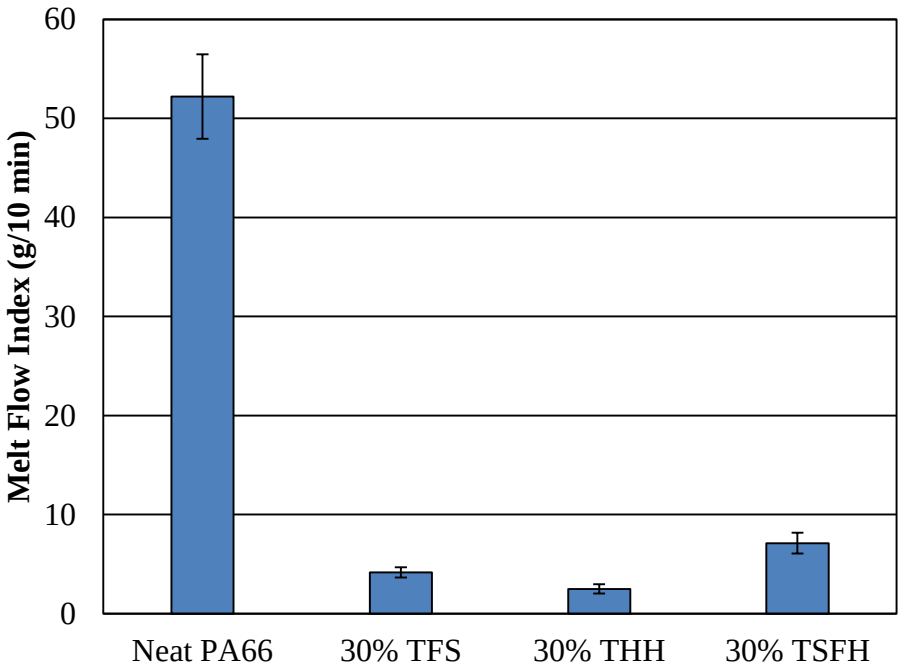

Figure 5.37: Melt flow index of neat PA66 and torrefied biomass filled PA66.

From the previous work done on TFS and TSFH filled PA6 composites, an attempt at producing PA66 biocomposites was made [32]. In that work the PA66 filled biocomposites contained very large voids on the order of two to six mm in width. The torrefaction of biomass through the use of microwave energy in this work was shown to successfully produce PA66 based biocomposites without the large voids seen in previous work. While the large scale voids were not seen small microscopic voids were present in the biocomposites. The THH PA66 biocomposite showed the largest void at approximately 100 µm, which directly relates to the lowest degree of torrefaction. Adding 30 wt% TSFH to PA66 produce biocomposites with 60 µm or smaller voids. The addition to TFS to PA66 showed to produce the smallest voids, 35 µm or

smaller, of the three feedstocks. The voids found within the biocomposites could have come from several sources. The first source is due to further degradation of the biomass during the composite processing. The other is due to moisture trapped within the biocomposite pellets after the extrusion process that was not properly driven off before injection molding. Both sources could be eliminated with minor changes to the final part production process or by finding the ideal degree of torrefaction for each biomass.

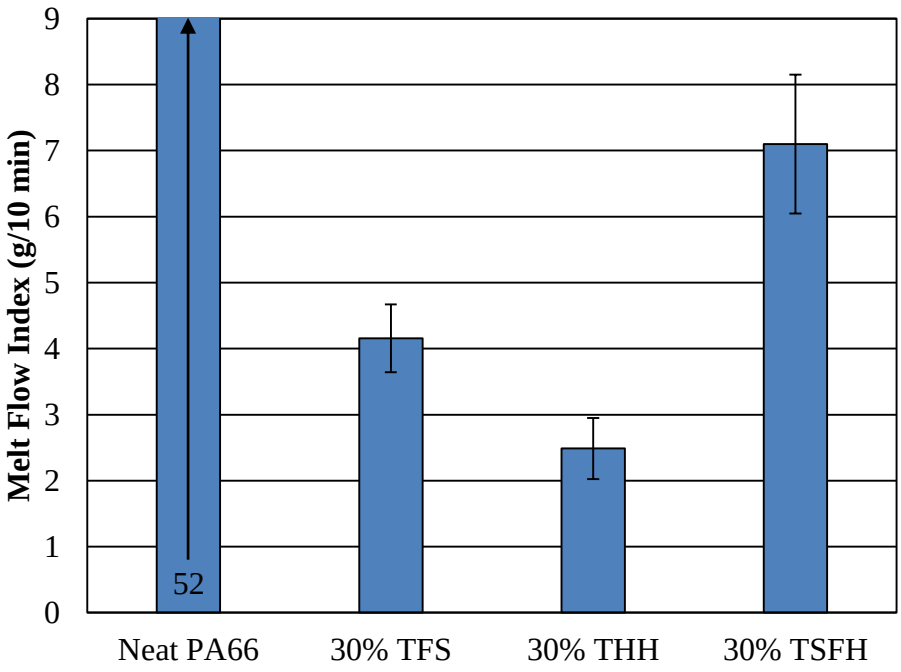

Figure 5.38: Melt flow index of neat PA66 and torrefied biomass filled PA66.

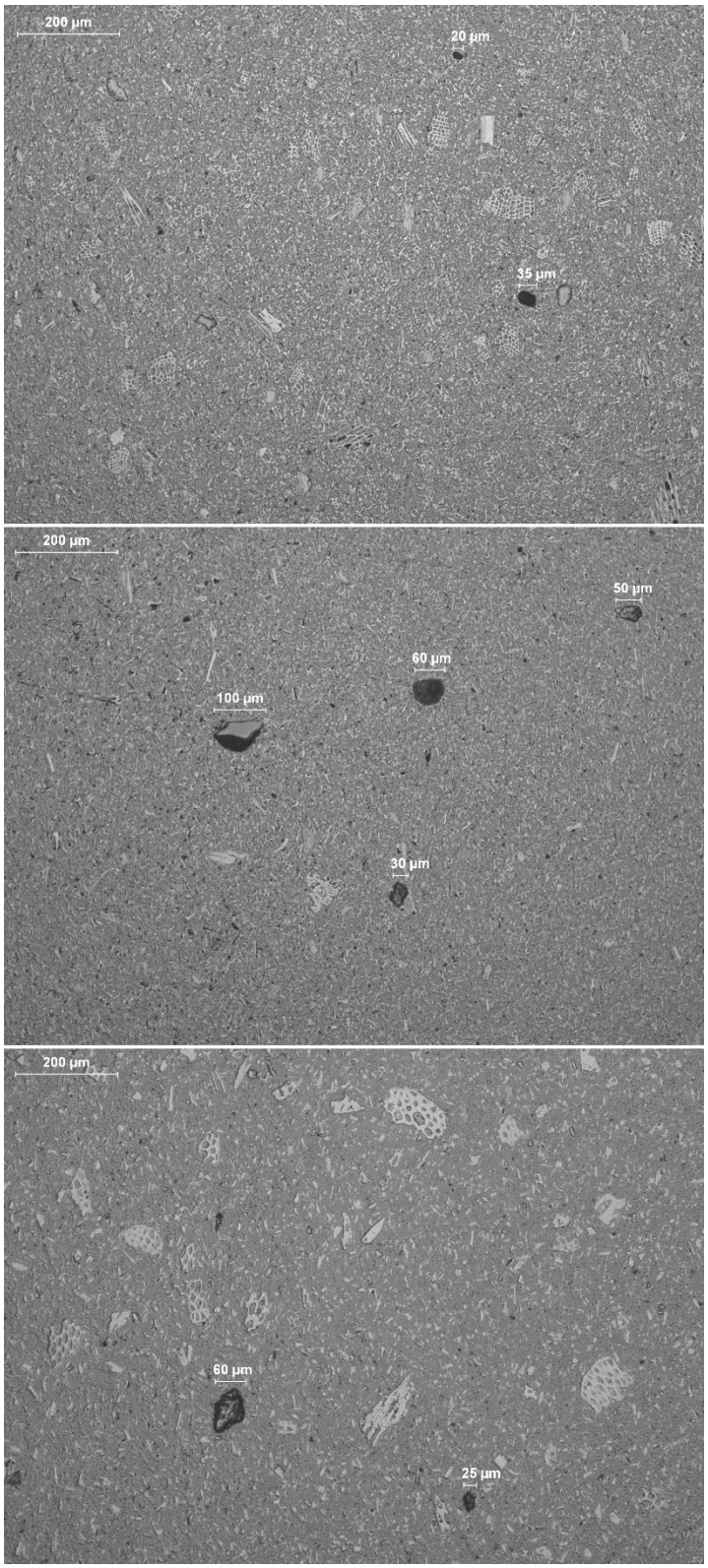

Figure 5.39: 10X optical microscopy images of TFS (top), THH (middle), and TSFH (bottom) filled PA66.

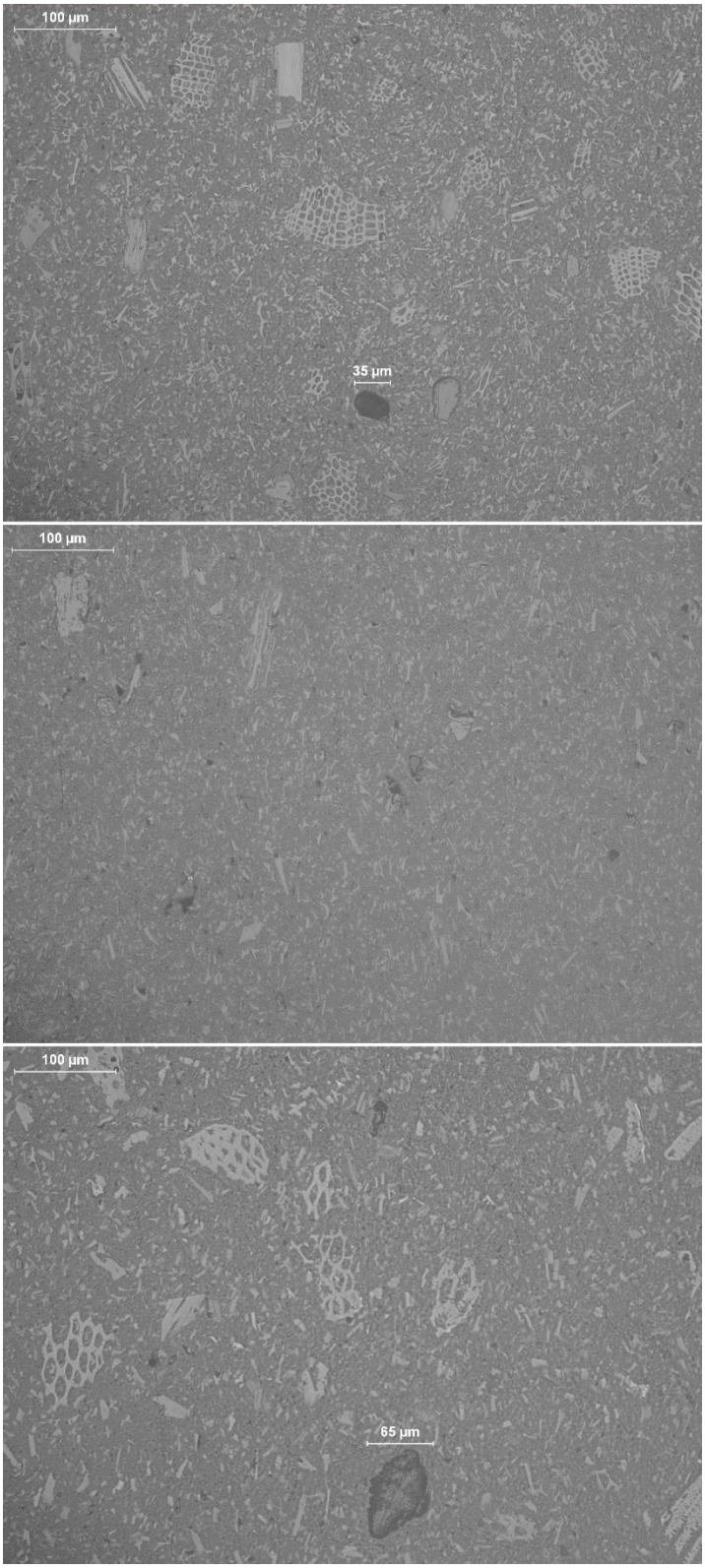

Figure 5.40: 20X optical microscopy images of TFS (top), THH (middle), and TSFH (bottom) filled PA66.

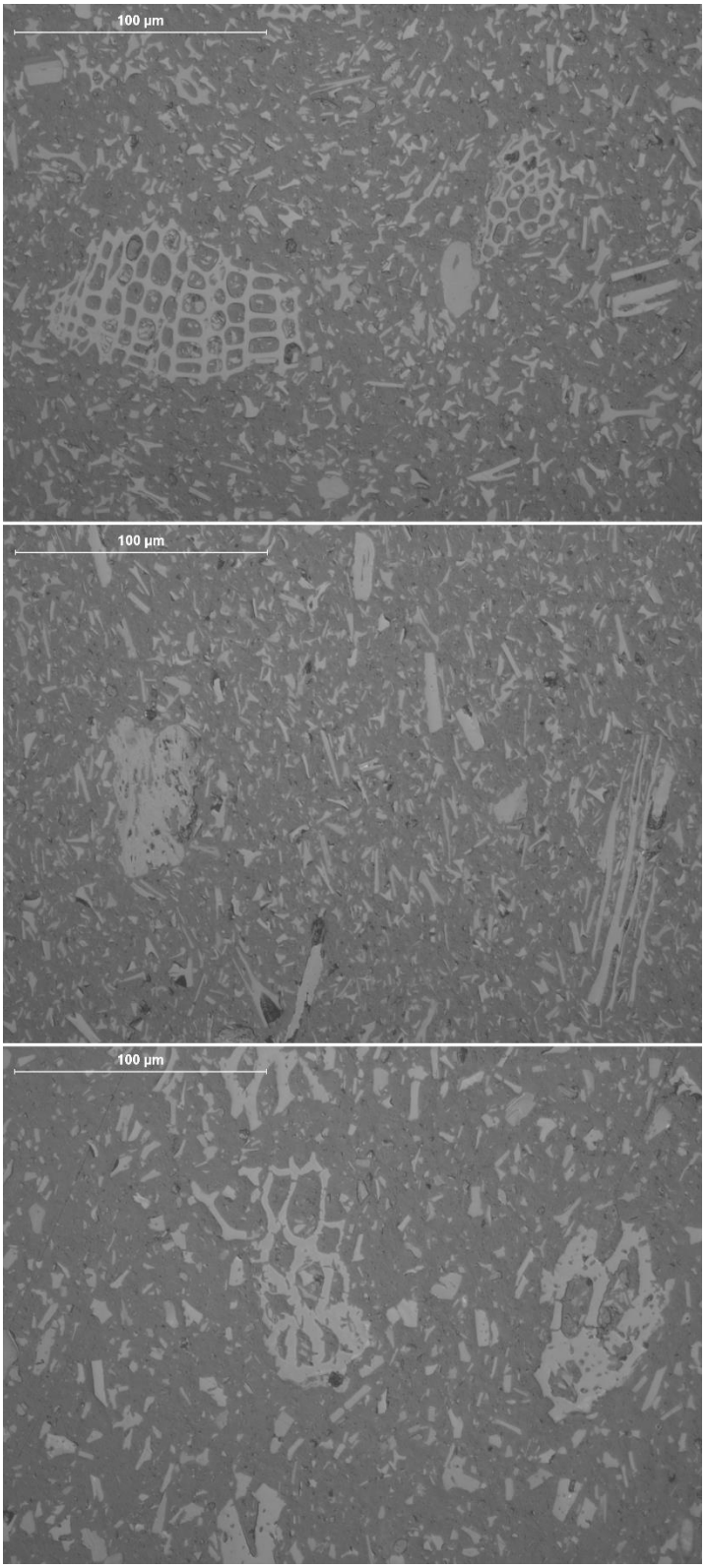

Figure 5.41: 50X optical microscopy images of TFS (top), THH (middle), and TSFH (bottom) filled PA66.

CHAPTER 6. CONCLUSIONS AND RECOMMENDATIONS

Through microwave torrefaction flax shive, hemp hurd, and sunflower hulls filled polyamide 6,6 biocomposites were successfully produced. Torrefaction was used to convert cellulose, lignin, hemicellulose, and low weight constituents within biomass to gases, liquids, and a thermally stable solid mass char which was utilized as filler in the biocomposites. These torrefied fillers were characterized to determine degree of torrefaction, elemental makeup, chemical structure, and degree of hydrophobicity.

Microwave torrefied biomass was shown to have added thermal stability over the untreated fibers. Flax shive that had undergone torrefaction had a thermal stability temperature 42% higher than the untreated fiber. Hemp hurd saw an increase in thermal stability temperature of 24% over the untreated biomass and sunflower hulls saw an increase of 48% from torrefaction.

Electron dispersive spectroscopy and fourier transform infrared spectroscopy were used to better understand the chemical structure present after the torrefaction treatment. Both methods showed that significant changes to the chemical structure and makeup were imposed on the torrefied biomass. In all three feedstocks the amount of carbon present increased by an average of 10% and the oxygen content decreased by an average of 15% indicating the successful conversion of low weight constituents from torrefaction. The chemical structure was also shown to be mostly carbon-carbon bonds with few carbon-oxygen bonds remaining. With the content of carbon being so high and chemical structure being mostly carbon-carbon bonds, the torrefaction parameters used from this work produced transition char containing little to no intact cellulose or lignin structures. For the overall goal of producing drop-in replacements for automotive parts

made of polyamides the biomasses used were over-torrefied. The late transition char is approaching the structure of carbon black which had some negative impacts on mechanical strength.

Scanning electron microscopy was used to examine the surface changes due to torrefaction on the biomass fibers. The conversion process induced by torrefaction increases the surface porosity of the fibers. Increased porosity is believed to aid in the surface interaction between the fibers and polyamide 6,6 matrix due to polymer penetrating the fiber surface.

The culmination of the chemical makeup, structure, thermal stability, and surface characteristics studies led to a better understanding of degree of torrefaction. This was more of a comparative analysis, but the foundation of the grading was the thermal stability increase. Hemp hurd was shown to have the lowest degree of torrefaction. Hemp hurd had the smallest changes in surface porosity, stability temperature, chemical makeup, and structure. Flax shive and sunflower hulls had similar degrees of torrefaction that were higher than the hemp hurd with sunflower hulls having a slightly higher grading.

The last characterization for the torrefied biomasses was the sorption and desorption of moisture from the environment. In the field of alternative energy torrefaction is used to both densify biomass and prevent bacterial growth. Bacterial growth is hindered due to the increased hydrophobicity of the torrefied biomass. This work looked to quantify this increase in hydrophobicity. It was shown through dynamic vapor sorption analysis that torrefaction decreased the affinity to water of the fiber by 30% or more with a direct relationship between increased degree of torrefaction and hydrophobicity.

With the characteristics of torrefied biomass better understood the next step of this study was to incorporate the torrefied flax shive, hemp hurd, and sunflower hulls into polyamide 6,6 at

30 wt%. These biocomposites were shown to have comparable mechanical properties to the unfilled polyamide 6,6 matrix. The torrefied biomass filled biocomposites were shown to have lower tensile and flexural strengths with increased elastic and tangent moduli. As with any rigid particle filled composites the impact toughness of the biocomposites was lower than the unfilled matrix. One of the advantages to using torrefied biomass as filler in polyamides over the conventional fiberglass fillers is the decreased density.

Thermal mechanical analysis of the biocomposites was also conducted. The addition of torrefied biomass to polyamide 6,6 showed to increase the thermal stability of the biocomposites over the unfilled matrix through heat deflection temperature analysis. Dynamic mechanical analysis also showed that torrefied filler increased the elastic behavior of the composites while decreasing the coefficient of linear thermal expansion. Melt flow indexing showed that the addition of torrefied biomass decreased the flow of the composite through the orifice by over 90% from the neat matrix. Through differential scanning calorimetry analysis the degree of crystallinity of polyamide 6,6 was shown to decrease by approximately 50% with the addition of torrefied fillers. This decrease in crystallinity is a large factor in the mediocre mechanical performance observed from the biocomposites.

While the increased thermal stability and similar mechanical properties of torrefied biomass filled biocomposites when compare to the neat matrix is promising; the decreased petroleum content of the final part is more important. This work showed that the addition of 30 wt% renewable fillers is a viable option for replacements of polyamide parts. Beyond the mechanical properties the economics must also line up to make torrefied fillers an appealing option for industrial applications. It was calculated that for a conventional torrefaction process taking eight hours at 300 °C it costs $7.68 for 150 g of torrefied biomass. By utilizing a

microwave running at a maximum of 500 W for 75 minutes at 400 °C it costs $0.24 for approximately 16 g. These costs come out to be $51.20/kg utilizing a conventional oven and $15.00/kg for the microwave torrefaction. That is a 70% savings by switching from conventional oven torrefaction to microwave torrefaction.

The production of torrefied biomass for the sole use of biocomposites may still not be that appealing due to the added man power needed to conduct the torrefaction. Another option is to utilize the solid by-product of an energy production process. Companies such as Proton Power based in Lenoir City, Tennessee use the syngas and liquids produced from the torrefaction of biomass to produce alternative clean energy. With no use for the carbonized solid by-product Proton Power sells it on the large industrial scale for $0.55/kg. This is an economical alternative to producing torrefied biomass in house.

One final aspect of this work was to develop a predictive modelling approach for torrefaction yield and 90% stability temperature. This model allows for the tailoring of torrefied biomass for particular polymer matrices or applications. The ideal stability temperature for a torrefied biomass would be just over the processing temperatures of the matrix (i.e. within 10 °C) it is to be introduced into. This will allow for the largest amount of surviving lignin and cellulose with the torrefied biomass without seeing further degradation during composite processing. Predicting the torrefaction yield is useful in project planning when estimating how long torrefying processes should last. In order to make the model presented in this work more useful it must be tested for ruggedness in future studies. The model needs to be tested across several biomass feedstocks not studied in this work as well as a larger range of torrefaction temperatures and times.

While this work is a good start on solving the issue of petroleum usage in high temperature thermoplastic biocomposites there is some work yet to be done. Much of the discussion on mechanical results revolved around the decreased crystallinity of the biocomposites from the neat matrix. The next step would be to work on increasing the degree of crystallinity. Throughout this work there were some indications that low molecular weight compounds may have been deposited on the surface of the fiber during torrefaction. Therefore, it would be useful to study how extraction of these compounds may improve the crystallinity of the biocomposites. The particulate size was not studied at all in this work in an effort to reduce the processing of fiber prior to introducing it into the polyamide 6,6 matrix. Moving forward with this work particle size studies after torrefaction are needed in order to fully understand how particle size would affect the properties of the biocomposites. It would be good to study the effects of degree of torrefaction on mechanical properties further as well through a test matrix based on one biomass feedstock with constant particle size at varying degrees of torrefaction incorporated into a polyamide 6,6 matrix.

REFERENCES

[1] D. K. Platt, *Engineering and High Performance Plastics Market Report*. A Rapra Market Report, 2003, p. 188.

[2] E. McHenry and Z. H. Stachurski, "Composite materials based on wood and nylon fibre," *Compos. Part A Appl. Sci. Manuf.*, vol. 34, no. 2, pp. 171–181, Feb. 2003.

[3] G. Sui, M. A. Fuqua, C. A. Ulven, and W. H. Zhong, "A plant fiber reinforced polymer composite prepared by a twin-screw extruder.," *Bioresour. Technol.*, vol. 100, no. 3, pp. 1246–51, Feb. 2009.

[4] P. Santos, M. Spinace, K. Fermoselli, and M. Depaoli, "Polyamide-6/vegetal fiber composite prepared by extrusion and injection molding," *Compos. Part A Appl. Sci. Manuf.*, vol. 38, no. 12, pp. 2404–2411, Dec. 2007.

[5] D. Bruce, R. Hobson, J. Farrent, and D. Hepworth, "High-performance composites from low-cost plant primary cell walls," *Compos. Part A Appl. Sci. Manuf.*, vol. 36, no. 11, pp. 1486–1493, Nov. 2005.

[6] M. A. Fuqua and C. A. Ulven, "Characterization of Polypropylene/Corn Fiber Composites with Maleic Anhydride Grafted Polypropylene," *J. Biobased Mater. Bioenergy*, vol. 2, no. 3, pp. 258–263, Sep. 2008.

[7] M. Avella, M. Malinconico, A. Buzarovska, A. Grozdanov, G. Gentile, and M. E. Errico, "Natural Fiber Eco-Composites," *Polym. Compos.*, vol. 28, no. 1, pp. 98–107, 2007.

[8] V. S. Chevali, M. A. Fuqua, S. Huo, and C. A. Ulven, “Utilization of Agricultural By-products as Fillers and Reinforcements in ABS,” *SAE Int. J. Mater. Manuf.*, vol. 3, no. 1, pp. 221–229, 2010.

[9] R. N. Rothon, Ed., *Particulate-Filled Polymer Composites*, 2nd ed. Rapra Technology Limited, 2003.

[10] M. Chanda and S. K. Roy, *Industrial Polymers, Specialty Polymers, and Their Applications*. CRC Press, 2009, p. 432.

[11] E. Carlson and K. Nelson, “Nylon Under the Hood: A History of Innovation,” vol. December. DuPont, 2003.

[12] W.-H. Chen and P.-C. Kuo, “Torrefaction and co-torrefaction characterization of hemicellulose, cellulose and lignin as well as torrefaction of some basic constituents in biomass,” *Energy*, vol. 36, no. 2, pp. 803–811, Feb. 2011.

[13] N. S. Murthy, “Hydrogen Bonding, Mobility, and Structural Transitions in Aliphatic Polyamides,” *J. Polym. Sci. Part B Polym. Phys.*, vol. 44, pp. 1763–1782, 2006.

[14] R. M. Rowell, “Chemical modification of wood: A short review,” *Wood Mater. Sci. Eng.*, vol. 1, no. 1, pp. 29–33, Mar. 2006.

[15] R. E. Ibach and C. M. Clemons, “Effect of Acetylated Wood Flour or Coupling Agent on Moisture , UV , and Biological Resistance of Extruded Woodfiber-Plastic Composites,” in *Wood Protection*, 2006, pp. 139–147.

[16] K. Segerholm, “Wood Plastic Composites made from Modified Wood - Aspects on Moisture Sorption, Micromophology, and Durability,” KTH Architecture and the Built Environment, 2007.

[17] S. Galland, “Microstructure and Micromechanical Studies of Injection Moulded Chemically Modified Woor/Poly(lactic acid) Composites,” Lulea University of Technology, 2009.

[18] H. P. S. A. Khalil, H. Ismail, H. D. Rozman, and M. N. Ahmad, “The effect of acetylation on interfacial shear strength between plant fibres and various matrices,” *Eur. Polym. J.*, vol. 37, pp. 1037–1045, 2001.

[19] J. Follrich, U. Muller, W. Gindl, and N. Mundigler, “Effects of Long-term Storage on the Mechanical Characteristics of Wood Plastic Composites Produced from Thermally Modified Wood Fibers,” *J. Thermoplast. Compos. Mater.*, vol. 23, no. 6, pp. 845–853, May 2010.

[20] W.-H. Chen and P.-C. Kuo, “A study on torrefaction of various biomass materials and its impact on lignocellulosic structure simulated by a thermogravimetry,” *Energy*, vol. 35, no. 6, pp. 2580–2586, Jun. 2010.

[21] M. Keiluweit, P. S. Nico, M. G. Johnson, and M. Kleber, “Dynamic molecular structure of plant biomass-derived black carbon (biochar).,” *Environ. Sci. Technol.*, vol. 44, no. 4, pp. 1247–53, Feb. 2010.

[22] J. J. Chew and V. Doshi, “Recent advances in biomass pretreatment – Torrefaction fundamentals and technology,” *Renew. Sustain. Energy Rev.*, vol. 15, no. 8, pp. 4212–4222, Oct. 2011.

[23] T. Bridgeman, J. Jones, I. Shield, and P. Williams, “Torrefaction of reed canary grass, wheat straw and willow to enhance solid fuel qualities and combustion properties,” *Fuel*, vol. 87, no. 6, pp. 844–856, May 2008.

[24] M. Prins, K. Ptasinski, and F. Janssen, “Torrefaction of woodPart 1. Weight loss kinetics,” *J. Anal. Appl. Pyrolysis*, vol. 77, no. 1, pp. 28–34, Aug. 2006.

[25] M. Prins, K. Ptasinski, and F. Janssen, “Torrefaction of woodPart 2. Analysis of products,” *J. Anal. Appl. Pyrolysis*, vol. 77, no. 1, pp. 35–40, Aug. 2006.

[26] P. C. A. Bergman, A. R. Boersma, R. W. R. Zwart, and J. H. A. Kiel, “Torrefaction for biomass co-firing in existing coal-fired power stations,” 2005.

[27] S. Panigrahi, A. Ghazanfari, and V. Meda, “Dehydrating of Flax Fiber with Microwave Heating for Biocomposite Production,” *J. Microw. Power Electromagn. Energy*, vol. 40, no. 2, pp. 69–77, 2006.

[28] V. L. Budarin, J. H. Clark, B. a Lanigan, P. Shuttleworth, and D. J. Macquarrie, “Microwave assisted decomposition of cellulose: A new thermochemical route for biomass exploitation.,” *Bioresour. Technol.*, vol. 101, no. 10, pp. 3776–9, May 2010.

[29] R. Luque, J. A. Menéndez, A. Arenillas, and J. Cot, “Microwave-assisted pyrolysis of biomass feedstocks: the way forward?,” *Energy Environ. Sci.*, vol. 5, no. 2, p. 5481, 2012.

[30] M. Guiotoku, C. R. Rambo, F. A. Hansel, W. L. E. Magalhães, and D. Hotza, "Microwave-assisted hydrothermal carbonization of lignocellulosic materials," *Mater. Lett.*, vol. 63, no. 30, pp. 2707–2709, Dec. 2009.

[31] M. J. Wang, Y. F. Huang, P. T. Chiueh, W. H. Kuan, and S. L. Lo, "Microwave-induced torrefaction of rice husk and sugarcane residues," *Energy*, vol. 37, no. 1, pp. 177–184, Jan. 2012.

[32] J. L. Lattimer, "North Dakota State University," North Dakota State University, 2012.

[33] Milestone, "How the PYRO Works," 2009. [Online]. Available: http://www.milestonesrl.com/analytical/products-microwave-ashing-pyro-how-pyro-works.html.

[34] G. Lardy and V. Anderson, "Alternative Feeds for Ruminants," *AS-1181,* 2009. [Online]. Available: http://www.ag.ndsu.edu/pubs/ansci/livestoc/as1182.html.

[35] "Hemp Architecture." [Online]. Available: http://www.hemparchitecture.com/hemp-plant/.

[36] "Hemp Technologies Global." [Online]. Available: http://www.hemp-technologies.com/.

[37] "American Hemp." [Online]. Available: http://www.americanhempllc.com/.

[38] "Hemp Industries Association." [Online]. Available: http://www.thehia.org/index.html.

[39] D. E. Akin, J. A. Foulk, R. B. Dodd, and D. D. McAlister, “Enzyme-retting of flax and characterization of processed fibers.,” *J. Biotechnol.*, vol. 89, no. 2–3, pp. 193–203, Aug. 2001.

[40] D. A. Montgomery, *Design and Analysis of Experiments*, Eighth. Johm Wiley & Sons, Inc., 2013.

[41] H. Yang, R. Yan, H. Chen, D. H. Lee, and C. Zheng, “Characteristics of hemicellulose, cellulose and lignin pyrolysis,” *Fuel*, vol. 86, pp. 1781–1788, 2007.

[42] S. Gaspard and M. C. Ncibi, Eds., *Biomass for Sustainable Applications: Pollution Remediation and Energy*. Cambridge: Royal Society of Chemistry, 2014.

[43] D. Pavia, G. Lampman, G. Kriz, and J. Vyvyan, *Introduction to Spectroscopy*, 5th ed. Stamford: Cengage Learning, 2009.

APPENDIX A. TEST MATRICES DATA TABLES

Table A.1: Particle Size and Sample Mass Test Matrix Data

Size and Mass Matrix			
Particle Size	Sample Mass (g)	Stability Temp (°C)	Yield (%)
200	50	279.69	40.00
200	25	264.26	38.40
750	25	282.97	39.60
AR	25	299.40	38.00
AR	50	285.84	38.80
750	50	282.87	39.40

Table A.2: Microwave Power Level and Torrefaction Time Test Matrix Data

Power Level Matrix				
Power Level (W)	Time (min)	Stability Temp (°C)	Yield (%)	Mass Lost per Degree Raised (%/°C)
400	30	247.20	88.60	0.065
500	20	253.37	83.40	4.396
500	30	263.28	66.20	0.086
500	40	293.16	37.80	0.137
400	20	237.90	91.20	0.068
600	30	292.80	40.20	0.182
300	40	261.60	78.00	4.836
300	30	234.79	91.40	0.063
600	40	315.83	35.40	0.061
400	40	258.77	66.00	0.102
300	20	226.75	92.80	0.140
600	20	250.47	78.60	0.102

Table A.3: Torrefaction Temperature and Torrefaction Hold Time Test Matrix Data

Temperature Matrix			
Temperature (°C)	Time (min)	Stability Temp (°C)	Yield (%)
300	10	271.67	50.20
400	30	329.23	31.80
350	20	302.34	38.80
400	10	303.38	35.20
350	10	300.30	39.60
350	30	309.61	37.40
300	30	286.25	43.20
300	20	281.41	45.60
400	20	343.47	34.20

APPENDIX B. YIELD AND STABILITY TEMPERATURE PREDICTION MATLAB CODE

```
clear all
close all
clc

%% Coefficient Calculations

% Quadratic relationship of change in constituents due to torrefaction temperature
cell = [1 25 25^2 100; 1 336.1111 336.1111^2 90; 1 900 900^2 6.5];
hemi = [1 25 25^2 100; 1 219.4444 216.4444^2 90; 1 900 900^2 20];
lig = [1 25 25^2 100; 1 125 125^2 90; 1 900 900^2 45.7];

C = rref(cell);
H = rref(hemi);
L = rref(lig);

cellconst = C(:,end);
hemiconst = H(:,end);
ligconst = L(:,end);

% Change in yield due to hold time
predictedyield = [67.1595 67.1595 67.1595 64.3138 64.3138 64.3138 61.2045 61.2045 61.2045];
actualyield = [50.2 45.6 43.2 39.6 38.8 38.4 35.2 34.2 31.8];
yieldchange = predictedyield - actualyield;
T = [300 350 400];
time = [10 20 30 10 20 30 10 20 30];

% Linear relationship between yield change and time at each temperature
sumy = sum(yieldchange(1:3));
sumx = sum(time(1:3));
sumx2 = sum(time(1:3).^2);
sumxy = sum(time(1:3).*yieldchange(1:3));
n = 3;

a03 = (sumy*sumx2 - sumx*sumxy)/(n*sumx2 - sumx^2);
a13 = (n*sumxy - sumx*sumy)/(n*sumx2 - sumx^2);

sumy = sum(yieldchange(4:6));
sumx = sum(time(4:6));
sumx2 = sum(time(4:6).^2);
sumxy = sum(time(4:6).*yieldchange(4:6));

a035 = (sumy*sumx2 - sumx*sumxy)/(n*sumx2 - sumx^2);
a135 = (n*sumxy - sumx*sumy)/(n*sumx2 - sumx^2);

sumy = sum(yieldchange(7:9));
sumx = sum(time(7:9));
```

```
sumx2 = sum(time(7:9).^2);
sumxy = sum(time(7:9).*yieldchange(7:9));

% Quadratic relationship between linear regression coefficients and
% temperature
a04 = (sumy*sumx2 - sumx*sumxy)/(n*sumx2 - sumx^2);
a14 = (n*sumxy - sumx*sumy)/(n*sumx2 - sumx^2);

A0 = [a03 a035 a04];
A1 = [a13 a135 a14];

sumx = sum(T);
sumx2 = sum(T.^2);
sumx3 = sum(T.^3);
sumx4 = sum(T.^4);
sumy = sum(A0);
sumxy = sum(A0.*T);
sumx2y = sum(A0.*T.^2);
n = length(3);

A0T = [n sumx sumx2 sumy; sumx sumx2 sumx3 sumxy; sumx2 sumx3 sumx4 sumx2y];
a0 = rref(A0T);

sumy = sum(A1);
sumxy = sum(A1.*T);
sumx2y = sum(A1.*T.^2);

A1T = [n sumx sumx2 sumy; sumx sumx2 sumx3 sumxy; sumx2 sumx3 sumx4 sumx2y];
a1 = rref(A1T);

%% Torrefaction Yield Prediction
again = 'Y';

while again ~= 'n' && again ~= 'N'
   cellulose = input('How much cellulose does the untorrefied fiber contain? ');
   hemicellulose = input('How much hemicellulose does the untorrefied fiber contain? ');
   lignin = input('How much lignin does the untorrefied fiber contain? ');
   temp = input('What temperature will the torrefaction occur at? ');
   time = input('How long will the fiber be held at temperature? ');

   % Amount of each constituent remaining after initial heating
   cellremain = cellconst(1) + cellconst(2)*temp + cellconst(3)*temp^2;
   hemiremain = hemiconst(1) + hemiconst(2)*temp + hemiconst(3)*temp^2;
   ligremain = ligconst(1) + ligconst(2)*temp + ligconst(3)*temp^2;

   yieldHEAT =  cellulose*cellremain/100 + hemicellulose*hemiremain/100 + lignin*ligremain/100;

   newa0 = a0(1,end) + a0(2,end)*temp + a0(3,end)*temp^2;
   newa1 = a1(1,end) + a1(2,end)*temp + a1(3,end)*temp^2;

   yieldTIME = newa0 + newa1*time;
```

```
    yield = yieldHEAT - yieldTIME;

    disp(['The predicted yield is ' num2str(yield) '%'])

    % 90% stability temperature prediction
    stability = -0.0019*yield^3 + 0.3864*yield^2 - 25.362*yield + 810.36;

    disp(['The predicted 90% stability temperature is ' num2str(stability) ' deg C'])

    again = input('Would you like to make another prediction? (y or Y for yes, n or N for no) ', 's');
end
```